ABSTRACT

Title of Thesis: RESPONSE OF FOUNDATIONS SUBJECTED TO VERTICAL DYNAMIC LOADING

Ghassan Sutaih, Master of Science, 2015

Thesis Directed By: Professor, M. Sherif Aggour, Department of Civil and Environmental Engineering

Design of machine foundations that are subject to dynamic loading require that their amplified displacement is within certain limit so that such displacement doesn't impede the operation of the machine they are supporting. For the design of such foundations, several methods are available that are based on a mathematical solution of the differential equation that represents dynamic loads on an elastic half space. When the soil conditions are not uniform, the response cannot be predicted accurately by these methods and hence numerical methods should be used to analyze the problem. This research presents a numerical solution to a foundation subject to dynamic loading considering: 1) the effect of soil layering on the dynamic response. Specifically, a footing rests on a finite soil layer over an elastic half space and 2) the effect of the depth of embedment of a foundation in a homogenous elastic half space on its dynamic response.

RESPONSE OF FOUNDATIONS SUBJECTED TO VERTICAL DYNAMIC LOADING

by

Ghassn Sutaih

Thesis submitted to the Faculty of the Graduate School of the
University of Maryland, College Park, in partial fulfillment
Of the requirements for the degree of
Master of Science
2015

Advisory Committee:
Professor M. Sherif Aggour, Chair
Professor Fu, Chung C.
Professor Goulias, Dimitrios G.

© Copyright by
Ghassan Sutaih
2015

Dedication

To my mother and my sisters, thank you for your continuous support.

Acknowledgements

I would like to thank to Professor M.S. Aggour who supervised my research. I would like to thank him for his guidance and support throughout this study. I would like to thank Professor Fu, Chung C and Professor Goulias, Dimitrios G.for taking and time and serving as committee member.

Table of Contents

List of Tables

List of Figures

1. Introduction

Design of machine foundations requires that amplification of the deformation of the supporting soil is to be minimized. If amplification is high it will cause excessive vibrations that will impede the operation of the supported machine and may cause failure. A designer of machines then requires that the deformations are very small. These very small deformations will result in very small strains within the soil medium so that an elastic soil can be assumed. Design of machine foundations would then require the study of wave propagation within an elastic medium, which involves solving partial differential equations that are very complex to obtain solutions that represent soil accurately. Several mathematical solutions are provided in the literature for different loading configurations (e.g. horizontal loads, vertical loads). Most of these solutions assume that soil is a homogenous elastic medium which is seldom the case. Although these solutions are limited in their ability to represent the soil, they provide practical methods of analysis that are quick and easy for engineers to apply. They are also fair good in representing many cases and provide adequate estimates of the foundation response (Richart & Whitman, 1967). An approximate solution provides a simple method by converting the soil-foundation system to a single degree of freedom dynamic problem that involves a mass, a spring, and a viscous damper. This trend to try to simplify the soil-structure interaction problem and converting it to an equivalent spring and/or spring with dashpot element is a trend in geotechnical engineering and is applied to both static and dynamic problems. This is done due to the complexity of obtaining solution to differential equations. Although numerical methods are available (most common Finite Element Method, Finite Difference

Method and Boundary Element Method) that can provide accurate solutions to the full 3D soil-structure interaction problem, they require more computing resources, an experienced engineer, more time and more money than conventional mathematical method. These numerical solutions are feasible when the resources are available. In addition to the previous requirements, the accuracy of the results is as good as the input of the parameters involved in solving the problem. Implementation of such methods would require more laboratory and field testing to better represent the problem they are used to solve. These solutions are not commonly used in practice. They are better used in research to help determine reasonable approximations that would provide designing engineers with practical guidance. This study involves numerical solutions using the finite element method for different cases that might face engineers in the field and where the provided solutions for homogenous soil profile are rendered inaccurate.

1.1. Problems statement and objectives

This study involves two problems. The first is the problem of a machine vibrating over two layers of elastic soil. The second is an embedded footing within the soil. In both problems the study will determine the equivalent single degree of freedom solution to the problem. The study is a continuation to the work of Lysmer and Richart (Lysmer & Richart, 1966) which is limited by the assumption of a homogenous soil layer. The study determined the representative spring and damping constants which are the main variables that control the response of a single degree of freedom dynamic system. The problem is presented graphically in Figure 1.1.

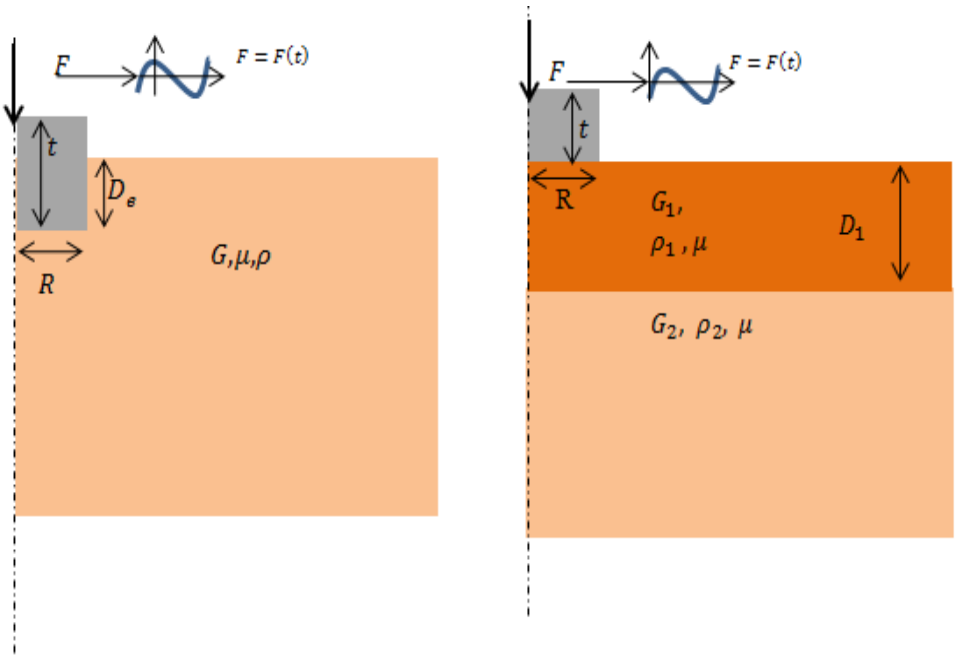

The two problems are simplified to

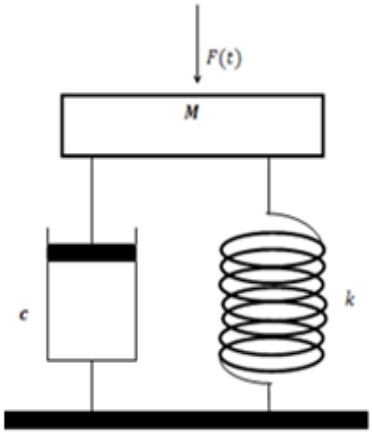

Figure 1.1: Problem definition presented graphically

In the first problem, the soil is divided into two elastic layers. The first layer has predefined depth and the second layer acts as an elastic half space. Variations in the depth of the first layer and the ratio of the shear modulus of the first layer to that of the second layer will be analyzed under a dynamic load at different frequencies. The response is determined at the center of the footing at the soil-footing interface. In addition the problem is analyzed statically to obtain the spring constant. Values of dynamic amplification (i.e. the ratio of dynamic displacement over the static displacement) are obtained. From these values the damping ratio that governs the dynamic response is obtained.

In the second study, the footing is embedded within the soil. The embedment depth is varied from partially embedded at different levels of embedment until full embedment is reached. The shear modulus of the soil is also varied. Static response provides the spring constant while dynamic response at different frequencies will provide the damping ratio.

In summary, the objectives of the study are:

1- Numerical analysis of footing on two layer elastic soils and another analysis of embedded footing in homogenous soil.
2- Obtain spring constant from static analysis of the problems.
3- Obtain the damping ratio from dynamic analysis of the problems.
4- Compare with available studies if applicable.
5- Provide charts that would help with practical applications and better understanding of the effect of the studied variables on the problem of machine foundations.

1.2. Thesis organization

The thesis is divided into 5 chapters other than this one and in brief these chapters are:

2. Review of literature: Provides an introduction to relative literature of soil dynamics covering waves in elastic medium, solutions for machine foundations and properties of dynamically loaded soil.
3. The Finite Element Method: covers the theory of the finite element method in the context of an axisymmetric element. In addition, solution schemes to static and dynamic analyses are provided.
4. Modeling and finite element implementation: this chapter serves as the methodology chapter. It covers the implementation of the finite element in the studied problems. It includes a detailed description of the problems studied and provides a flow chart of the solution approach from modeling, data acquisition to data interpretation.
5. Results and discussion: this is a presentation of the interpreted data. These data are provided in charts that would assist in better understanding the effect of the study's variables on the response of soil to dynamic loads.
6. Conclusion: this chapter summarizes the work done and the outcomes.

2. Literature Review

2.1. Vibrating Systems

Consider a system of a single degree of freedom system as shown in figure 2.1. Such system consists of a rigid mass, a supporting elastic spring and viscous dashpot damper. Applying a force F to the system; in which F is dynamic in nature that varies with time t. In such a system the inertia takes effect and Newton's second equation of motion applies to the system. The following differential equation can be used

$$M\frac{d^2u}{dt^2} = F(t) \tag{2.1}$$

In Equation 2.1, M is the mass and u is the displacement. In said system, the spring will respond to the displacement caused by the force while the damper will respond to the velocity. Equation 2.1 is now adjusted to include the spring and damper reactions to becomes

$$M\frac{d^2u}{dt^2} + c\frac{du}{dt} + ku = F(t) \tag{2.2}$$

Where, c is the damper viscosity coefficient and k is the spring constant. Understanding such a system is critical in Machine foundation and soil dynamics in general. In many cases the soil response to an applied dynamic load is reduced to an analogous spring and a viscous dashpot damper. This makes the problem easy to solve. The engineers only need to conduct experiments to determine c and k values and solve the problem.

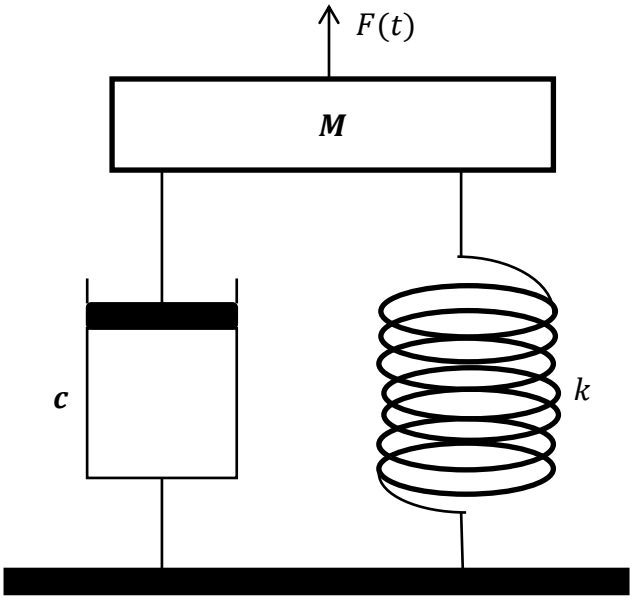

Figure 2.1: Single degree of freedom system consists of a mass, a spring and a viscous damper

2.2. Free Vibrations

If the force F is set to zero, i.e. the system is unloaded; the system will then vibrate freely for a period of time and then stops. Equation 2.2 then becomes

$$\mathrm{M}\frac{\mathrm{d}^2\mathrm{u}}{\mathrm{dt}^2} + \mathrm{c}\frac{\mathrm{du}}{\mathrm{dt}} + \mathrm{ku} = 0 \qquad (2.3)$$

Depending on the damping of the system and the value of the displacement at the time the force is set to zero , the response can be identified mathematically. Defining the damping ratio of the system which is the ratio of the damper coefficient on the critical damping of the system is Mathematically represented by

$$\zeta = \frac{\mathrm{c}}{2\sqrt{\mathrm{kM}}} \qquad (2.4)$$

Where the denominator is the value of the critical damping of the system. Also the natural frequency ω_0 of such a system can be written as

$$\omega_0 = \frac{f_n}{2\pi}\left(\frac{radians}{second}\right) \; where \; f_n = \sqrt{\frac{\kappa}{M}}(Hz) \tag{2.5}$$

The response of the system can be characterized by using the response time t_r also called the relaxation time which is defined as

$$t_r = c/k \tag{2.6}$$

The value of t_r defines the response time of the system. At any time less than the response time, the system is considered stiff and the response depends on the damper. The system response depends more on the spring when the time is greater than the response time. From equations 2.4, 2.5 and 2.6 the damping coefficient can be related to the damping ratio and the natural frequency of the system as $c = 2\zeta\omega_0$. Using $c = 2\zeta\omega_0$ into equation 2.3 gives the following

$$M\frac{d^2u}{dt^2} + 2\zeta\omega_0\frac{du}{dt} + \omega_0^2 u = 0 \tag{2.7}$$

Equation 2.7 represents a differential equation in which the solution can be assume to take the form

$$u = Ae^{\alpha t} \tag{2.8}$$

Where A is a constant related to the initial value of the displacement when F was set to zero. and α is unknown value. Substituting equation 2.8 in equation 2.7 will give

$$\alpha^2 + 2\zeta\omega_0\alpha + \omega_0^2 = 0 \tag{2.9}$$

α now can be found by finding the roots of equation 2.9. The solution might be real or complex and in general it takes the form

$$\alpha_{1,2} = -\zeta\omega_0 \pm \omega_0\sqrt{\zeta^2 - 1} \tag{2.10}$$

It is clear from equation 2.10 that the response of the system depends on the value of the damping ratio ζ. In general, three outcomes can be obtained as shown below:

2.2.1. When the Damping Ratio is Less Than 1

When the damping ratio ζ is less than 1($\zeta < 1$), the solution of equation 2.10 takes the form complex roots.

$$\alpha_{1,2} = -\zeta\omega_0 \pm i\omega_0\sqrt{1 - \zeta^2} \tag{2.11}$$

Where i is the imaginary part of the complex number and($i = \sqrt{-1}$). The dynamic displacement u can be obtained as

$$u = A_1\, e^{i\omega_1 t}\, e^{-\zeta\omega_0 t} + A_2\, e^{i\omega_1 t}\, e^{-\zeta\omega_0 t} \tag{2.12}$$

And $\omega_1$is defined as the damped natural frequency where $\omega_1 = \omega_0\sqrt{1 - \zeta^2}$. $e^{i\omega_1 t}$ Can be rewritten as $\cos(\omega_1 t) + i\sin(\omega_1 t)$. Equation 2.12 then becomes

$$u_d = C_1 \cos(\omega_1 t)\, e^{-\zeta\omega_0 t} + C_2 \sin(\omega_1 t)\, e^{-\zeta\omega_0 t} \tag{2.13}$$

Where C_1 and C_2 values depend on the displacement u_0 which is the displacement when the force F is set to zero. Finally the solution of the dynamic displacement u_d relative to the initial displacement u_0 can be given as

$$\frac{u}{u_0} = \frac{\cos(\omega_1 t - \psi)}{\cos(\psi)}\, e^{-\zeta\omega_0 t} \tag{2.14}$$

Where ψ is the phase angle and $\tan(\psi) = \frac{\omega_0 \zeta}{\omega_1}$. This behavior of the system is represented graphically in figure 2.2 for various damping values. In general, the system will continue to vibrate in a sinusoidal form but its amplitude will decay depending on the exponent of the damping $e^{-\zeta \omega_0 t}$. This decay will continue until it reaches at rest conditions.

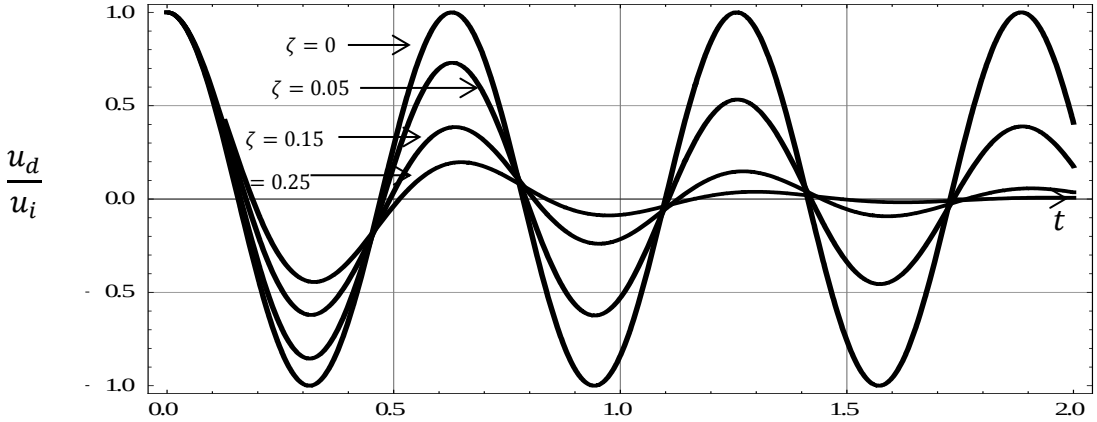

Figure 2.2: Free vibration of damped systems

2.2.2. Critically Damped Systems

When the Damping Ratio of the system is set to 1 (i.e. $\zeta = 1$) the system is said to be critically damped. The response is entirely different than that when $\zeta < 1$. The sinusoidal behavior is no longer applicable here; instead a smooth curve is obtained for the decay of the amplitude with time. This behavior is represented in figure 2.3. The solution of equation 2.9 has two roots of equal values and $\alpha_1 = \alpha_2 = -\omega_0$. The ratio of the amplitude of the displacement at any time to that at $t = 0$ is given by

$$\frac{u}{u_0} = (1 + \omega_0 t)\, e^{-\omega_0 t} \qquad (2.15)$$

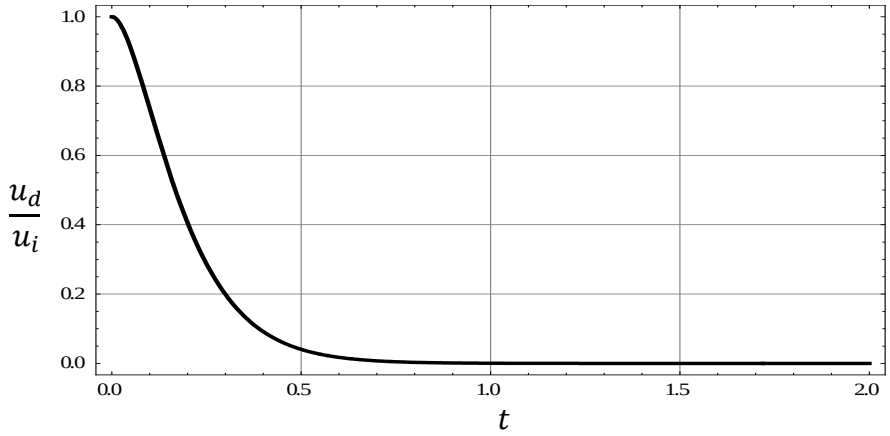

Figure 2.3: Critically damped systems

2.2.3. When the Damping Ratio is Greater than 1

In such a case where $\zeta > 1$, the solution to equation 2.9 has two roots that are real and different. The following equation describes the ratio of the amplitude of displacement at any time relative to that at $t = 0$.

$$\frac{u_d}{u_0} = \frac{\omega_2}{\omega_2 - \omega_0}\, e^{-\omega_1 t} - \frac{\omega_1}{\omega_2 - \omega_1}\, e^{-\omega_2 \tau} \tag{2.16}$$

2.3. Forced Vibrations

The previous sections dealt with the solution of the dynamic differential equation 2.2 when the force F equals zero (i.e. free vibration). In this section the response of the system is investigated under a loading that varies with time. The loading considered is periodic sinusoidal in nature and in general takes the form

$$F(t) = F_0 \cos(\omega t) \tag{2.18}$$

Where ω is the frequency of the periodic load in $radians/seconds$. The solution of equation 2.2 is now obtained and is

$$u = u_d\, Cos(\omega t - \psi) \tag{2.19}$$

Where u_d is the dynamic displacement and is given by

$$u_d = \frac{F_0/k}{\sqrt{\left(1-\frac{\omega^2}{\omega_0^2}\right)^2 + \left(2\zeta\frac{\omega}{\omega_0}\right)^2}} \tag{2.20}$$

Where ζ and ω_0 are defined as per equations 2.4 and 2.5 respectively. Equation 2.20 can also be written in terms of k and c only as shown in the following equation

$$u_d = \frac{F_0/k}{\sqrt{\left(1-m\frac{\omega^2}{k}\right)^2 + \left(c\frac{\omega}{k}\right)^2}} \tag{2.21}$$

If the system has no mass the solution is reduced to

$$u_d = \frac{F_0/k}{\sqrt{1+\left(c\frac{\omega}{k}\right)^2}} \tag{2.22}$$

Equations 2.20 is represented graphically in figure 2.4. It is important to note that $u_s = F_0/k$ and u_s is defined as the static displacement.

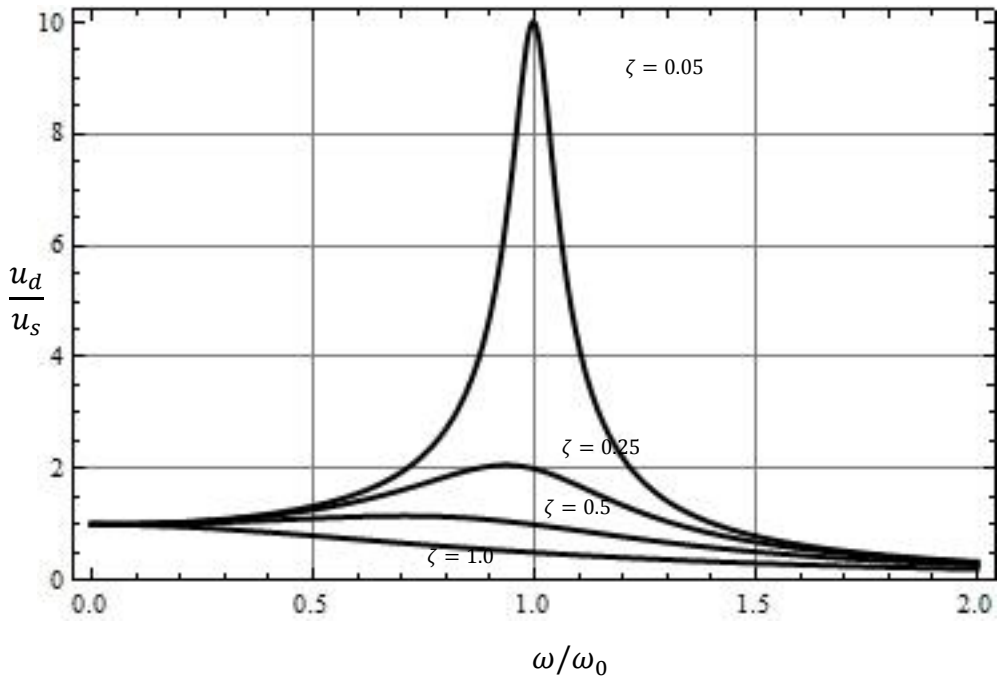

Figure 2.4: Oscillation of forced vibration

So far, an introduction to vibrating systems of a single degree of freedom is presented in the previous sections based on texts (Das & Ramana, 2010; Verruijt, 2010). It is convenient to use such systems to represent the response of the soil to a footing subjected to periodic loading. It is also can be used for single piles in a homogenous elastic half space (Verruijt, 2010). While the finite element method and the boundary element method can be used in engineering practices, it is easier and faster to deal with the reduced system. It also allows the engineers to focus on the problem at hand not on the complexity that is associated with using the numerical methods. This also allows making changes on the problem parameters and decision making much faster and easier. In the upcoming sections a review of the developments of the soil dynamics field with a focus on the response of the soil supporting shallow foundation subjected to a harmonic load shall be presented.

2.4. Waves in a Three Dimensional Elastic Medium

Waves in the soil are better represented by a three dimensional elastic half space. This section will present the mathematical preliminaries required for waves in a three dimensional space.

2.4.1. The Equation of Motion in a Three Dimensional Elastic Medium

For a small finite elastic cube similar to that shown in figure 2.5 (a), If that cube has experienced motion in any directions it would be similar to that presented in figure 2.5 (b). The differential equations that represent this are driven by summing the forces in all directions.

$$\frac{\partial \sigma_x}{\partial x} + \frac{\partial \tau_{yx}}{\partial y} + \frac{\partial \tau_{zx}}{\partial z} = \rho \frac{\partial^2 u}{\partial t^2} \tag{2.23}$$

$$\frac{\partial \sigma_y}{\partial y} + \frac{\partial \tau_{xy}}{\partial x} + \frac{\partial \tau_{zy}}{\partial z} = \rho \frac{\partial^2 v}{\partial t^2} \tag{2.24}$$

$$\frac{\partial \sigma_z}{\partial z} + \frac{\partial \tau_{xz}}{\partial x} + \frac{\partial \tau_{yz}}{\partial y} = \rho \frac{\partial^2 w}{\partial t^2} \tag{2.25}$$

Where $u, v \; and \; w$ are the displacements in the $x, y \;\; and \; z$ directions respectively, σ_i is the normal stress on the i axis, τ_{ij} is the shear stress acting normal on The i plane and its directed towards the j axis and ρ is the mass density of the medium. Strain which is defined as the change in shape relative to the original shape and is given by

$$\varepsilon_x = \frac{\partial u}{\partial x} \tag{2.26}$$

$$\varepsilon_y = \frac{\partial v}{\partial y} \tag{2.27}$$

$$\varepsilon_z = \frac{\partial w}{\partial z} \tag{2.28}$$

$$\gamma_{xy} = \frac{\partial v}{\partial x} + \frac{\partial u}{\partial y} \tag{2.29}$$

$$\gamma_{yz} = \frac{\partial w}{\partial y} + \frac{\partial v}{\partial z} \tag{2.30}$$

$$\gamma_{z\chi} = \frac{\partial w}{\partial x} + \frac{\partial u}{\partial z} \tag{2.31}$$

Where ε_ι is the normal strain in the i direction, γ_{ij} is the shear strain acting normal on the i axis directed towards the j axis. The rotation about a certain axis is defined by

$$\overline{\omega}_x = \frac{1}{2}\left(\frac{\partial w}{\partial y} - \frac{\partial v}{\partial z}\right) \tag{2.32}$$

$$\overline{\omega}_y = \frac{1}{2}\left(\frac{\partial u}{\partial z} - \frac{\partial w}{\partial x}\right) \tag{2.33}$$

$$\overline{\omega}_z = \frac{1}{2}\left(\frac{\partial v}{\partial x} - \frac{\partial u}{\partial y}\right) \tag{2.34}$$

Where $\overline{\omega}_\iota$ is the rotation around the i axis. The mathematical derivation of those equations is given in many books on the Theory of elasticity such as Elasticity and Soil Mechanics by (Davis & Selvadurai, 1996).

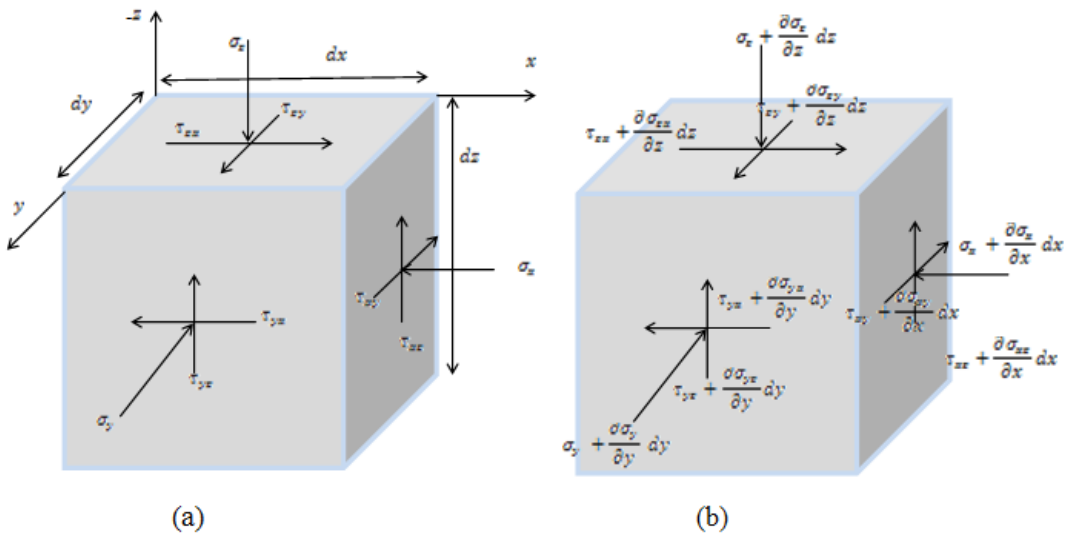

Figure 2.5: (a) Finite cube under static stress. (b) Same cube undergoing some motion

2.4.2. Hooke's Law

In a linear elastic medium the stress and strain are related by Hooke's Law and are given by

$$\varepsilon_x = \frac{1}{E}[\,\sigma_x - \mu(\sigma_y + \sigma_z)] \tag{2.35}$$

$$\varepsilon_y = \frac{1}{E}[\,\sigma_y - \mu(\sigma_x + \sigma_z)] \tag{2.36}$$

$$\varepsilon_z = \frac{1}{E}[\,\sigma_z - \mu(\sigma_y + \sigma_x)] \tag{2.37}$$

Where E is Young's Modulus of Elasticity and μ is Poisson's ratio. Similarly the shear stresses and strains are related by

$$\tau_{xy} = G\gamma_{xy} \tag{2.38}$$

$$\tau_{yz} = G\gamma_{yz} \tag{2.39}$$

$$\tau_{zx} = G\gamma_{zx} \tag{2.40}$$

G is the shear modulus and is related the Young's Modulus Poisson's ratio by

$$G = \frac{1}{2}\, E\,(1+\mu) \tag{2.41}$$

The solution to equations 2.35 to 2.37 that relates the normal stresses to the normal strains is

$$\sigma_x = \lambda\overline{\varepsilon} + 2G\varepsilon_x \tag{2.42}$$

$$\sigma_y = \lambda\overline{\varepsilon} + 2G\varepsilon_y \tag{2.43}$$

$$\sigma_z = \lambda\overline{\varepsilon} + 2G\varepsilon_z \tag{2.44}$$

Where

$$\lambda = \mu E/[(1+\mu)(1-2\mu)] \tag{2.45}$$

$$\overline{\varepsilon} = \varepsilon_x + \varepsilon_y + \varepsilon_z \tag{2.46}$$

2.4.3. Equations for Compression Stress Waves in an Infinite Elastic Medium

Equation 2.23 can be rewritten using equations 2.38, 2.40 and 2.42 to become

$$\rho\frac{\partial^2 u}{\partial t^2} = \frac{\partial}{\partial x}(\lambda\overline{\varepsilon} + 2G\varepsilon_x) + \frac{\partial}{\partial y}\left(G\gamma_{xy}\right) + \frac{\partial}{\partial z}(G\gamma_{xz}) \tag{2.47}$$

The values of ε_x, γ_{xy} and γ_{xz} can be substituted using equations 2.26, 2.29 and 2.31 so that equation 2.47 becomes

$$\rho\frac{\partial^2 u}{\partial t^2} = \frac{\partial}{\partial x}(\lambda\overline{\varepsilon} + 2G\varepsilon_x) + G\frac{\partial}{\partial y}\left(\frac{\partial v}{\partial x} + \frac{\partial u}{\partial y}\right) + G\frac{\partial}{\partial z}\left(\frac{\partial w}{\partial x} + \frac{\partial u}{\partial z}\right) \tag{2.48}$$

The previous equation can be rearranged so that it becomes

$$\rho\frac{\partial^2 u}{\partial t^2} = \lambda\frac{\partial \overline{e}}{\partial x} + G(\frac{\partial^2 u}{\partial x^2} + \frac{\partial^2 v}{\partial x \partial y} + \frac{\partial^2 w}{\partial x \partial z} + \frac{\partial^2 u}{\partial x^2} + \frac{\partial^2 u}{\partial y^2} + \frac{\partial^2 u}{2\partial z^2}) \tag{2.49}$$

Yet $\overline{\varepsilon} = \varepsilon_x + \varepsilon_y + \varepsilon_z$ which values can be taken from equations 2.26, 2.27 and 2.28 so that

$$\frac{\partial^2 u}{\partial x^2} + \frac{\partial^2 v}{\partial x \partial y} + \frac{\partial^2 w}{\partial x \partial z}$$

can be rewritten as $\frac{\partial \overline{\varepsilon}}{\partial x}$. Using the previous derivation, equation 2.49 is simplified to be

$$\rho\frac{\partial^2 u}{\partial t^2} = (\lambda + G)\frac{\partial \overline{\varepsilon}}{\partial x} + G\nabla^2 u \tag{2.50}$$

Where

$$\nabla^2 = \frac{\partial^2}{\partial x^2} + \frac{\partial^2}{\partial y^2} + \frac{\partial^2}{\partial z^2} \tag{2.51}$$

Similarly in the y and z directions

$$\rho\frac{\partial^2 v}{\partial t^2} = (\lambda + G)\frac{\partial \overline{\varepsilon}}{\partial y} + G\nabla^2 v \tag{2.52}$$

$$\rho\frac{\partial^2 w}{\partial t^2} = (\lambda + G)\frac{\partial \overline{\varepsilon}}{\partial z} + G\nabla^2 w \tag{2.53}$$

By differentiating equations 2.50, 2.52 and 2.53 with respect to x, y and z respectively and then summing the equations all together, the result would be

$$\rho \frac{\partial^2 \overline{\varepsilon}}{\partial t^2} = (\lambda + 2G)(\nabla^2 \overline{e}) \tag{2.54}$$

By dividing both sides on ρ

$$\frac{\partial^2 \overline{\varepsilon}}{\partial t^2} = \frac{(\lambda + 2G)}{\rho} \nabla^2 \overline{\varepsilon} = v_p \nabla^2 \overline{\varepsilon} \tag{2.55}$$

Where $v_p$is defined as the compressional wave velocity and is given by

$$v_p = \frac{\lambda + 2G}{\rho} \tag{2.56}$$

For the rest of this text, Compression waves can be referred to as Primary waves or P-waves.

2.4.4. Equations for Shear Waves in an Infinite Elastic Medium

By differentiating equation 2.52 with respect to z and equation 2.53 with respect to y the following equations are obtained

$$\rho \frac{\partial^2}{\partial t^2}\left(\frac{\partial v}{\partial z}\right) = (\lambda + G) \frac{\partial \overline{\varepsilon}}{\partial y \partial z} + G \nabla^2 \frac{\partial v}{\partial z} \tag{2.57}$$

$$\rho \frac{\partial^2}{\partial t^2}\left(\frac{\partial w}{\partial y}\right) = (\lambda + G) \frac{\partial \overline{\varepsilon}}{\partial y \partial z} + G \nabla^2 \frac{\partial w}{\partial y} \tag{2.58}$$

By subtracting the two previous equations, the following is obtained

$$\rho \frac{\partial}{\partial t^2}\left(\frac{\partial w}{\partial y} - \frac{\partial v}{\partial z}\right) = G \nabla^2 \left(\frac{\partial w}{\partial y} - \frac{\partial v}{\partial z}\right) \tag{2.59}$$

And it is already known from equation 2.32 that $\left(\frac{\partial w}{\partial y} - \frac{\partial v}{\partial z}\right) = 2\overline{\omega}_x$. Equation 2.59 can be rewritten as

$$\rho \frac{\partial^2 \overline{\omega}_x}{\partial t} = \frac{G}{\rho} \nabla^2 \overline{\omega}_x = v_s^2 \nabla^2 \overline{\omega}_x \tag{2.60}$$

Where v_s is defined as the shear wave velocity. For the rest of this text Shear waves are refereed to S-Waves.

2.4.5. Rayleigh Waves (R-Wave)

Another type of elastic waves is the Rayleigh wave. This type travels at or near the free surface boundary of an elastic medium. Its velocity is close to that of a shear wave. Firgue.2.6 shows variation of v_r/v_s with the Poisson's ratio. Where v_r is the Rayleigh wave velocity.

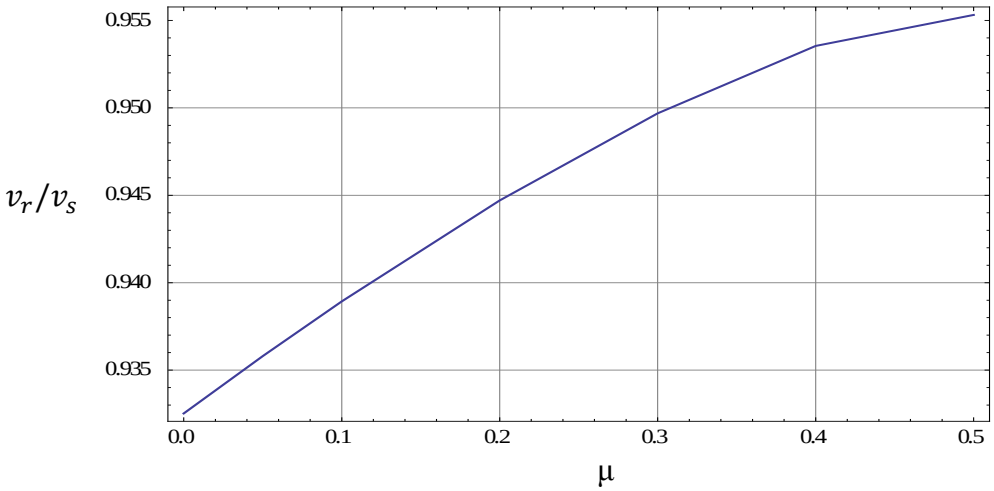

2.6: Variation of v_r/v_s with the Poisson's ratio.

2.4.6. Attenuation of Elastic Waves with Distance from a Source

As waves travel through an elastic medium they lose energy. Part of this energy is absorbed within the medium due to what is known as damping, geometrical

and hysteretic. Geometrical damping is the loss of amplitude due to spreading away from the source, while the hysteretic damping of the medium is related to the material properties or dry friction of a medium in case of soil. Body waves decay with distance faster than surface waves and Rayleigh waves. The decay of elastic waves follows the equation

$$u_{ydr} = \frac{u_{yd0}}{r^n} \tag{2.61}$$

Where

$$n = \begin{cases} 2\ for\ compression\ and\ shear\ wave\ at\ the\ surface \\ 1\ for\ body\ waves\ within\ the\ elastic\ medium \\ \frac{1}{2}\ for\ Rayleigh\ Waves \end{cases}$$

In figure 2.7-a, a disturbance at a source point is shown and in figure 2.7-b, the arrival time and amplitudes of the waves is shown. From figure 2.7, it is obvious that a Rayleigh wave will arrive last at time close to the S-wave and the R-wave will have the highest amplitude than the compressional and shear wave. A P-wave is the fastest among the waves.

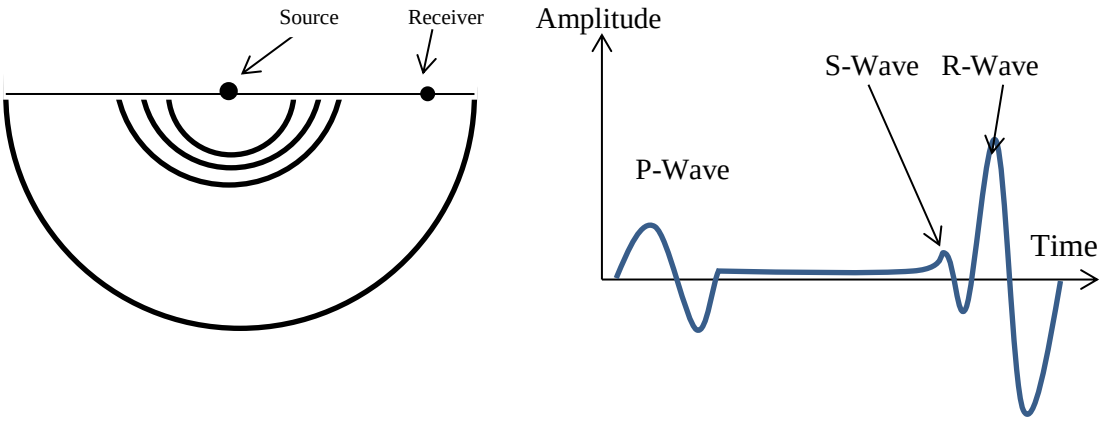

Figure 2.7: (a) Disturbance caused at a point on the surface. (b) the amplitude of different wave and their arrival time

2.5. Refraction and Reflection of Elastic Waves within a Horizontally Layered Elastic Medium

When traveling body waves (P-waves and S-waves) reached the boundary between two elastic layers with different elastic properties, some of the waves will be reflected and some will be refracted and will continue traveling through the second layer. P-waves and S-waves behave differently in multilayered systems. The particle motion in the case of P-wave propagation is continuous to the original P-wave ray (see figure 2.8-a), whereas the particle motion of in the case of S-wave propagation can be divided to two directions:

1- SH-waves which cause the particles to move in the plane of propagation as presented in figure 2.8-b.

2- SV-waves that cause the particles to move in a direction that is perpendicular to the plane of propagation as shown in figure 2.8-c.

In the case of a P-wave at the interface of two layers, there will be two reflected waves and two refracted waves. The first of the reflected waves will be of the same nature of the source wave, a P-wave, while the second one will be of the nature of an SV-wave. As for the refracted waves, the same applies; a P-wave and SV-wave will be generated (see figure 2.8-a).

For the first type of an S-wave which is an SH-wave, there would be a reflected SH-wave and a refracted SH-wave as result of facing a new elastic layer. See figure 2.8-b.

As for SV-waves, the result of facing a new layer would be two reflected wave which are a P-wave and an SV-wave and two refracted waves, a P-wave and an SV-wave as shown in figure 2.8-c.

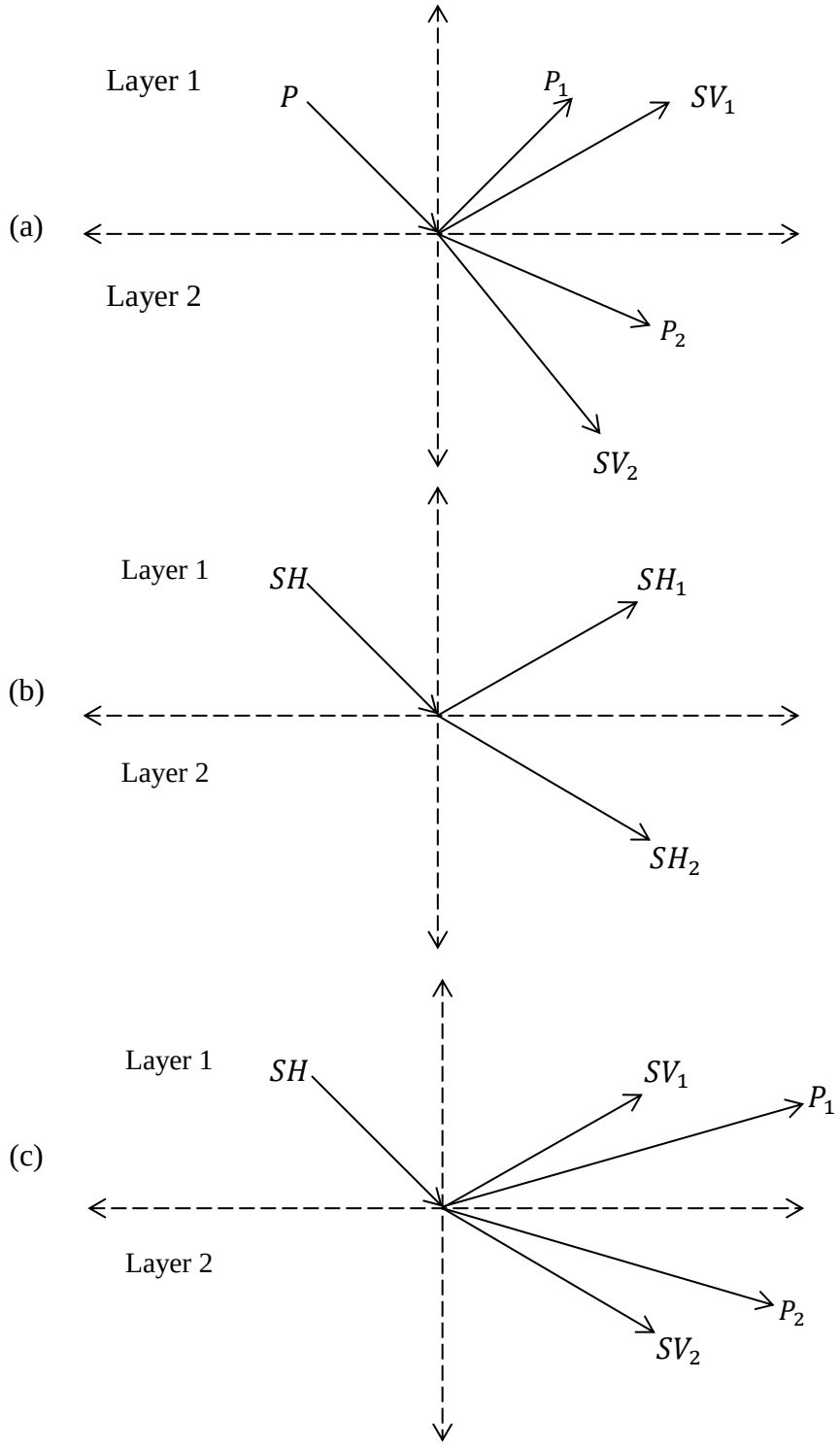

Figure 2.8: Reflection and refraction of body waves at the interface between two elastic layers

2.6. Theories and applications for dynamic soil-foundation interaction.

Consider a footing similar to that presented in figure 2.9. The footing has a mass, m, a radius, r_0 and is subject to a dynamic force Q with an amplitude of Q_0. The elastic properties of the half space are the shear modulus, G, Poisson's ratio, μ, and a mass density ρ. Several solutions for such a problem exist to find the dynamic displacement of the elastic half space under such conditions. The upcoming sections will present some of these solutions along with assumptions made to simplify the problem. Furthermore, a comparison between some of the theories and field testing will also be presented

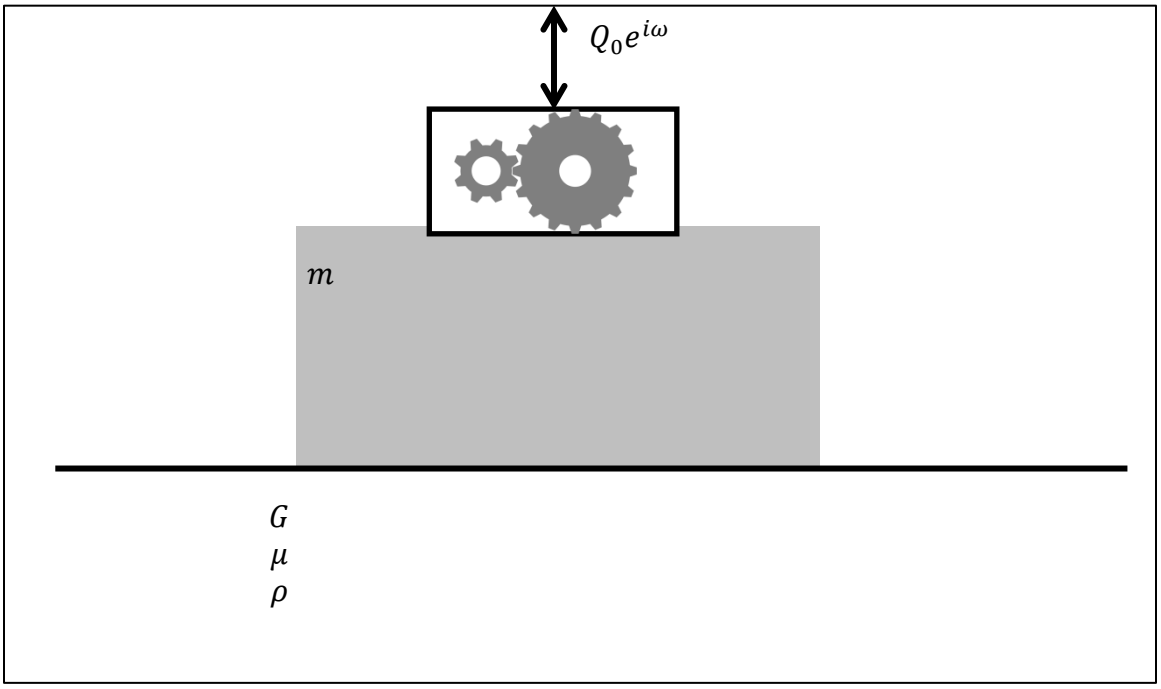

Figure 2.9: Foundation subject to dynamic load

2.4.7. The work of Reissner

Lambe in 1904 studied the problem of a vertical point load acting dynamically over an elastic half space. The problem is known as "the Dynamic Boussinesq Problem". (Reissner, 1936) studied the case where a uniformly distributed load is

acting dynamically on circular flexible foundation. The nature of the pressure distribution under the footing for such a load case is presented in figure 2.10-a. This was done by integrating the problem of a point load which was studied by (Lambe, 1904). The vertical displacement was found to be

$$u = (\frac{Q_0 e^{i\omega\tau}}{G r_0})(f_1 + f_2) \tag{2.62}$$

where Q_0 is the amplitude of the load applied, u is the dynamic displacement at the center of the foundation, G is the shear modulus of the elastic medium, r_0 is the radius of the foundation and f_1 and f_2 are called displacement functions which are functions of a dimensionless frequency a_0 and are shown in figure 2.11 and figure 2.12 respectively, while a_0 is obtained as per equation 2.63.

$$a_0 = \frac{\omega r_0}{v_s} \tag{2.63}$$

Where ω is the frequency of motion in radians per second and v_s is the shear wave velocity in meters per second and r_0 is the radius of said footing.

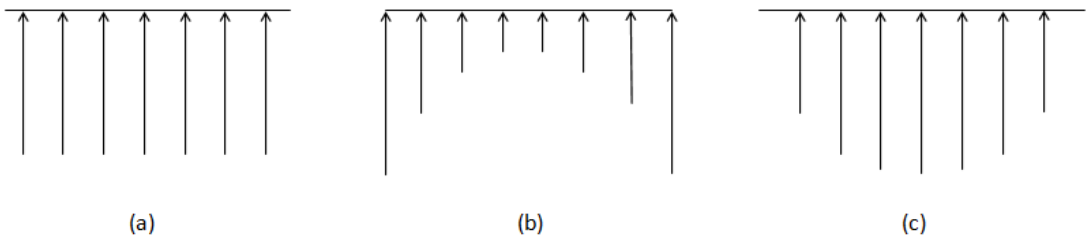

Figure 2.10: Pressure distribution under footing subject to dynamic load. (a) Uniform pressure distribution, (b) Pressure distribution under a rigid footing and (c) Parabolic pressure distribution

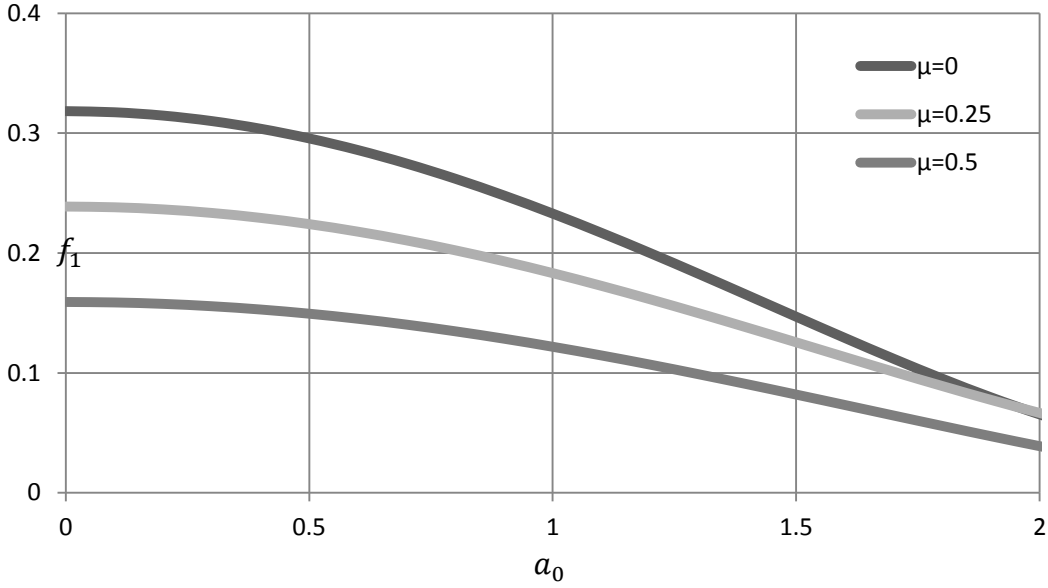

Figure 2.11: Values of f_1 vs. dimensionless frequency a_0 for different Poisson's ratios

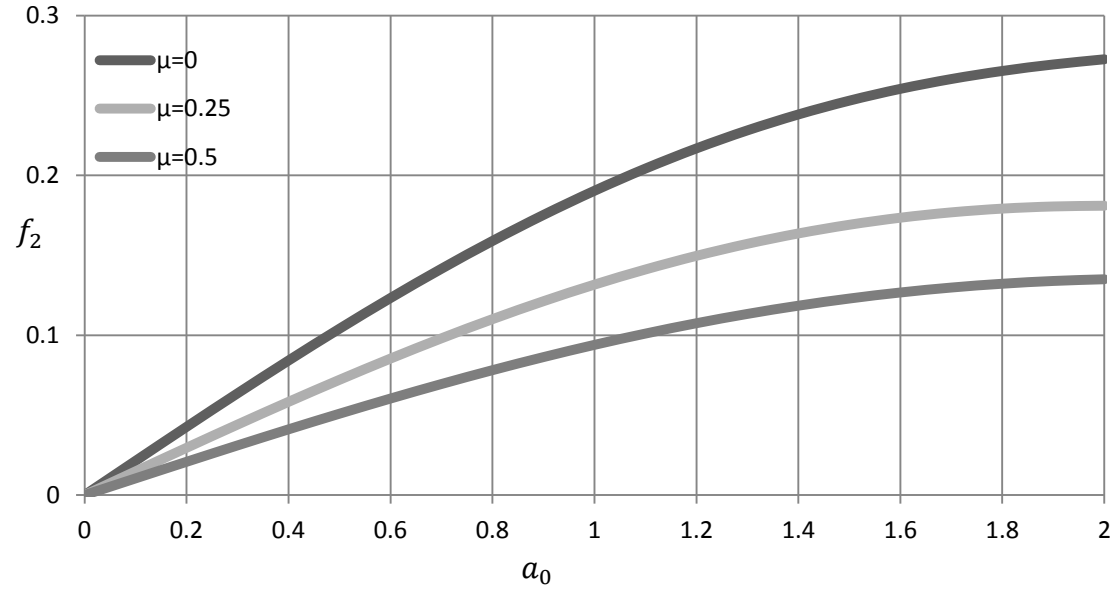

Figure 2.12: Values of f_2 vs. dimensionless frequency a_0 for different Poisson's ratios

Using equation 2.62 and applying equilibrium in forces, the following equation for the amplitude of motion can be derived

$$A_z = \left(\frac{Q_0}{Gr_0}\right) Z \tag{2.64}$$

Where Z is a dimension-less amplitude and is given by

$$Z = \sqrt{\frac{f_1^2 + f_2^2}{(1 - ba_0^2 f_1)^2 + (ba_0^2 f_2)^2}} \tag{2.65}$$

The term b refers to a dimensionless mass ratio that relates the mass of the foundation, m, and the machine with the mass density of the soil, ρ, and is defined as

$$b = \frac{m}{\rho r_0^3} = \frac{W}{\gamma r_0^3} \tag{2.66}$$

Where γ is the unit weight of the soil and W is the weight of the foundation plus that of the machine. So far the dynamic elastic response for the case of a uniformly distributed pressure on a flexible foundation was given (figure 2.10-a). (Quinlan, 1953) and (Sung, 1953) picked up on Reissner's work and studied the response of a load distribution that is similar to that show in figure 2.10-b and 2.10-c. equations 2.64 and 2.65 applies to the case of a rigid foundation (figure 2.10-b) but the values of f_1 and f_2 are different and are shown in figure 2.13 and 2.14.

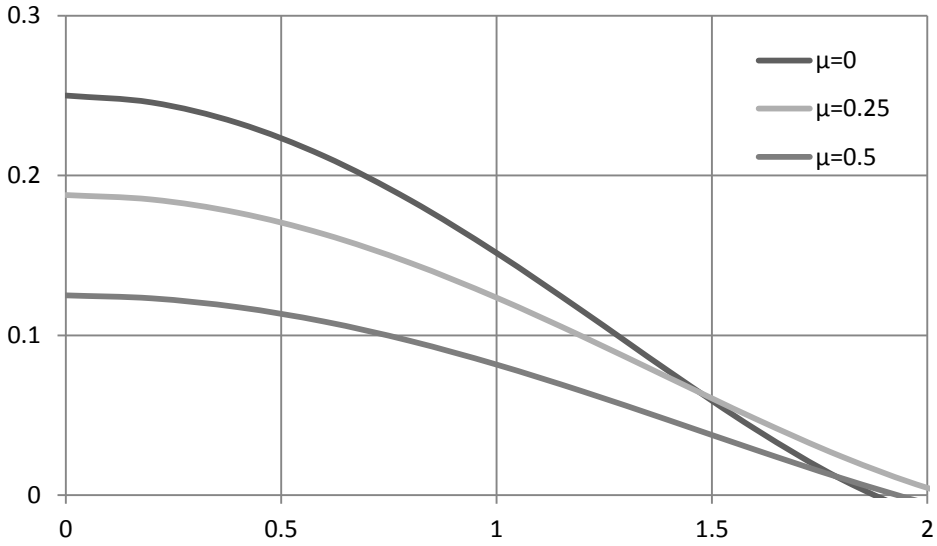

Figure 2.13: Values of f_1 for a rigid foundation

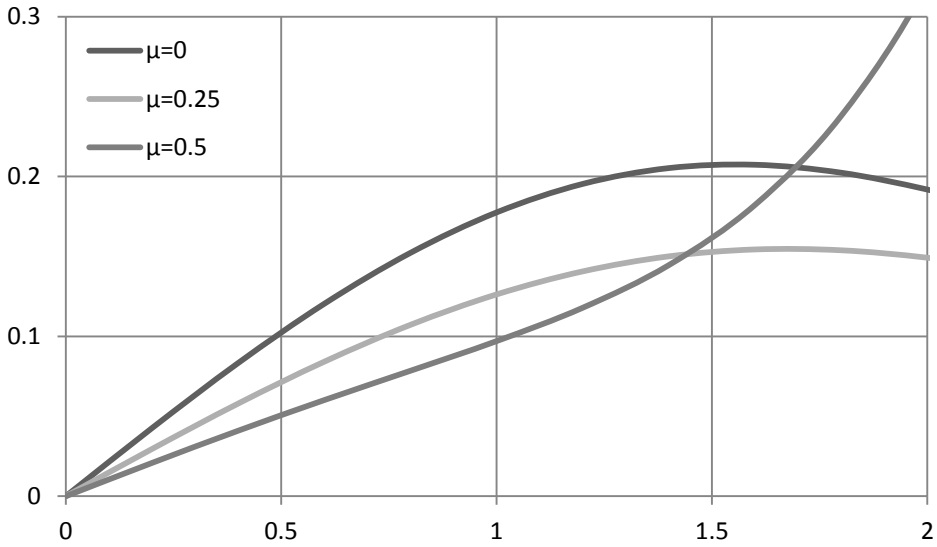

Figure 2.14: Values of f_2 for a rigid foundation

2.4.8. The Work of Lysmer and Richart on Lumped Parameter System for Vertical Motion

(Lysmer & Richart, 1966) work reduces the problem of the elastic half space theory to a model of a single degree of freedom consists of a mass, a spring and a dashpot damper similar to that shown in figure 2.1. The required spring and dashpot constants are obtained from the elastic theory. The mass is equal to the mass of the vibrating machine and the supporting footing. Generally the equations for calculating the required parameters are

$$k = \frac{4Gr_0}{1-\mu} \tag{2.67}$$

$$c = \frac{3.4}{1-\mu} r_0^2 \sqrt{\rho G} \tag{2.68}$$

Where G is the shear modulus of the soil, ρ is the density of the soil, μ is Poisson's Ratio, and r_0 is the radius of the supporting footing. After these two constants are calculated, the response of the soil can be obtained using the procedure presented in sections 2.1-2.3 to calculate the response of the single degree of freedom system.

Lysmer and Richart work is of importance because of its simplicity. Moreover, his work showed that any elastic dynamic system can be reduced to a single degree of freedom at the point of interest by identifying the equivalent spring and dashpot constants. Since then development in the area of machine vibrations has continued with different loading settings (e.g. horizontal and rocking vibrations) different ground conditions (e.g. rock base). The mass ratio B, spring constant k, and

damping ratio D for a rigid foundation under different types of loading are in shown Table 2.1. The equations in Table 2.1 are based on continuation of Lysmer Solution.

Table 2. 1: Values of mass ratio, spring constant and damping ratio for different types of dynamic loadings

Degree of freedom	Mass ratio	Spring constant	Damping ratio
Vertical	$B_v = \frac{(1-\mu)}{4}\frac{m}{\rho r_0^3}$	$K_v = \frac{4Gr_0}{1-\mu}$	$D_v = \frac{0.425}{\sqrt{B_z}}$
Sliding	$B_h = \frac{(7-8\mu)}{32(1-\mu)}\frac{m}{\rho r_0^3}$	$K_h = \frac{8Gr_0^3}{2-\mu}$	$D_h = \frac{0.288}{\sqrt{B_h}}$
Rocking	$B_r = \frac{3(1-\mu)}{8}\frac{I_r}{\rho r_0^3}$	$K_r = \frac{8Gr_0^3}{3(1-\mu)}$	$D_r = \frac{0.15}{(1+B_r)\sqrt{B_r}}$
Torsional	$B_t = \frac{I_t}{\rho r_0^3}$	$k_t = \frac{16Gr_0^3}{3}$	$D_t = \frac{0.5}{1+2B_t}$

2.7. Dynamic properties of soil

Although soil is not an elastic medium nor it is homogeneous, the dynamic properties and mathematics of an elastic medium can be used to obtain reasonable approximations for the response of soil to dynamic loading. The mathematics of a dynamic elastic medium forms the basis of theories presented before. It is then of importance to be able to obtain the dynamic properties of soil. Several laboratory tests

are available to determine these mechanical properties that are needed to apply the theory of elasticity to soil dynamics. From these tests several correlations between soil properties are made to further aid in the analysis.

Soil tends to behave nonlinearly when under stress. If the applied loading is cyclic, the behavior is called the backbone curve and looks like that shown in figure 2.15. This nonlinear behavior can be reduced to a linear behavior using two parameters, the shear modulus and the damping ratio. It is important that this reduction will require prior knowledge of the expected strain level the soil will be exposed to. This is due to the fact that the two said parameters; the shear modulus and the damping ratio; vary with the strain level. With a prior knowledge of the strain level, a dynamic soil test can be selected to determine the required parameters. When the shear modulus and the damping ratio are obtained the soil behavior can be modeled within a reasonable accuracy using the elastic theory.

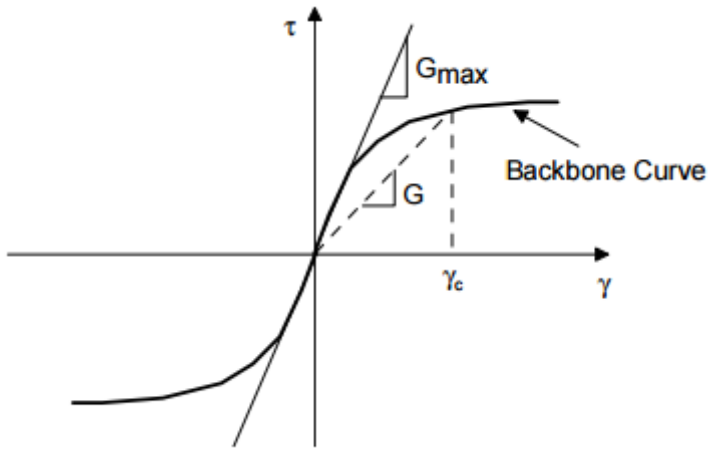

Figure 2.15: Backbone curve

2.7.1. Laboratory testing and correlations for dynamic soil properties

2.7.1.1.Resonant Column Test

In the Resonant column test, a soil sample is excited to vibrate until it reaches one of its natural modes. Once resonated, the frequency at resonance is obtained to calculate the wave velocity of the soil. If the soil is excited in torsion, the wave velocity calculated will be that of a shear wave. On the other hand, if the soil is excited longitudinally, the wave velocity obtained will be that of the compression wave.

Two types of the resonant column test are used. They differ in the applied boundary conditions on the soil sample. The two types are free-fixed and free-free boundary conditions. Figure 2.16 shows a schematic drawing of the setup for the resonant column test. Sinusoidal force is applied into the specimen through the power source and an amplifier. Together, they deliver the force into the driver. The pick-up end is used to obtain the soil specimen response. Obtaining of dynamic soil properties $(G\ and\ \zeta)$ depends on the type of the boundary condition and the force (vertical or torsional) applied to the soil sample.

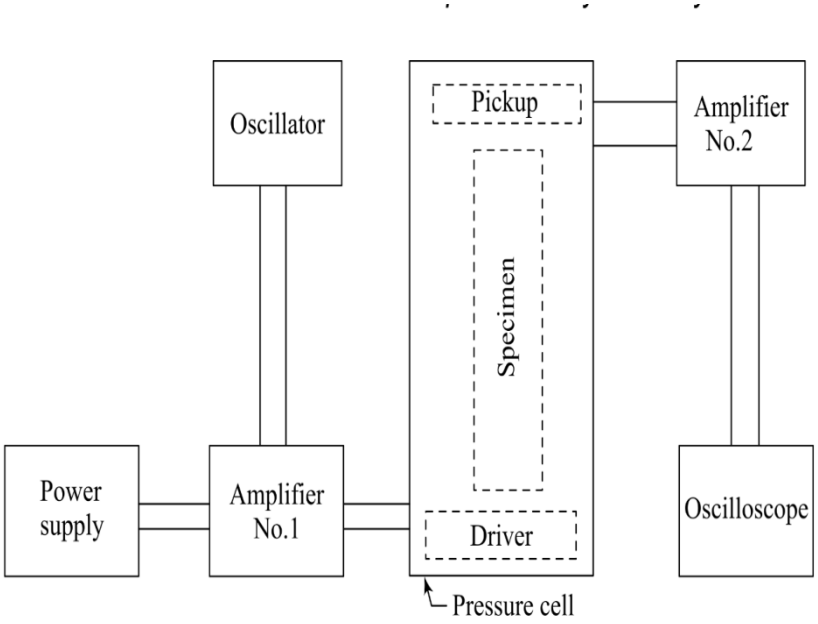

Figure 2.16: Schematic drawing of the resonant column test

Equations for obtaining E and v_p from a fixed free resonant column test with vertical dynamic loading are

$$E = 39.48\left(\frac{f_n^2 * L^2}{\alpha^2}\right)\rho \tag{2.69}$$

$$v_p = \frac{2\pi f_n L}{\alpha} \tag{2.70}$$

Where $\alpha\tan(\alpha) = \frac{AL\gamma}{W}$, L is the length of the specimen, W is the weight of the attachments on top of the soil sample, γ is the unit weight of the soil sample, f_n is the natural frequency obtained and ρ is the density of the soil sample.

Similarly, equations from a torsional load applied to the soil for obtaining v_s and G of the soil sample are

$$G = 39.48\left(\frac{f_n L}{\alpha}\right)^2 \rho \tag{2.71}$$

$$v_s = \frac{2\pi f_n L}{\alpha} \tag{2.72}$$

Here, $a = \frac{2\pi f_n}{v_s}\tan\left(\frac{2\pi f_n L}{v_s}\right) = \alpha\tan(\alpha)$. Other symbols definitions are similar to that of equations 2.69 and 2.70.

Other laboratory tests include cyclic shear test and cyclic triaxial test. These tests are better used to determine soil strength parameters for large strains and when nonlinearity is expected. Figure 2.17 shows different laboratory and field tests with the range of strain level each test will produce.

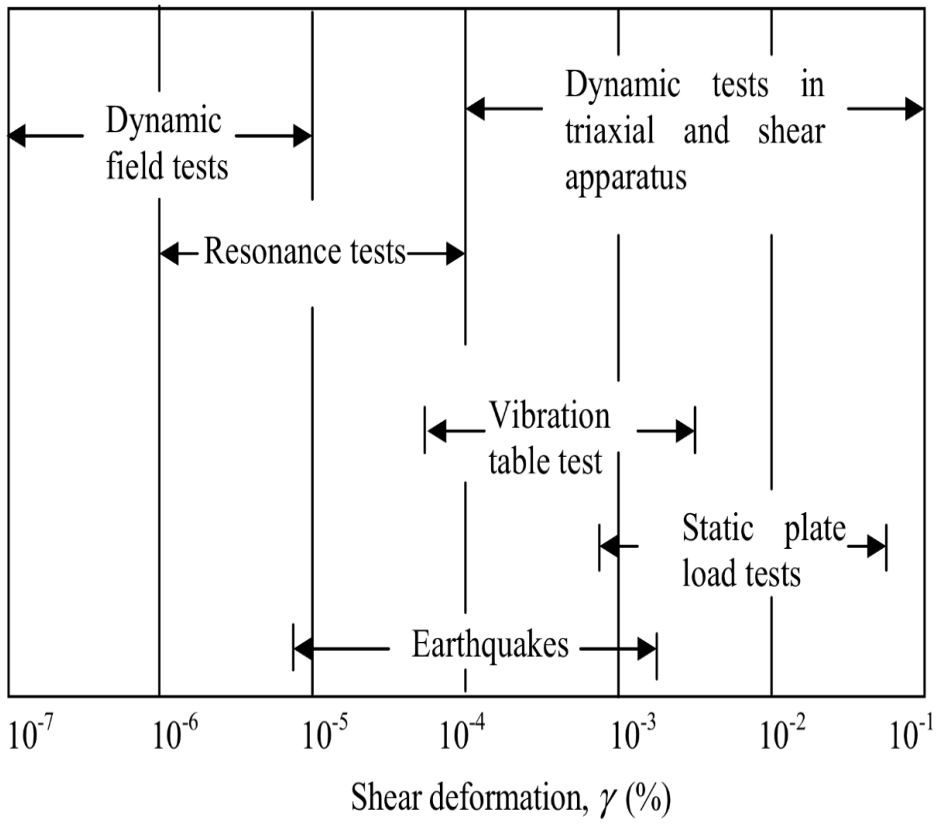

Figure 2.17: Range of strain levels produced by different shear tests (Das & Ramana, 2010)

2.7.1.2.Correlations for shear modulus at low strains in cohesion-less soils

(B O Hardin & Richart, 1963) conducted several resonant column tests on dry Ottawa sands. The shear strain amplitude was at 10^{-3} %. The results of their experiments showed that the shear wave velocity is independent of the grain-size distribution, soil gradation and the relative density of the specimen. Instead, the resulting shear wave velocities were dependent on the void ratio and the effective confining pressure. The results of these experiments are shown in figure 2.18.

From figure 2.18, it can be seen that the higher the confining pressure, the higher the resulting shear wave velocities. This finding is with accordance to the fact

that at deeper earth strata, the shear wave velocities are higher than those at shallower depths. It is also shown in figure 2.15 that at the same confining pressure higher void ratios has shear wave velocity that is lower than at low void ratios (i.e. the shear wave velocity is inversely correlated with the void ratio). The correlation of the shear wave velocity with the confining pressure and the void ratio apply indirectly with the shear modulus.

2.7.1.3.Correlations for shear modulus at low strains for normally consolidated cohesive soils

(B. O. Hardin & Black, 1968) experimented with normally consolidated kaolinite and Boston Blue clay with a resonant column test. Their findings are presented in figure 2.19. The shear modulus was found dependent on the void ratio at a certain confining pressure and can be estimated as

$$G = 1230\frac{(2.973 - e)^2}{(1 + e)}\sigma_c'^{\,1/2} \tag{2.69}$$

In equation 2.69 the shear modulus G and the effective confining pressure are both in lbs/in^2.

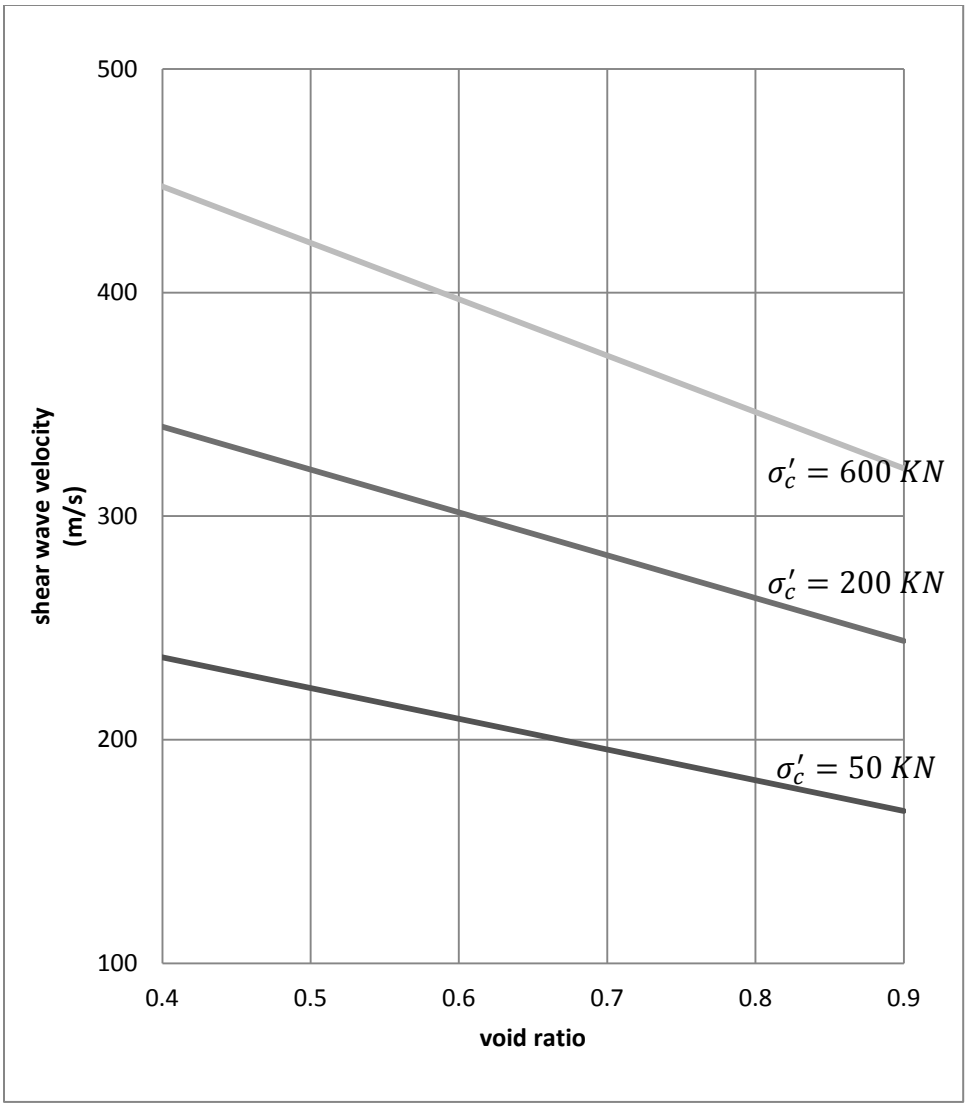

Figure 2.18: Variation of shear wave velocity with the void ratio for different confining pressures (B O Hardin & Richart, 1963)

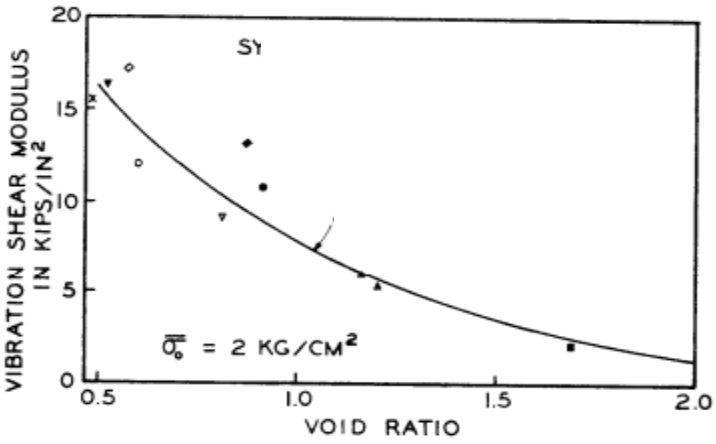

Figure 2.19: Correlation of shear modulus with void ratio for normally consolidated clays. After (B. O. Hardin & Black, 1968)

2.7.1.4.Correlations for shear modulus at low strains for overly consolidated cohesive soils

(B. O. Hardin & Black, 1968) consolidated some specimens before testing to see how pre-consolidation pressure might affect the correlation between shear modulus and void ratio. Equation 2.69 will be modified so that the shear modulus will be calculated as

$$G = 1230\frac{(2.973 - e)^2}{(1 + e)}(OCR)^k {\sigma_c'}^{1/2} \tag{2.70}$$

In (2.70) the term k depends on the plasticity index of the clay specimen. This variation is shown in figure 2.20.

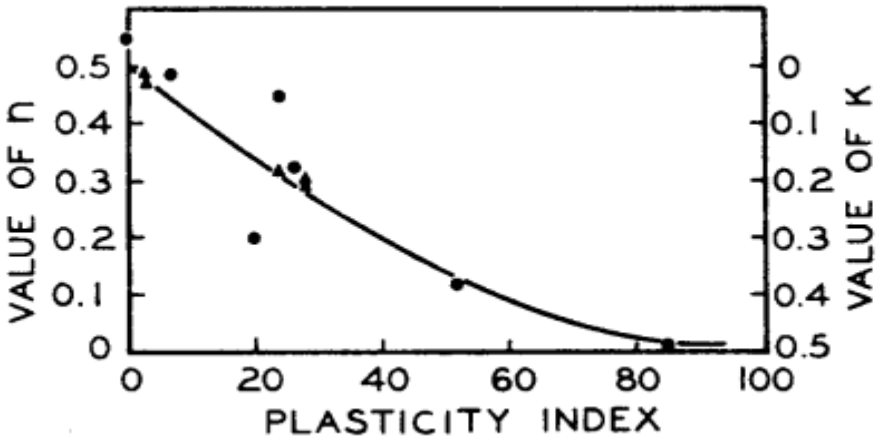

Figure 2.20: Variation of the term *k* in equation 2.70 with the plasticity index. after(B. O. Hardin & Black, 1968)

2.7.1.5. Correlations for shear modulus and damping ratio with strain level

In order to obtain reliable approximation of soil response to a dynamic load, the shear modulus and the damping ratios must be identified correctly and at the strain level for the case at hand. A machine generating a dynamic load of low amplitude will induce a low strain in the soil skeleton. At this low strain level, the shear modulus and the damping ratio will defer greatly from those at higher strain level produced by something like an earthquake or an explosion. Generally, at low strains, the soil will respond with a high shear modulus and a low damping. At higher strains, the soil will respond with a low shear modulus but with a higher damping. This unique relation is reported by several scholars of geotechnical engineering and their results are show in figure 2.21 for the shear modulus and in figure 2.22 for the damping ratio.

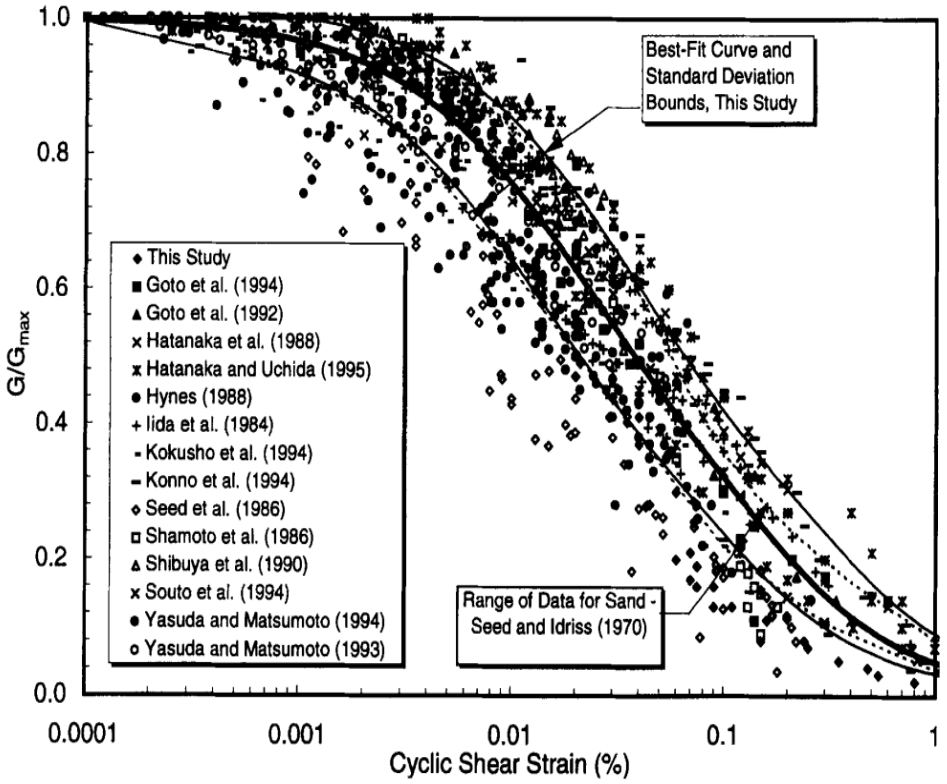

Figure 2.21: Normalized shear modulus values at different strain levels after

(Rollins & Evans, 1998)

From the data a best fit curve reported by (Rollins & Evans, 1998) is shown in figure 2.21. The curve is a hyperbolic curve and the shear modulus according to this curve is

$$\frac{G}{G_{max}} = \frac{1}{1.2 + 16\gamma(1 + 10^{-20\gamma})} \tag{2.70}$$

Where G is the shear modulus and G_{max} is the maximum shear modulus, which is the shear modulus measured at very low strain level of $10^{-4}\%$ (Rollins & Evans, 1998).

Similar correlation for the damping ratio with the shear strain is reported by (Rollins & Evans, 1998). The damping is correlated with shear strain as

$$D = 0.8 + 18(1 + 0.15\gamma^{-0.9})^{-0.75} \quad (2.71)$$

These relations are important to accurately and easily model a dynamic problem. If the expected strain level is known, the non-linear soil stress-strain curve can be reduced to an equivalent shear modulus and damping ratio. This correlation will also help aid in selecting the proper dynamic soil testing method as some testing methods produce higher strains than others which will yield a higher damping ratio while the shear modulus will be lower than a low strain inducing laboratory test.

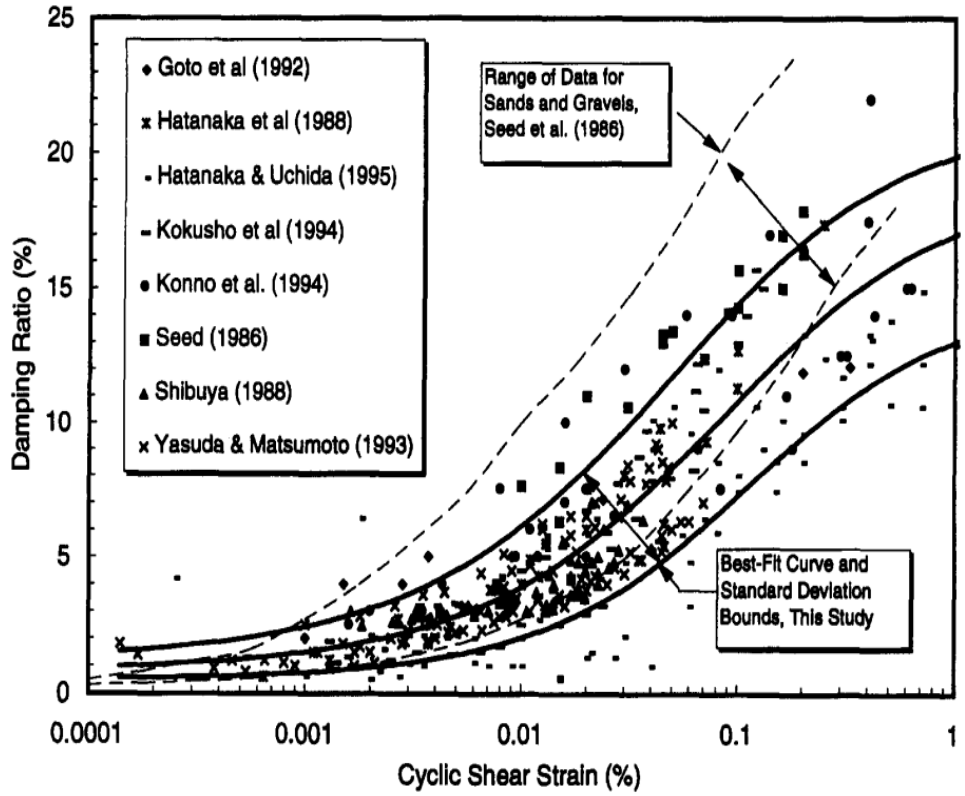

Figure 2.22: Damping ratio of soil at different strain levels after (Rollins & Evans, 1998)

3. The Finite Element Method

The finite element method (to be referred to as FEM or FEA throughout the rest of this text) is a numerical method that discretizes a continuum into small finite sub-structures. The sub-structure element is mathematically defined in how it transports a certain quantity (e.g. stress, temperature, or a fluid) to the adjacent element. Boundary conditions and material models are to be defined in order for the solution of the differential equations to be numerically obtained and to approximate the material behavior in the real problem. Basically, FEM is a numerical method used to solve approximately differential equations of field problems. The field problem can be one, two or three dimensional of any shape and configuration. In this research, the finite element method is used to simulate the problem of a machine foundation resting on soil medium. Since the foundation is circular and the problem is axisymmetric, the use of the axisymmetric finite element will yield the same result of a full three-dimensional model of the problem while being efficient in the use of computer resources and will save considerable amount of time. An axisymmetric representation of a three-dimensional solid of revolution is shown in figure 3.1.

This chapter will serve as an introduction to the finite element method based on (Bathe, 2006; Logan, 2007). In this chapter, the axisymmetric element and how to derive the required matrices to solve the differential equations will be discussed. The sparse and iterative solvers of the equilibrium equations will be introduced. Finally, integration schemes in time of the dynamic problem will be presented. After the presentation of the basics of the finite element method, application to the current research is discussed. This discussion will include the type of integration scheme

used, mesh size, time step size and boundary conditions. To be certain of proper selection of these variables a comparison study is made. This study compares the finite element solution of a machine under a vibrating vertical load resting on an elastic half-space with the theoretical solution of the problem provided by Lysmer and discussed in section 2.4.8.

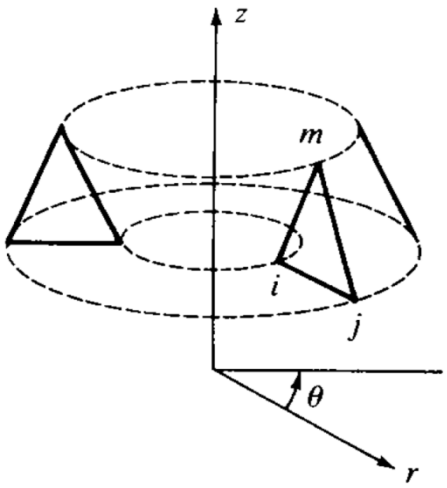

Figure 3.1: Body rotating around the z-axis with a triangular element used to model it.

3.1. Mathematical preliminaries for the finite element method

In a linear elastic material the stress-strain relationship is defined by

$$\{\sigma\} = [C]\{\varepsilon\} \tag{3.1}$$

Where $\{\sigma\}$ is the stress matrix, $[C]$ is a constitutive matrix that relates the stress to the strain and $\{\varepsilon\}$ is the strain matrix.

From the constitutive matrix, a local elemental stiffness matrix $[k]$ can be calculated as

$$\{k\} = \int [B]^T [C][B] dV \tag{3.2}$$

The matrix $[B]$ depends on the geometry and coordinates of the finite element and is defined by

$$[B] = \{\partial\}[N] \tag{3.3}$$

In 3.3, $\{\partial\}$is a differential operator of the shape functions matrix$[N]$.

The final equilibrium equation for a static problem is

$$\{F\} = [K]\{D\} \tag{3.4}$$

Where $[F]$ is the global nodal forces matrix and $[U]$ is the global nodal displacement matrix. They are defined by

$$\{F\} = \sum_{i=0}^{n} f_i \tag{3.5}$$

$$\{D\} = \sum_{i=0}^{n} d_i \tag{3.6}$$

f_i and u_i are the force and displacement at node i respectively. n is the total number of nodes in the problem.

$[K]$ is the global stiffness matrix and is obtained by

$$\{K\} = \sum_{j=0}^{n} \sum_{i=0}^{n} k_{ij} \tag{3.7}$$

$\{F\}$ and $\{U\}$ depends on the boundary conditions of the problem (i.e. applied loads and prescribed displacements). After defining all the required matrices equation 3.4 can be solved to obtain unknown forces or displacements at any node in the continuum. All the above equation will depend on the problem at hand. The number of nodes n will vary greatly between one-dimensional, two-dimensional or three dimensional. Generally the more nodes there are the longer it will take a computer to solve the problem. This will be important to reduce analysis time in dynamic problems as the equilibrium equations are solved multiple times at discretized time steps.

3.2. The axisymmetric element

An axisymmetric element is a finite element used to model a three-dimensional body that is symmetrical around an axis in regards to geometry and boundary conditions. Due to symmetry around the z-axis as shown in figure 3.1, the stresses and strains are independent of the value of θ. The stresses then are dependent on the coordinates of the plane $z - r$. The following is a derivation of the matrices required to solve a finite element problem with a triangular axisymmetric element. See figure 3.2 for the triangular element with vertices $i, j, and\ m$; each has the coordinates (z, r). The element has two degrees of freedom per node ($u\ and\ w$). Let the element has the following displacement functions

$$u(r,z) = a_1 + a_2 r + a_3 z \tag{3.8}$$

$$w(r,z) = a_4 + a_5 r + a_6 z \tag{3.9}$$

Note that the total number of the coefficients a is the same as the number of the degrees of freedom. (6 $a_i's$ for 6 degrees of freedom). The nodal displacement matrix is

$$\{d\} = \begin{Bmatrix} d_i \\ d_j \\ d_m \end{Bmatrix} = \begin{Bmatrix} u_i \\ w_i \\ u_j \\ w_j \\ u_m \\ w_m \end{Bmatrix} \tag{3.10}$$

At any node i, u and w are evaluated as

$$u(r_i, z_i) = a_1 + a_2 r_i + a_3 z_i \tag{3.11}$$

$$w(r_i, z_i) = a_4 + a_5 r_i + a_6 z_i \tag{3.12}$$

In matrix form the displacement function is represented as

$$\{\psi\} = \begin{bmatrix} 1 & r & z & 0 & 0 & 0 \\ 0 & 0 & 0 & 1 & r & z \end{bmatrix} \begin{Bmatrix} a_1 \\ a_2 \\ a_3 \\ a_4 \\ a_5 \\ a_6 \end{Bmatrix} \tag{3.13}$$

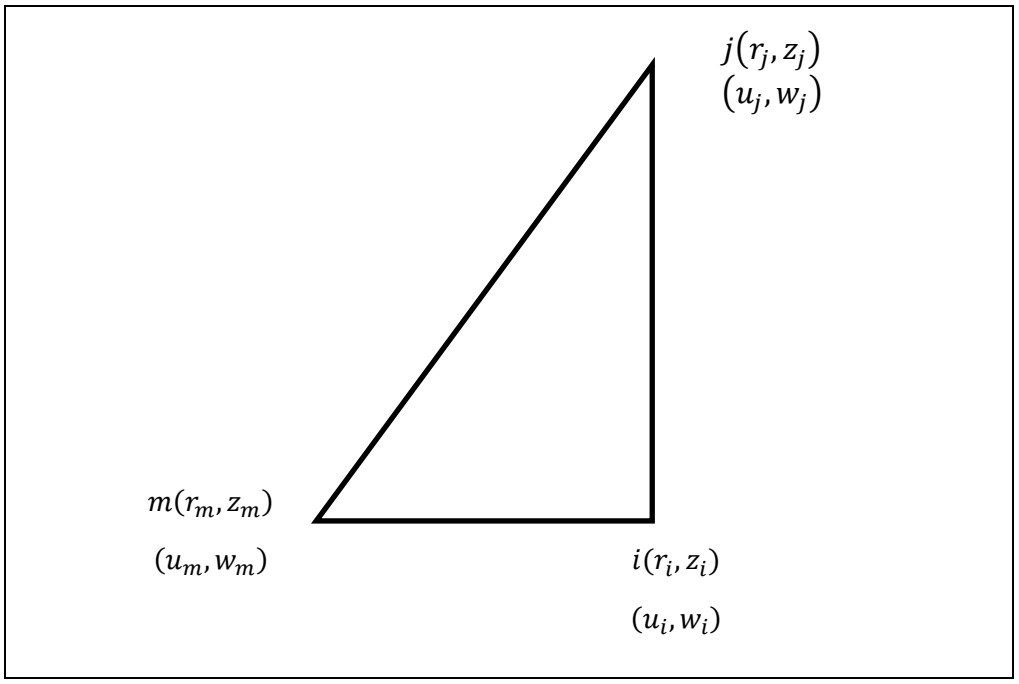

Figure 3.2: Triangular axisymmetric element

Rearranging equation 3.13 and substituting the coordinates of each vertex on the element yields:

$$\begin{Bmatrix} a_1 \\ a_2 \\ a_3 \end{Bmatrix} = \begin{bmatrix} 1 & r_i & z_i \\ 1 & r_j & z_j \\ 1 & r_m & z_m \end{bmatrix}^{-1} \begin{Bmatrix} u_i \\ u_j \\ u_m \end{Bmatrix} \tag{3.14}$$

$$\begin{Bmatrix} a_4 \\ a_5 \\ a_6 \end{Bmatrix} = \begin{bmatrix} 1 & r_i & z_i \\ 1 & r_j & z_j \\ 1 & r_m & z_m \end{bmatrix}^{-1} \begin{Bmatrix} w_i \\ w_j \\ w_m \end{Bmatrix} \tag{3.15}$$

After performing the inversion in equations 3.14 and 3.15 they become

$$\begin{Bmatrix} a_1 \\ a_2 \\ a_3 \end{Bmatrix} = \frac{1}{2A} \begin{bmatrix} \alpha_\iota & \alpha_j & a_m \\ \beta_\iota & \beta_j & \beta_m \\ \gamma_i & \gamma_j & \gamma_m \end{bmatrix} \begin{Bmatrix} u_i \\ u_j \\ u_m \end{Bmatrix} \tag{3.16}$$

$$\begin{Bmatrix} a_4 \\ a_5 \\ a_6 \end{Bmatrix} = \frac{1}{2A} \begin{bmatrix} \alpha_\iota & \alpha_j & a_m \\ \beta_\iota & \beta_j & \beta_m \\ \gamma_i & \gamma_j & \gamma_m \end{bmatrix} \begin{Bmatrix} w_i \\ w_j \\ w_m \end{Bmatrix} \tag{3.17}$$

Where:

$$\begin{array}{lll} \alpha_\iota = r_j z_m - z_j r_m & \alpha_j = r_m z_i - z_m r_i & \alpha_m = r_i z_j - z_i r_j \\ \beta_i = z_j - z_m & \beta_j = z_m - z_i & \beta_m = z_i - z_j \\ \gamma_i = r_m - r_j & \gamma_j = r_i - r_m & \gamma_m = r_j - r_i \end{array} \tag{3.18}$$

The shape functions are then defined as:

$$N_i = \frac{1}{2A}(\alpha_i + \beta_i r + \gamma_i z) \tag{3.19}$$

$$N_j = \frac{1}{2A}(\alpha_j + \beta_j r + \gamma_j z) \tag{3.20}$$

$$N_m = \frac{1}{2A}(\alpha_m + \beta_m r + \gamma_m z) \tag{3.21}$$

The displacement matrix of the element is:

$$\begin{Bmatrix} u(z,r) \\ w(z,r) \end{Bmatrix} = \begin{bmatrix} N_i & 0 & N_j & 0 & N_m & 0 \\ 0 & N_i & 0 & N_j & 0 & N_m \end{bmatrix} \begin{Bmatrix} u_i \\ w_i \\ u_j \\ w_j \\ u_m \\ w_m \end{Bmatrix} \tag{3.22}$$

From continuum mechanics and elasticity the strains can be defined as

$$\varepsilon_r = \frac{\partial u}{\partial r} \qquad \varepsilon_\theta = \frac{u}{r} \qquad \varepsilon_z = \frac{\partial w}{\partial z} \qquad \gamma_{rz} = \frac{\partial u}{\partial z} + \frac{\partial w}{\partial r} \tag{3.23}$$

Using equations 3.8 and 3.9 with 3.23 the following is obtained

$$\{\varepsilon\} = \begin{Bmatrix} a_2 \\ a_6 \\ \frac{a_1}{r} + a_2 + \frac{a_3 z}{r} \\ a_3 + a_5 \end{Bmatrix} \tag{3.24}$$

Equation 3.24 can be rewritten as

$$\begin{Bmatrix} \varepsilon_r \\ \varepsilon_z \\ \varepsilon_\theta \\ \gamma_{rz} \end{Bmatrix} = \begin{bmatrix} 0 & 1 & 0 & 0 & 0 & 0 \\ 0 & 0 & 0 & 0 & 0 & 1 \\ \frac{1}{r} & 1 & \frac{z}{r} & 0 & 0 & 0 \\ 0 & 0 & 1 & 0 & 1 & 0 \end{bmatrix} \begin{Bmatrix} a_1 \\ a_2 \\ a_3 \\ a_4 \\ a_5 \\ a_6 \end{Bmatrix} \tag{3.25}$$

Substituting Equations 3.16 and 3.17 in 3.25 with simplification, the following equation is obtained

$$\{\varepsilon\} =$$

$$\frac{1}{2A} \underbrace{\begin{bmatrix} \beta_i & 0 & \beta_j & 0 & \beta_m & 0 \\ 0 & \gamma_i & 0 & \gamma_j & 0 & \gamma_m \\ \frac{\alpha_i}{r} + \beta_i + \frac{\gamma_i z}{r} & 0 & \frac{\alpha_j}{r} + \beta_j + \frac{\gamma_j z}{r} & 0 & \frac{\alpha_m}{r} + \beta_m + \frac{\gamma_m z}{r} & 0 \\ \gamma_i & \beta_i & \gamma_j & \beta_j & \gamma_m & \beta_m \end{bmatrix}}_{[B]} \begin{Bmatrix} u_i \\ w_i \\ u_j \\ w_j \\ u_m \\ w_m \end{Bmatrix} \tag{3.26}$$

The stresses are given by equation 3.1 where the constitutive matrix $[C]$ is according to the following equation

$$[C] = \frac{E}{(1+\mu)(1-2\mu)} \begin{bmatrix} 1-\mu & \mu & \mu & 0 \\ \mu & 1-\mu & \mu & 0 \\ \mu & \mu & 1-\mu & 0 \\ 0 & 0 & 0 & \frac{1-2\mu}{2} \end{bmatrix} \tag{3.27}$$

The axisymmetric element stiffness matrix is calculated according to the volume integral in equation 3.2 and in the cylindrical coordinates equation 3.2 becomes

$$[k] = 2\pi \iint [B]^T [C][B]\, r\, dr\, dz \tag{3.28}$$

So far the element stiffness matrix of an axisymmetric element is derived. Boundary conditions (i.e. nodal forces and prescribed displacements) are applied on each node and placed in the proper location in the forces and displacement matrices. In the case of surface forces (i.e. surface traction and/or pressure) the process is more involved to obtain equivalent nodal forces. The process is explained with the aid of figure3.3. In figure 3.3, an axisymmetric element is presented with forces acting on the surface of the element. One force is a pressure force and the other is a surface traction force. In general surface forces can be found by

$$\{f_s\} = \iint [N_s]^T \{T\}\, dS \tag{3.29}$$

Where $\{f_s\}$ is the element forces matrix and $[N_s]$ is the shape function matrix evaluated along the surface where the surface forces act. In the case of the element presented in figure 3.3, equation 3.29 becomes

$$\{f_s\} = \iint [N_s]^T \begin{Bmatrix} p_r \\ p_z \end{Bmatrix} dS \tag{3.30}$$

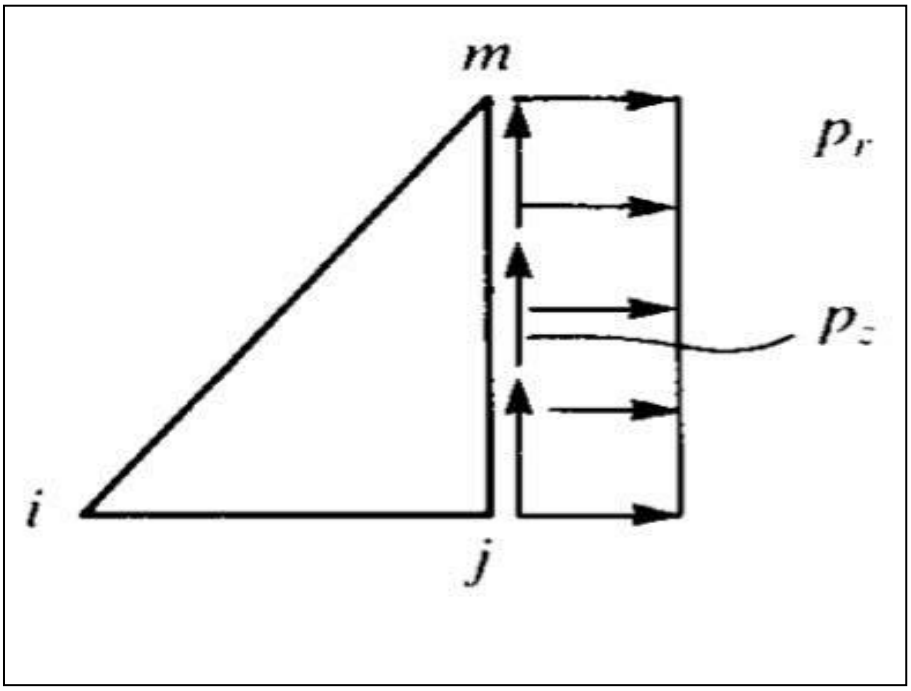

Figure 3.3: Example of surface forces acting on an axisymmetric element

The evaluation of $[N_s]$ is obtained from equations 3.19, 3.20, and 3.21. For each node the integral is evaluated individually to obtain the equivalent forces at the node. For example at node j the integral in equation 3.30 and with the aid of equation 3.20 becomes

$$\{f_{sj}\} = \int_{z_j}^{z_m} \frac{1}{2A} \underbrace{\begin{bmatrix} \alpha_j + \beta_j r + \gamma_j z & 0 \\ 0 & \alpha_j + \beta_j r + \gamma_j z \end{bmatrix}}_{\text{Evaluated at } r = r_j \text{ and } z = z} \begin{Bmatrix} p_r \\ p_z \end{Bmatrix} 2\pi r_j \, dz \tag{3.31}$$

After performing the integration at each node the forces matrix can be calculated and at each node the final force matrix becomes

$$\{f_s\} = \frac{2\pi r_j (z_m - zj)}{2} \begin{Bmatrix} 0 \\ 0 \\ p_r \\ p_z \\ p_r \\ p_z \end{Bmatrix} \tag{3.32}$$

Finally the global stiffness, forces and displacements are formed by summation of the values at each node according to equations 3.5, 3.6, and 3.7.

3.2. Solution of the static equilibrium equation

For static analysis equation 3.4 needs to be solved. Several techniques are available to solve the equation. The software used is capable of using two methods. The first is a sparse solver and the second is an iterative solver. The following sections will give an in-depth look at each technique.

3.2.1. Direct solution of the static equilibrium equation in linear analysis

Gauss Elimination method is used in the direct solution to the equilibrium equations in linear elastic finite elements. The process of the Gauss elimination is better explained with the aid of the following equation

$$\begin{bmatrix} k_{11} & k_{12} & k_{13} & k_{14} \\ k_{21} & k_{22} & k_{23} & k_{24} \\ k_{31} & k_{32} & k_{33} & k_{34} \\ k_{41} & k_{42} & k_{43} & k_{44} \end{bmatrix} \begin{Bmatrix} u_1 \\ u_2 \\ u_3 \\ u_4 \end{Bmatrix} = \begin{Bmatrix} f_1 \\ f_2 \\ f_3 \\ f_4 \end{Bmatrix} \tag{3.33}$$

The mathematical steps to the solution of the system of equations above are:

1. For the second row get

$$k_{2,j} - \frac{k_{2,1} k_1, j}{k_{1,1}}$$

This means that for $i = 2\ and\ j = 1$ the entry will be $k_{2,1} - \frac{k_{2,1}k_{1,1}}{k_{1,1}} = 0$

For the third row get

$$k_{3,j} - \frac{k_{3,1}k_{1},j}{k_{1,1}}$$

This means that for $i = 3\ and\ j = 1$ the entry will be $k_{3,1} - \frac{k_{2,1}k_{1,1}}{k_{1,1}} = 0$

The process is then repeated for all the rows and columns until the first column of entries in the matrix $= 0$ and in one equation step one is summarized is summarized as

$$k_{i,j} - \frac{k_{i,1}k_{1},j}{k_{1,1}} \quad i = 2,3,\ldots.to\ the\ number\ of\ rows$$
$$j = 1,2,3,\ldots\ldots to\ the\ number\ of\ columns \tag{3.34}$$

2. Starting from the third row apply the following equation

$$k_{i,j} - \frac{k_{i,2}k_{2},j}{k_{2,2}} \quad i = 3,4,\ldots.to\ the\ number\ of\ rows$$
$$j = 2,3,4\ldots\ldots to\ the\ number\ of\ columns \tag{3.35}$$

This result will be that the second column of entries zeros starting from the third row will be zeros.

3. The process is repeated for the fourth row until a triangle of zeros is made below the diagonal of the matrix similar to equation 3.36

$$\begin{bmatrix} k_{11} & k_{12} & k_{13} & k_{14} \\ 0 & k'_{22} & k'_{23} & k'_{24} \\ 0 & 0 & k'_{33} & k'_{34} \\ 0 & 0 & 0 & k'_{44} \end{bmatrix} \begin{Bmatrix} u_1 \\ u_2 \\ u_3 \\ u_4 \end{Bmatrix} = \begin{Bmatrix} f_1 \\ f_2 \\ f_3 \\ f_4 \end{Bmatrix} \tag{3.36}$$

$k'_{i,j}$ is the new entry calculated as per steps $1\ to\ 3$.

4. A simultaneous solution can now be obtained as

$$u_4 = \frac{f_4}{k'_{44}}$$

$$u_3 = \frac{f_3 - k'_{34}u_4}{k'_{33}}$$

$$u_2 = \frac{f_2 - k'_{23}u_3 - k'_{24}u_4}{k'_{22}} \qquad (3.37)$$

$$u_1 = \frac{f_1 - k_{12}u_2 - k_{13}u_3 - k_{14}u_4}{k_{11}}$$

The process of obtaining the solution is then made directly until all unknowns are identified. This solution will yield the exact solution for the set of equilibrium equations given that the problem is defined correctly. Considering the sparsity of the stiffness matrix (i.e many entries are zeros in the matrix) programming algorithms are built with consideration to take advantage of this sparsity and solve fewer equations since the zero entries in the stiffness matrix do not affect the solution of the equations.

3.2.2. Iterative solution of the static equilibrium equation in linear analysis

The Iterative solution presented here is based on that developed by (Varga, 2009). Basically, the solution to equations of static equilibrium is calculated iteratively by trial and error as

$$U_i^{t+1} = K_{ii}^{-1}\left(F_i - \sum_{j=1}^{i-1} K_{ij}\, U_j^{t+1} - \sum_{j=i+1}^{n} k_{ij} U_j^{t} \right) \qquad (3.38)$$

Where U_i^{t+1} and F_i are the i^{th} component of U and F and t represents the trial number. The trials are continued until the following equation is satisfied

$$\frac{|U^{t+1} - U^t|}{|U^{s+1}|} < tolerance \tag{3.39}$$

Tolerance is a preset value depends on the user. The iterative solution will always converge given that K is positive and definite.

So far coverage of the finite element method was limited to the axisymmetric element in static and linear elastic analysis. The derivation of the stiffness matrix and treatment of surface forces was presented.

3.3. Dynamic analysis

The upcoming sections will cover dynamic finite element analysis and the solution to equilibrium equations in dynamic analysis.

3.3.1. Mass matrix of an axisymmetric element

Before delving into dynamics it is important to introduce the mass matrix. The mass matrix divides the element total mass on its nodes. It is of importance in dynamic problems since inertia forces are part of the dynamic equation of equilibrium as will be shown later and they play an important role in the dynamic response of any structure. The mass matrix of an axisymmetric element is obtained using the following equation

$$[m] = \iiint \rho [N]^T [N] dV \tag{3.40}$$

This mass matrix is called the consistent mass matrix and it is a full and symmetric matrix. By using the shape functions given in equations 3.19, 3.20 and 3.21, the mass matrix can be obtained for the axisymmetric element.

3.4. Integration of the dynamic equation of equilibrium in time

The following integration schemes are summarized from (Bathe, 2006; Logan, 2007) textbooks.

The equation of equilibrium in dynamics is

$$\{F(t)\} = \{K\}\{d\} + [M]\{\ddot{d}\} \tag{3.41}$$

In 3.41, the force is transient and is a function of time, $[M]$ is the global mass matrix and $\{\ddot{d}\}$ is the acceleration. The acceleration is defined as the second derivative of the displacement over time. Several methods are used to integrate equation 3.41 over time. The methods are called direct integration methods and under the direct integration method there is the explicit method which is known as the central difference method and there are the implicit methods such as Newmark-Beta (to be referred to as Newmark's method) and the Wilson-Theta method (to be referred to as Wilson's method). Each method has its advantages and disadvantages. A brief description is given in the upcoming sections.

3.4.1. the Central difference method

The finite difference equations for velocity is

$$\{\dot{d}_i\} = \frac{\{d_{i+1}\} - \{d_{i-1}\}}{2(\Delta\tau)} \tag{3.42}$$

And for acceleration

$$\{\ddot{d}\} = \frac{\{\dot{d}_{i+1}\} - \{\dot{d}_{i-1}\}}{2(\Delta t)} \tag{3.43}$$

In 3.43 and 3.42 the subscripts indicates the current time step for a time increment Δt.this means that $d\{(t)\} = \{d_i\}$ and $\{d(t + \Delta t)\}$.

With 3.42 and 3.43 an equation that relates the displacement with the acceleration can be obtained as

$$\{\ddot{d}\} = \frac{\{d_{i+1}\} - 2\{d_i\} + \{d_{i-1}\}}{(\Delta t)^2} \tag{3.44}$$

Given those previous two equations the procedure for the solution is

1- To start solving, $\{d_0\}$, $\{\dot{d}_i\}$, $\{\ddot{d}\}$, and $\{F_i(t)\}$ must be known

2- If $\{\ddot{d}\}$ is not known, it should be calculated by rearranging equation 3.41 as

$$\{\ddot{d}_0\} = [M]^{-1}(\{F_0\} - [K]\{d_0\}) \tag{3.45}$$

3- After obtaining $\{\ddot{d}_0\}$, $\{d_{-1}\}$ is calculated as

$$\{d_{-1}\} = \{d_0\} - (\Delta t)\{\dot{d}_0\} + \frac{(\Delta t)^2}{2}\{\ddot{d}_0\} \tag{3.46}$$

4- $\{d_1\}$ is now needed to be calculated as

$$\{d_1\} = [M]^{-1}\{\ (\Delta t)^2\{F_0\} + \left[2[M] - (\Delta t)^2[K]\right]\{d_0\} - [M]\{d_{-1}\}\ \} \tag{3.47}$$

5- $\{d_2\}$ can now be calculated as

$$\{d_2\} = [M]^{-1}\{ (\Delta t)^2\{F_1\} + \left[2[M] - (\Delta t)^2[K]\right]\{d_1\} - [M]\{d_0\} \} \quad (3.48)$$

6- $\{\ddot{d}_1\}$ is calculated as

$$\left\{\ddot{d}_1\right\} = [M]^{-1}(\{F_1\} - [K]\{d_1\}) \quad (3.49)$$

7- The velocity is calculated as

$$\left\{\dot{d}_1\right\} = \frac{\{d_2\} - \{d_0\}}{2(\Delta t)} \quad (3.50)$$

8- Repeating steps 5 to 7 for all other time steps while increasing the subscripts in equations 3.48, 3.49, and 4.50 by 1 to complete the integration in time.

3.4.2. Newmark's method

Newmark's equations that will be used to solve finite element problems in dynamics are

$$\left\{\dot{d}_{i+1}\right\} = \left\{\dot{d}_i\right\} + (\Delta t)[(1-\gamma)\left\{\ddot{d}_i\right\} + \gamma\left\{\ddot{d}_{i+1}\right\}] \quad (3.51)$$

And

$$\{d_{i+1}\} = \{d_i\} + (\Delta t)\left\{\dot{d}_i\right\} + (\Delta t)^2[\left(\frac{1}{2} - \beta\right)\left\{\ddot{d}_i\right\} + \beta\left\{\ddot{d}_{i+1}\right\}] \quad (3.52)$$

In Newmark's equations the parameters γ and β are selected by the analyzer. The steps to solve a dynamic problem using Newmark's method are:

1- With the load varying in time and known at every time step proceed to calculate the displacements, velocity, and acceleration for every time step.

2- Initially at $t = 0$, $\{d_0\}$ and $\{\dot{d_0}\}$ are know from the boundary conditions.

3- The initial acceleration $\{\ddot{d}_0\}$; unless it is also know; is calculated as

$$\{\ddot{d}_0\} = [M]^{-1}(\{F_0\} - [K]\{d_0\}) \tag{3.53}$$

4- Using $\{d_0\}$, $\{\dot{d}_0\}$, and $\{\ddot{d}_0\}$, $\{d_1\}$ is calculated as

$$[K']\{d_1\} = \{F_1'\} \tag{3.54}$$

Where

$$[K'] = [K] + \frac{1}{\beta(\Delta t)^2}[M] \tag{3.55}$$

And

$$\{F_1'\} = \{F_1\} + \frac{[M]}{\beta(\Delta t)^2}[\,\{d_0\} + (\Delta t)\{\dot{d}_0\} + \left(\frac{1}{2} - \beta\right)(\Delta t)^2\{\ddot{d}_0\}\,] \tag{3.56}$$

5- $\{\ddot{d}_1\}$ is calculated by rearranging equation 3.52 as

$$\{d_1\} = \frac{1}{\beta(\Delta t)^2}[\,\{d_1\} - \{d_0\} - (\Delta t)\{\dot{d}_0\} - (\Delta t)^2\left(\frac{1}{2} - \beta\right)\{\ddot{d}_0\}] \tag{3.57}$$

6- The velocity at $i = 1$, is calculated from equation 3.51

7- With the results from steps 5 and 6, the steps are repeated starting from step 4 while increasing the subscript i by a 1.

3.4.3. Wilson's method

Wilson equations that will be used are

$$\{\dot{d}_{i+1}\} = \{\dot{d}_i\} + \frac{\theta(\Delta t)}{2}\,(\{\ddot{d}_{i+1}\} + \{\ddot{d}_i\}) \tag{3.58}$$

And

$$\{d_{i+1}\} = \{d_i\} + \theta(\Delta t)\{\dot{d}_i\} + \frac{\theta^2(\Delta t)^2}{6}\left(\{\ddot{d}_{i+1}\} + 2\{\ddot{d}_i\}\right) \tag{3.59}$$

The steps for integration in time using Wilson's method are

1- From initial boundary and velocity conditions at time $t = 0$, the displacement $\{d_0\}$ and the velocity $\{\dot{d}\}$ are known.

2- If the initial acceleration $\{\ddot{d}_0\}$ is not known, it is calculated as

$$\{\ddot{d}_0\} = [M]^{-1}(\{F_0\} - [K]\{d_0\}) \tag{3.60}$$

3- $\{d_1\}$ is calculated a s

$$[K']\{d_1\} = \{F_1'\} \tag{3.61}$$

Where

$$[K'] = [K] + \frac{6}{(\theta\Delta t)^2}[M] \tag{3.62}$$

And

$$\{F_1'\} = \{F_1'\} + \frac{[M]}{(\theta\Delta t)^2}[6\{d_0\} + 6\theta(\Delta t)\{\dot{d}_1\} + 2(\theta\Delta t)^2\{\ddot{d}_0\}] \tag{3.63}$$

4- $\{\ddot{d}_1\}$ is calculated as

$$\{\ddot{d}_1\} = \frac{6}{\theta^2(\Delta t)^2}(\{d_1\} - \{d_0\}) - \frac{6}{\theta(\Delta t)}\{\dot{d}_0\} - 2\{\ddot{d}_0\} \tag{3.64}$$

5- $\{\dot{d}_1\}$ is calculated as

$$\{\dot{d}_1\} = \frac{3}{\theta(\Delta t)}(\{d_1\} - \{d_0\}) - 2\{\dot{d}_0\} - \frac{\theta(\Delta t)}{2}\{\ddot{d}_0\} \quad (3.65)$$

6- Steps 3 to 5 are repeated with the subscript increased by one each time a repetition is made.

3.4.4. Notes on the dynamic finite element solvers

Solving the dynamic finite element is more involved than solving static problems. The time step size is essential to the accuracy of the results and in case of using Newmark's method, the variables β and γ will affect the solution accuracy and stability. Usually, β is selected from between 0 and $\frac{1}{4}$; while γ is selected as $\frac{1}{2}$. If β is set as 0 and γ is set as $\frac{1}{2}$, Newmark's equations 3.51 and 3.52 become similar to the central difference equations. Similarly, If Wilson's method is used; the choice of the variable θ will also have an impact on the accuracy of the solution. (Bathe, 2006) gives a great discussion about the stability and the accuracy of the Integration schemes discussed in the previous sections.

In order to obtain accurate results, the integration of equation 3.41 must be accurae. The time step size chosen must be small but not miniscule that computer and time resources are wasted. If the time step is large, the response of a structure can be amplified and inaccurate and the solution is called unstable. (Bathe, 2006) specifies two types of stability of an integration scheme. The first is called conditionally stable solution which means that there is no amplification in the initial conditions of the solution regardless of the time step chosen. (Bathe, 2006) states that Newmark's

method is unconditionally stable when $\gamma = \frac{1}{2}$ and $\beta = \frac{1}{4}$. The discussion provided by (Bathe, 2006) formed the basis for using Newmark's method as a dynamic integration scheme of this study.

4. Modeling and Finite Element Implementation

In this chapter the process of modeling the geometry of the problem, the boundary conditions, the choice of time step size, the element size and a comparison of obtained results with existing solutions will be presented. Wave propagation using the finite element method requires adequate input of solution parameters such as mesh size, time step and boundary conditions. To make sure that selection of solution parameters is made properly, recommendations from the literature were taken into consideration and their implementation were tested using against the solution of Lysmer.

The general problem of a vibrating load over an elastic half-space is presented in figure.4.1-a. This study covers a dual layer system and different embedment depths to see how variations in Layering and depth of embedment affect the response a footing under a dynamic vertical load. Different optimizations in the modeling process were made throughout the study, but in general the parameters that control the finite element results are mostly the same. These parameters are the mesh size, time step and the boundary conditions.

4.1. Mesh size

In order to allow of proper traveling for the waves across a continuum, a mesh size limitation should be implemented. The maximum mesh size is controlled by the shear wave length, v_s and is given by (Zhang & Tang, 2007) as

$$maximum\ l_{element} = \frac{1}{8} \sim \frac{1}{5} v_s \tag{4.1}$$

Throughout this study the mesh size was selected as the upper limit to be $\frac{1}{5}v_s$. The mesh size also was refined near the stress concentration area. This area is beneath the foundation. This latter refinement is required to obtain results that would match that of Lysmer's solution. this is mostly required at low frequencies where the selected meshing criterion yields a large element size ($l_{element} > 0.5\,m$). The results of the analysis deviate greatly from Lysmer's method and erroneous amplifications are obtained, if this refinement is not implemented. Testing at a frequency of 20 Hz is used to see when the results stabilize.

Figure4.2 shows the results. In figure.4.2, the error is calculated as the difference between 2 readings at different refinement radiuses. This means that when it gets closer to zero no further refinement is needed. A radius of refinement of 5 m is selected based on this test and an element size of $0.1\,m$ is used to mesh the $5\,m$ area. Testing against Lysmer's solution (shown later in this chapter) shows great agreement at the current element size and the furtherly applied refinement. Figure.4.3 shows the mesh and the area refined.

4.2. Time step

In wave propagation using the finite element method, the time step must be small enough so that the wave doesn't travel more than the element length at each step. Otherwise, the results will not be reliable. The time step then depends on the wave with the highest velocity which is the p-wave. The maximum time step size used should be according to (Bathe, 2006)

$$maximum\ time\ step = l_e/v_p \qquad (4.2)$$

where l_e is the element length and v_p is the compression wave velocity and it is calculated as

$$v_p = \frac{\lambda + 2G}{\rho} \tag{4.3}$$

Where λ is Lame's parameter, G is the shear modulus and ρ is the mass density of the continuum.

4.3. Boundary conditions

The problem of a machine vibrating over an elastic half space assumes an infinite medium. This is not possible using the finite element method but it is possible to simulate the infinite medium using a) a vast finite domain with fixed boundaries at the edges or b) viscous boundary conditions at the edges. In the case of large finite field with fixed boundaries, the geometry has to be large enough that no reflection of waves at the edges will corrupt the results at the point of interest. Even if viscous boundaries at the edges are used they have to be far enough, that they don't influence the solution. In this study a large finite domain is used with fixed boundaries so that the amplitude of the waves near the edges is very small that it is practically zero and will not influence the solution at the footing where the results need to be obtained.

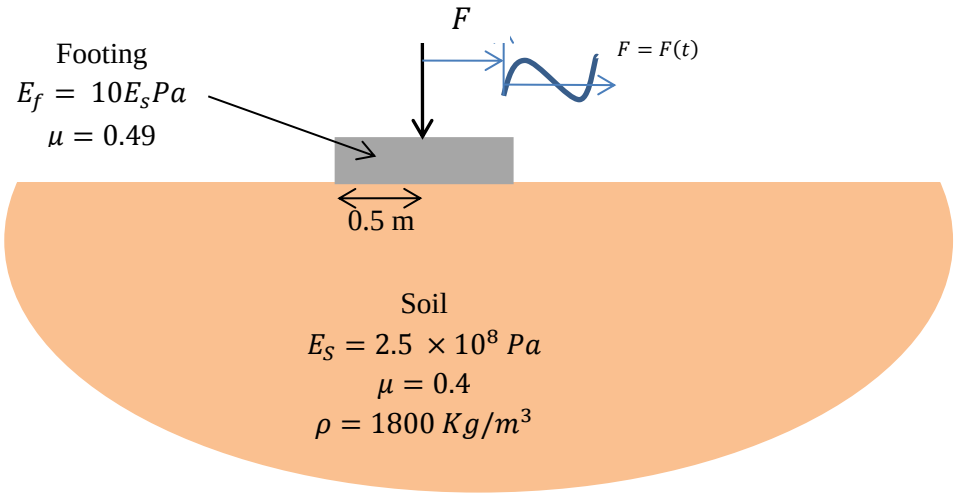

(a)

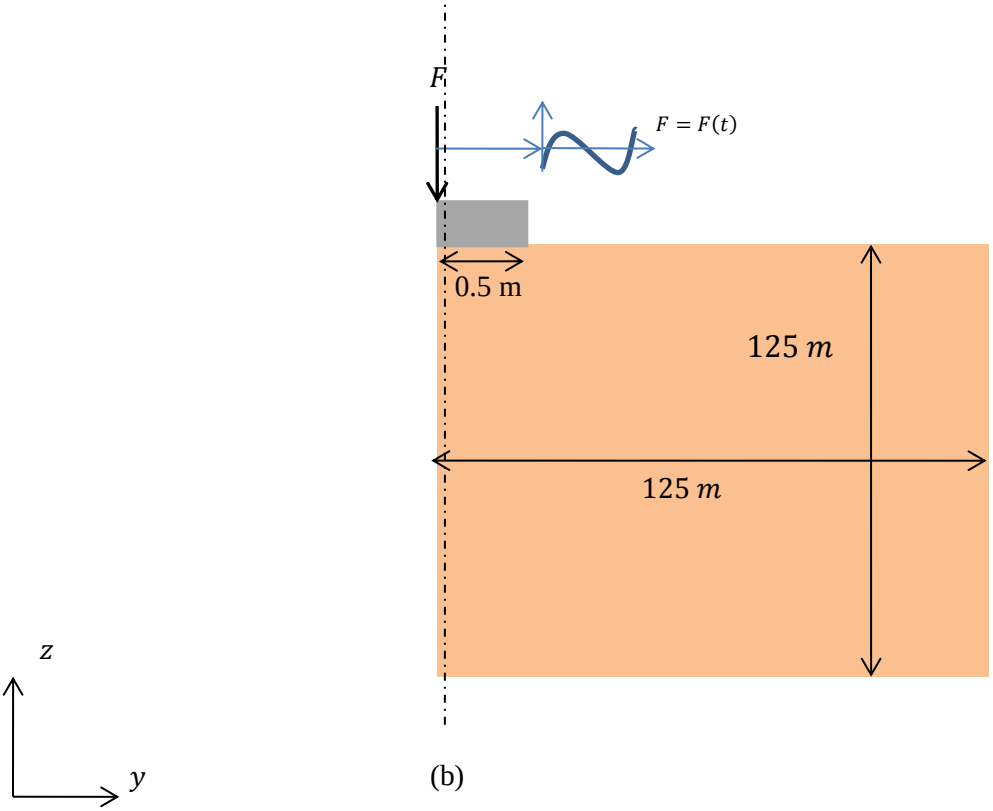

(b)

Figure 4.1: Finite element model geometry

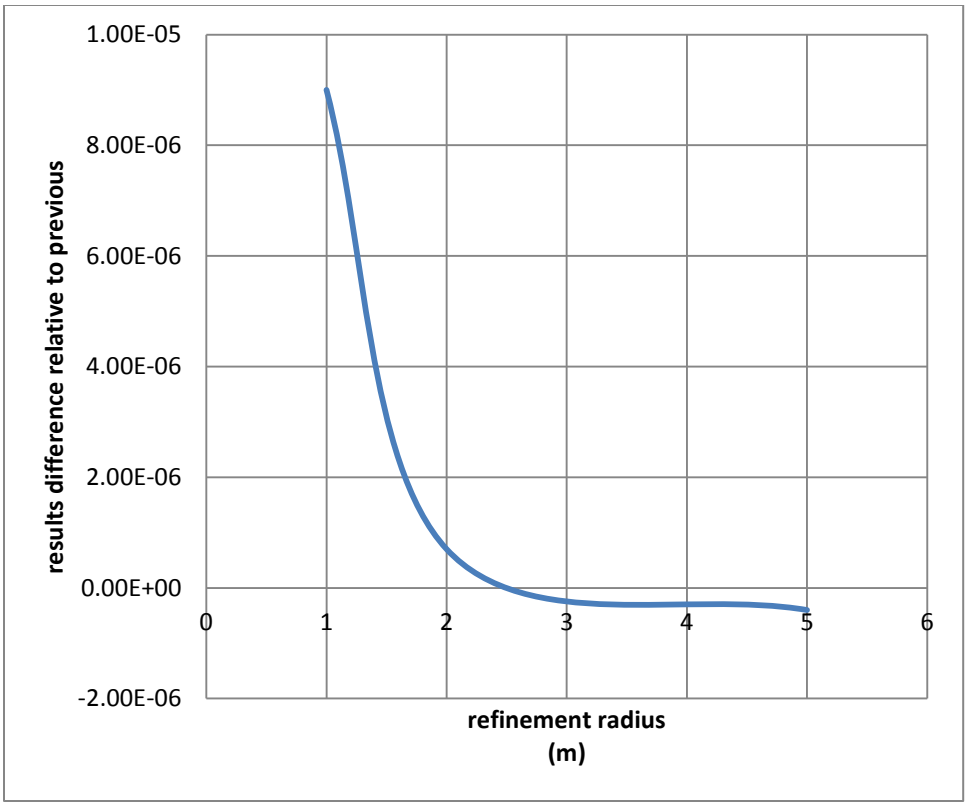

Figure 4. 2:Plot of refinement against results' difference at 20 Hz

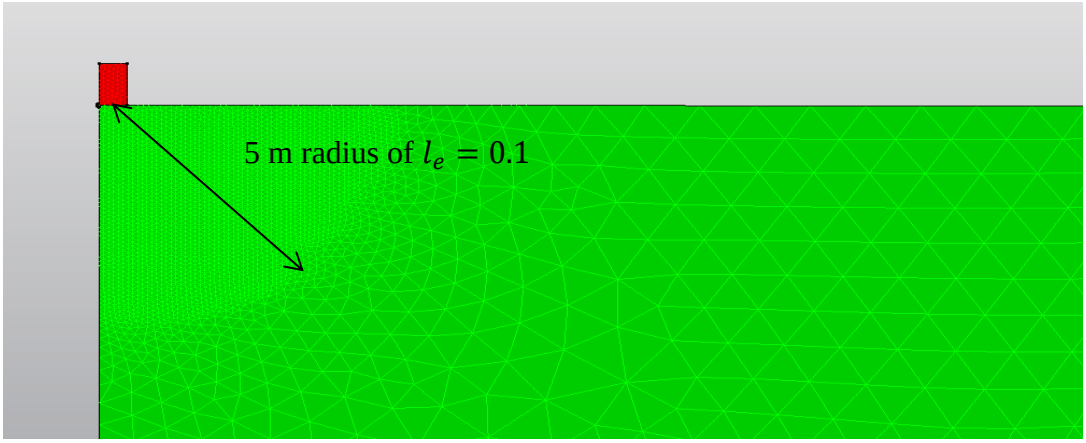

Figure 4.3:Finite element model mesh

4.4. Verifying model parameters used in FEM analysis

The modeling parameters recommendations given in sections 4.1 to 4.3 apply to any problem of wave propagation solved by the finite element method. To verify the adequacy of the modeling parameters, a comparison between Lysmer's Solution (section 2.4.8) ; the solution of the problem of a vibrating load on a circular rigid foundation on the surface of an elastic half space; with the finite element solution of the problem.

The model is similar to that presented in figure.4.1-a, while the finite element approximation is shown on in figure.4.1-b. Due to symmetry of the problem around the vertical z-axis, axisymmetric elements were used. This is reduces the number of elements significantly compared to using a fully 3D model. The result of such reduction is reflected on saving computing resources and reducing analysis time. Two studies were conducted; one that had a massless footing and the other had a footing with a mass. Analysis without mass was done to check reflection. Any reflection of waves from the fixed boundaries will be obvious. The response of the soil to vibrating massless footing doesn't amplify the static displacement (i.e. the amplitude o the dynamic displacement at any frequency is always less than the static displacement). If reflection takes place, it will result into amplified dynamic displacement (i.e. the amplitude of the dynamic displacement will be greater than the static displacement). The analysis was performed with mass mostly as Results will detect reflection (i.e. the response will be amplified than what they should be). It will also detect that if the footing was modeled correctly. If mesh size is too big in the footing the elements will

resonate at different frequencies result in irregular response with several peaks rather than one. (i.e. the system will not act as a single degree of freedom).

In the first study, the footing had no mass, while it had a modulus of elasticity that is $10E_s$, where E_s is the soil modulus of elasticity. This was done to ensure rigidity of the footing and that no internal stresses within the footing body would affect the result. To further ensure rigidity and prevent the footing from moving in the horizontal direction, all nodes within the footing were supported in the horizontal direction. The footing had a diameter of $1\,meter$. The soil was selected as homogenous linear elastic material. The soil had a modulus of elasticity of $2.5 \times 10^8\ Pascals$, a Poisson's ratio of 0.4 and a mass density of $1800\ kg/m^3$. This yielded a shear modulus of $8.93 \times 10^7\ Pascals$. The load applied on top of the footing is a uniformly distributed pressure that has a sinusoidal function of $22000\ Sin(\omega t)$, where ω is the frequency in $radians/seconds$ and t is the time in $seconds$. The load would have a maximum amplitude of $22000\ N/m\text{^}2$.

Using Lysmer's solution presented in (2.4.8) to solve the problem, the applied maximum amplitude is $F = P\ (Area) = 22000(\pi r_0^2) = 17280\ KN$, the spring constant k according to equation (2.67) is $2.98 \times 10^8\ N/m$, from table 2.1, the mass ratio $B_v = 1.256$ and the vertical geometrical damping ratio $D_v = 0.38$. Using the finite element method a uniform pressure was applied to the circular rigid footing with a sinusoidal curve. The static displacement was found to be 5.2×10^{-5} and 6.3×10^{-5} for the finite element solution and that of Lysmer respectively. A plot of the dimensionless frequency a_0 and the resulting amplification for both Lysmer and the finite element solution is given in figure 4.4. A fitted polynomial curve for the

finite element solution is also drawn the statistical R^2 value for the fitted curve was found to be 0.954. From figure.4.4, a comparison between the finite element solution and Lysmer solution is provided and showas that the finite element implementation with the selected analysis parameters (i.e. time step, element type, element size, and axisymmetric analysis) agrees with Lysmer's solution for a massless footing.

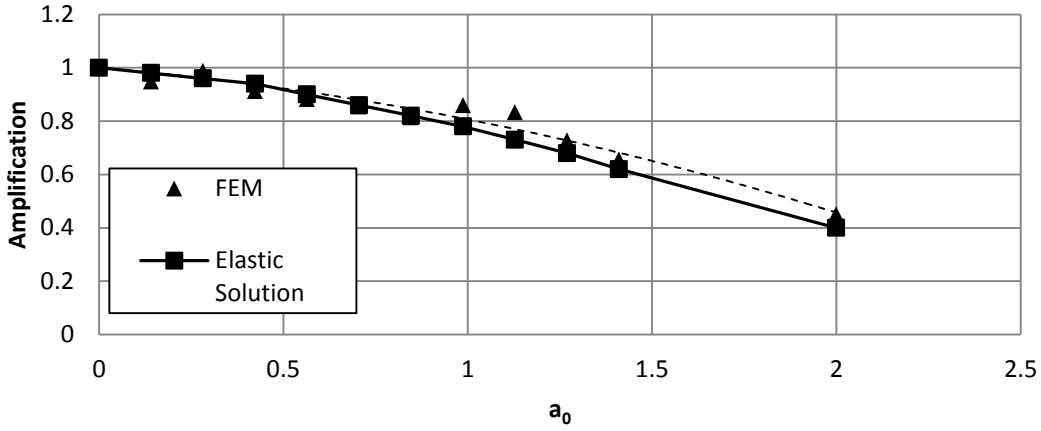

Figure 4.4: Comparison between the finite element solution and Lysmer's Solution for a mass-less footing

The second study was performed with a rigid foundation that had a mass of 6430 kg. The soil also had different Poisson's ratio of 0.3. Other properties are identical to that of the first study. Lysmer's solution parameters B_v and D_v are 5 and 0.19 respectively. A plot of both finite element solution and Lysmer's solution is shown in figure 4.5. Comparable results are obtained using the finite element method.

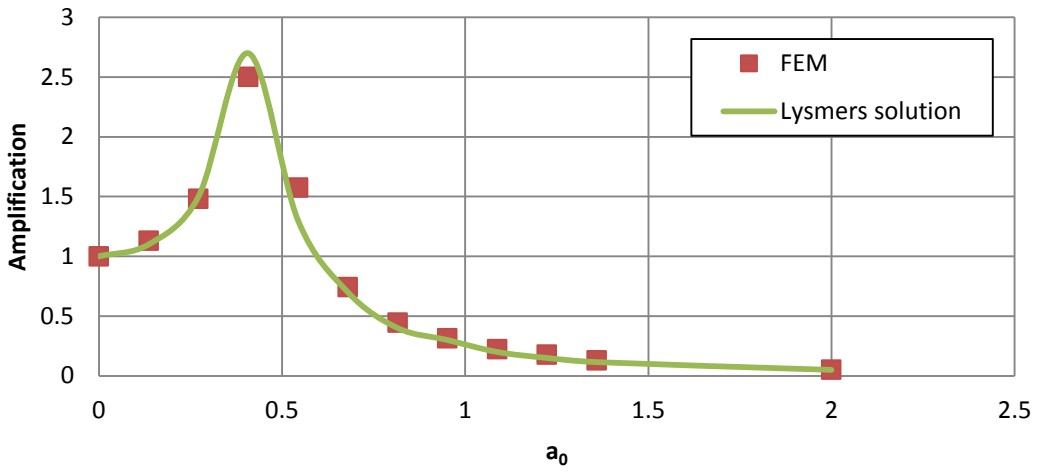

Figure 4.5: Comparison between the finite element solution and Lysmer's solution for a footing with mass

In summary element size, time step and boundary conditions are essential in dynamic simulation of soil dynamics problem. Proper selection of those model properties is critical to obtain correct results. The choice of these properties was based on various recommendations and testing against Lysmer showed high agreement between finite element simulation and the analytical solution of Lysmer. After selecting the model parameters, the effects of a two layer system and different embedment depths are studied. The simulations will have the same finite element parameters as discussed.

4.5. Study plan for the effect of a 2-Layer system

For the effect of layering, a top layer of a particular depth was placed beneath the foundation and over the elastic half space. The layer depth was varied and at each layer depth the strength parameters of both the top and the bottom layer was changed. The load is applied dynamically at different frequencies. Comparing the dynamic displacement against the static one allows for obtaining the single degree of freedom model parameters (spring constant k and damping ratio ζ) using statistical curve

fitting capabilities of Mathematica®. A Flow chart of this plan is shown in figure 4.7 with detailed geometry and problem definition given in figure 4.6 and Table 4.1 is given for symbols definition. Actual values used for the study variables given in table 4.2 for the constants and table 4.3 for the controlled variables. firgure 4.6 shows that the boundaries used were fixed at $125\ m$ beyond the depth of the first layer D_1. Mesh size was according to the discussion in section 4.1 with a further refiniemeent of element size of $0.1\ m$ applied from the center of the footing to a radius of $(D_1 + 5)\ m$ so that the refinement peentrates $5\ m$ into the second layer.

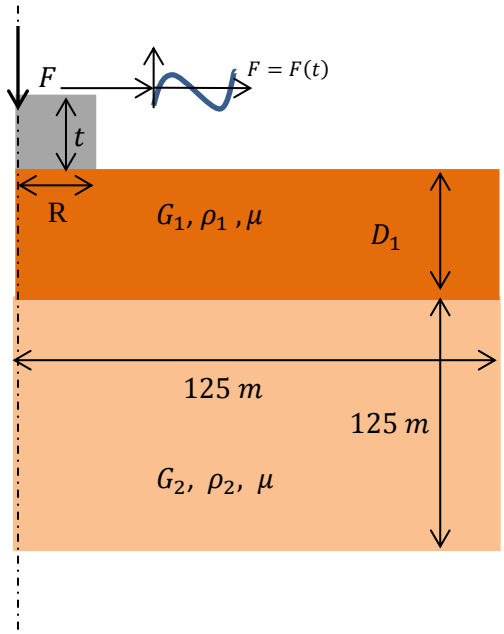

Figure 4.6:Geometry used in modeling effect of 2 layers

Table 4.1: Symbols Definition for study of 2-Layer effect

Symbol Used	Definition
t	Footing thickness
F	Force applied on footing
D_1	Depth of top layer
R	Footing radius
G_1	Shear modulus of top layer
G_2	Shear modulus of second layer (i.e. Elastic half space)
f	Frequency of force applied (values were taken between 10 to 90 Hz)
u_d	Dynamic displacement

u_s	Static displacement
k	Spring constant
ζ	Damping
G_{eq}	Equivalent shear modulus to represent G_1 and G_2 (i.e. $G_{eq} = F(G_1, G_2, D_1)$). Where F means a function
μ	Poisson's ratio of both layers
ρ_f	Footing density
ρ_s	Soil density for both top and elastic half space layers
v_{s1}	Shear wave velocity of top layer
v_{s2}	Shear wave velocity of bottom layer

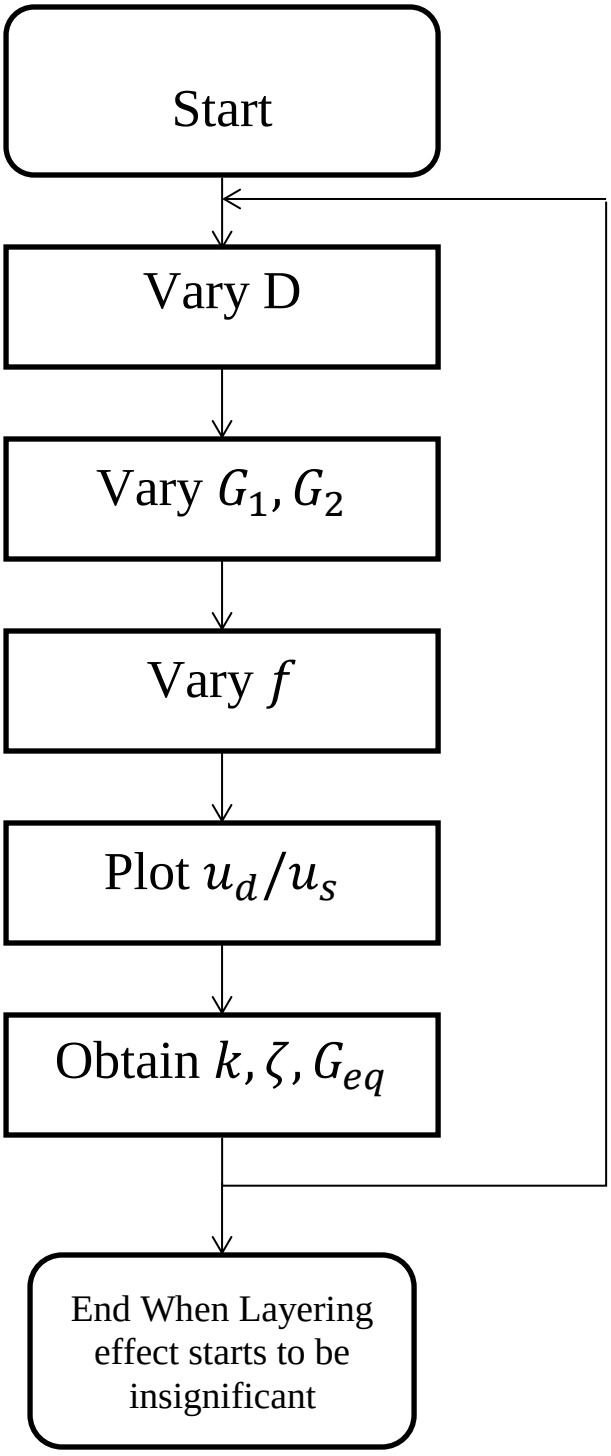

Figure 4.7:Flow chart for the study of layering effect on dynamic response

Table4.2: Constants used in study of 2-layers effect

Constants				
$\boldsymbol{R}$ (m)	$\boldsymbol{\rho_f}$ (Kg/m^3)	$\boldsymbol{\rho_s}$ (Kg/m^3)	$\boldsymbol{F}$ (KN)	$\boldsymbol{t}$ (m)
0.5	2400	1800	17280	1

Table 4.3: Controlled variables for the study of 2layrs effect

D_1 (m)	V_{s1} (m/s)	V_{s2} (m/s)
0.5	145	244
		359
		154
		293
	154	146
	199	
	244	146
1	145	244

1	145	359
		154
		293
	154	146
	199	
	244	
1.5	145	244
		359
		154
		293
	154	146
	199	
	244	
2	145	244
		359
		154
		293
	154	146
	199	
	244	

4.6. Study plan for the effect of footing embedment

The effect of embedment is investigated by varying the embedment depth and at each embedment the shear modulus of the elastic half-space is varied. A plot of the dynamic amplification and the frequency will allow obtaining$k\ and\ \zeta$ at different embedment depths. Symbols definition is given in table 4.4. The values for the constants and variables of the simulation are provided in table 4.5 and 4.6 respectively. The geometry and problem definition is given in figure 4.8 and. A flow chart of the study is provided in figure 4.9.

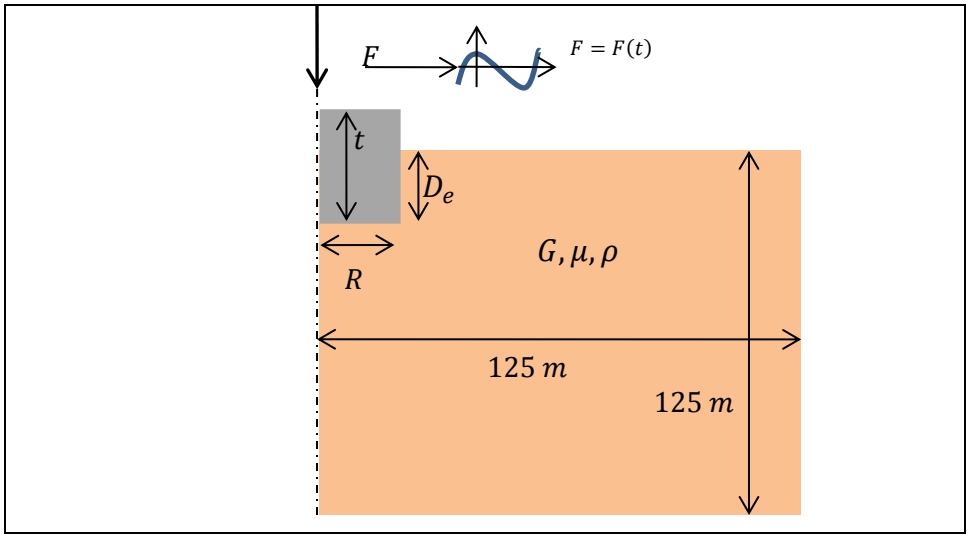

Figure 4.8:Geometry used in simulating the effect of footing embedment

Table 4.4: Symbols Definition for study of embedment effect

t	Footing thickness
F	Force applied on footing
D_e	Depth of embedment
R	Footing radius
G_s	Shear modulus of soil
f	Frequency of force applied
u_d	Dynamic displacement
u_s	Static displacement
k	Spring constant
ζ	Damping
ρ_f	Footing density
ρ_s	Soil density
v_s	Shear wave velocity of soil

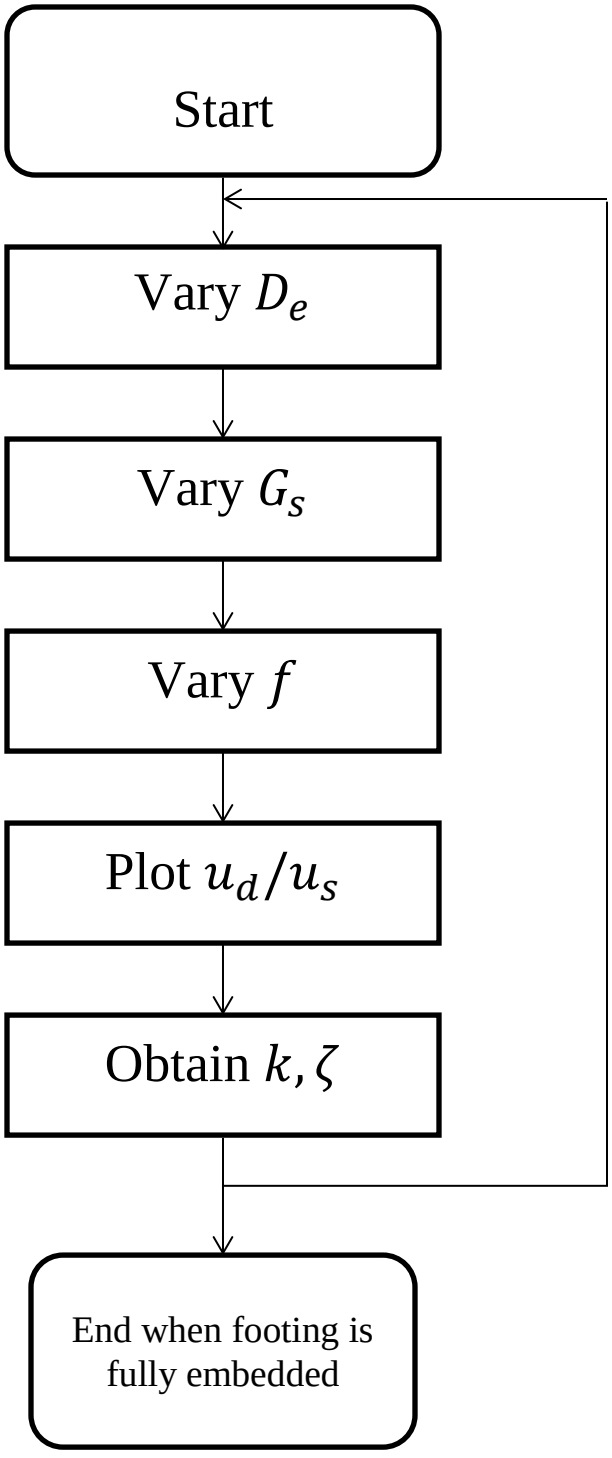

Figure 4.9: Flow chart for simulating the effect of footing embedment

Table 4.5: Constants used in study of footing embedment effect

Constants				
$\boldsymbol{R}$ (m)	$\boldsymbol{\rho_f}$ (Kg/m^3)	$\boldsymbol{\rho_s}$ (Kg/m^3)	$\boldsymbol{F}$ (KN)	$\boldsymbol{t}$ (m)
0.5	2400	1800	17280	1

Table 4.6: Controlled variables used in study of embedment effect

D_e (m)	V_s (m/s)
0.2	244
	199
	142
0.4	244
	199
	142
0.6	244

0.6	199
	142
0.8	244
	199
	142
1	244
	199
	142

5. Results and Discussion

After modeling with the finite element, readings of u_d/u_s against the frequency f were obtained. The static stiffness and equivalent shear modulus were calculated from the static analysis. From the dynamic analysis, using equation 2.20 values of the geometric damping ζ were calculated. This is illustrated step by step in the following section.

5.1. Procedure of interpreting results

1- At each variation in the depth of the top layer D_1 and the shear modulus of the top and bottom layer G_1 and G_2respectively, a static analysis is performed and the static displacement u_s is obtained from a point at the center of the footing at the footing-soil interface. From this static displacement the spring constant k is calculated as

$$k = F/u_s \qquad (5.1)$$

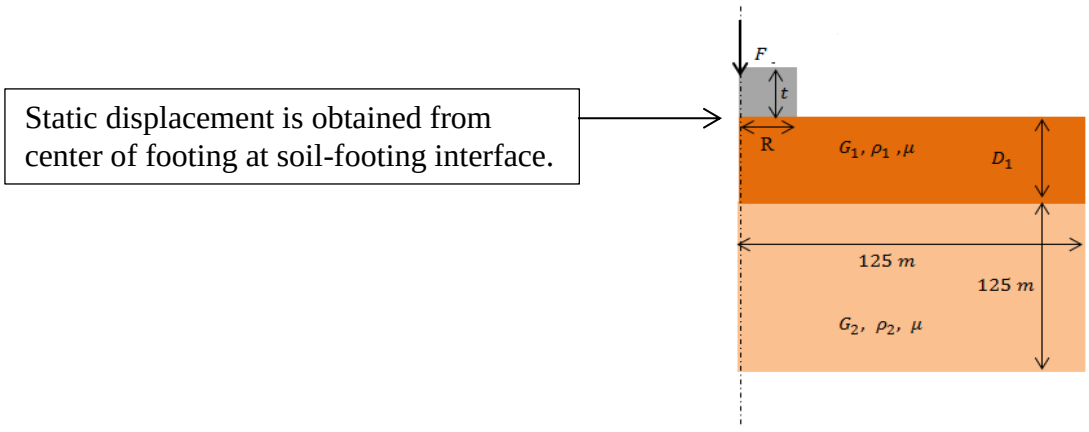

2- A dynamic analysis is performed with a sinusoidal force that has a maximum amplitude equal to that applied in the static one (i.e., $(t) = Fsin(\omega t)$) where

ω is the frequency in $radians/seconds$ and t is the time in seconds. The force also has a specific frequency.

The curve of such force at 20 Hz is as shown:

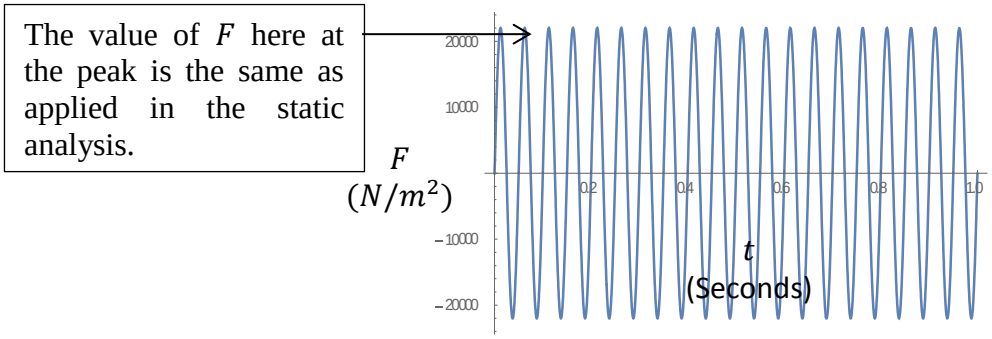

3- Another dynamic analysis is performed at a different frequency.

4- From the dynamic analyses the dynamic displacement u_d variation with time is obtained at the same location that the static displacement was determined from. The dynamic displacement has to be determined when a steady state is reached. In this study this was observed generally after the first cycle. The variation of dynamic displacement with time looks like the following curve for 20 Hz

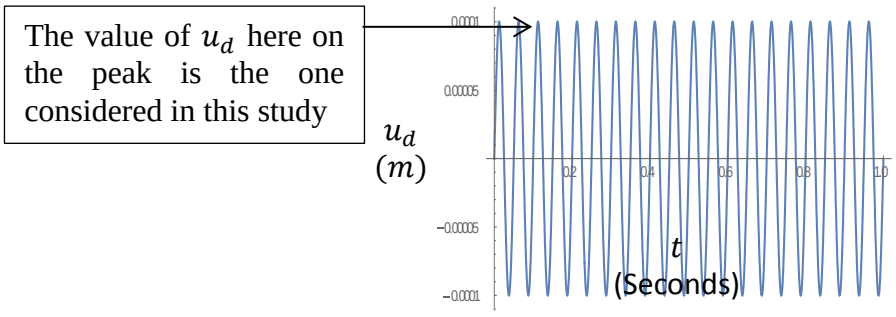

The value of the dynamic displacement at the peak is obtained and is the one used in this study. Values in the previous figure are just for presentation and are not actual analysis values.

5- A plot of the dynamic displacement over the static one u_d/u_s against different frequencies (i.e. amplification curve) is obtained and typically looks like the following curve

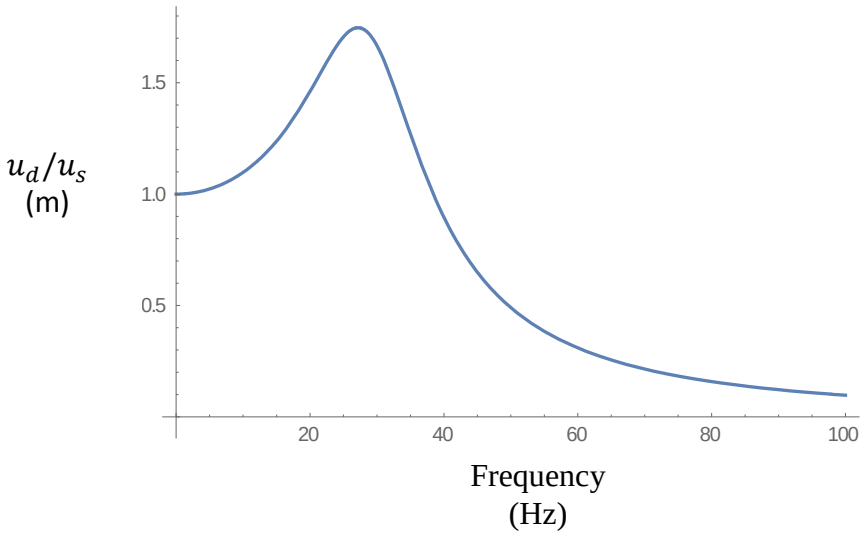

The previous curve is just for illustration and numbers are no actual numbers obtained in the study

6- From the previous plot data points are then inserted in the following equation

$$u_d/u_s = \frac{1}{\sqrt{\left(1-\frac{\omega^2}{\omega_0^2}\right)^2+\left(2\zeta\frac{\omega}{\omega_0}\right)^2}} \qquad (5.2)$$

Where u_d is the dynamic displacement, ω is the frequency of the load in radians/seconds, ω_0 is the natural frequency and ζ is the geometric damping. Values of ω are an input. Values of u_d/u_s are know from finite element analysis. ω_0 is calculated by the following equation

$$\omega_0 = 2\pi\sqrt{k/m} \tag{5.3}$$

Where k is the spring constant and m the mass of the footing. Plugging these equation into Mathematica with the command that is used to find the best value of the geometric damping ζ. The program then finds the geometric damping value that will yield the least residual on the input data.

The described procedure is used to obtain the spring constant and damping ratio at different study parameters to see what effect these parameters will have on these values of the spring constant and geometric damping. A sample calculation of the procedure described is given in appendix A1.

5.2. Results and discussion for footing on 2-Layer soils

5.2.1. Effect on static response

From the static displacement obtained from the finite element analysis the value of the spring constant for two layers, k is obtained as:

$$k = \frac{F}{u_s} \tag{5.4}$$

Where F is the static force that is applied and u_s is the static displacement obtained by the finite element analysis due to the applied load.

The spring constant can also be calculated directly by other available formula. Work done by (Hadjian & Luco, 1977) provided results which were used in (Gazetas, 1983)

to come up with a formula for the static spring constant of two soil layers. The formula for calculating k is

$$k = \frac{4G_1R}{1-\mu_1}\frac{1+\frac{1.28R}{H}}{1+\frac{1.28R}{H}\frac{G_1}{G_2}} \tag{5.5}$$

Where G_1 and G_2 is the shear modulus of the top and bottom layer respectively. H is the depth of the top layer. R is the radius of the footing. μ_1 is Poisson's ratio of the top layer.

After obtaining k for two layers, a value of an equivalent shear modulus G_{eq} was obtained by rearranging the equation for k_v from table 2.1 as

$$G_{eq} = (1-\mu)\frac{k}{4R} \tag{5.6}$$

Since μ of the top and bottom layer in this study were the same, equal to 0.4 and were not varied, equation 5.6 can be used when μ is close for both layers and around 0.4. Care should be taken when the current model is applied to cases where μ is other value than 0.4. Gazetas, 1983 argues that static stiffness of foundation under vertical loads is sensitive to Poisson's ratio. Whether variations in poison's ratio of top and bottom layer will affect predictions of dynamic response made by the current model has to be investigated. It would be unlikely from the author's point of view, since shear wave velocities of both top and bottom layers, which control the geometric damping of the system, depend on the shear modulus and the mass density and no Poisson's ratio are not in the formulas. G_{eq} is a function of the depth of the top layer, the shear modulus of the top layer and the shear modulus of the bottom layer (i.e.

$D_1, G_1, and\ G_2$ respectively). For simplification G_{eq} can be normalized by dividing it by G_1 and the ratio G_{eq}/G_1 is then considered as a correction factor applied to G_1. The relationship of G_{eq} with the normalized depth over radius (i.e., D_1/R) is plotted in Figure 5.1 for different cases of G_1/G_2. The ratio G_{eq}/G_1 seems to get close to 1 as D_1/R increases (at $D_1/R = 4$ the range of G_{eq}/G_1 = (0.82 to 1.39).

A comparison of calculated vertical spring constant k for a two layer system using the proposed model and that of (Gazetas, 1983) is presented in Figure 5.2. Figure 5.2 shows that spring constants calculated in this study are in general higher than that calculated by (Gazetas, 1983), which were based on data provided by (Hadjian & Luco, 1977). In general this study predicts higher vertical static stiffness than that predicted by Equation 5.5. This higher stiffness predicted here is most likely a result of the footing stiffness being part of the FEM solution while Equation 5.5 considers only the radius of the footing with no consideration of its strength parameters.

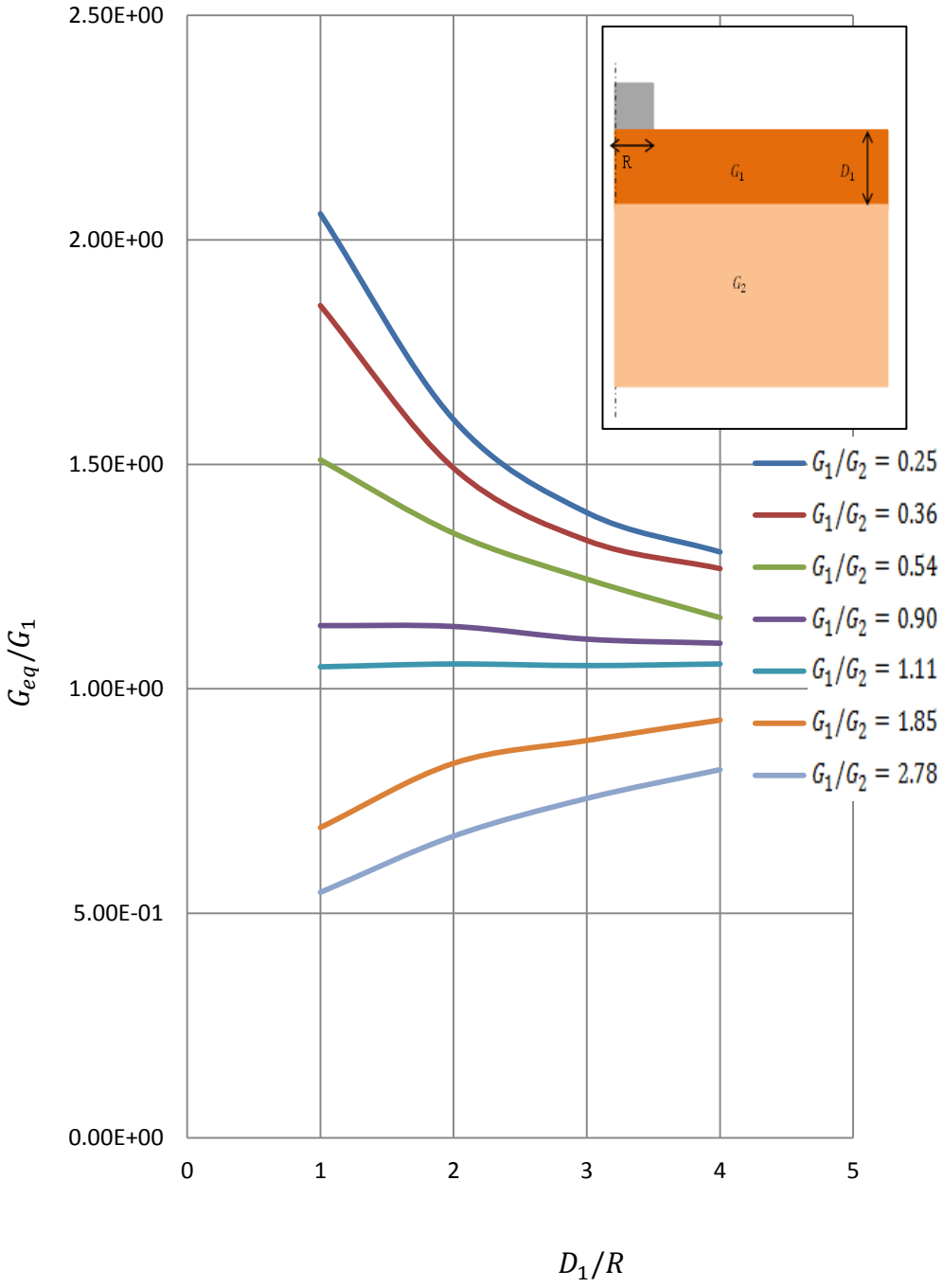

Figure 5.1: Variations of G_{eq}/G_1 with D_1/R for different values of G_1/G_2

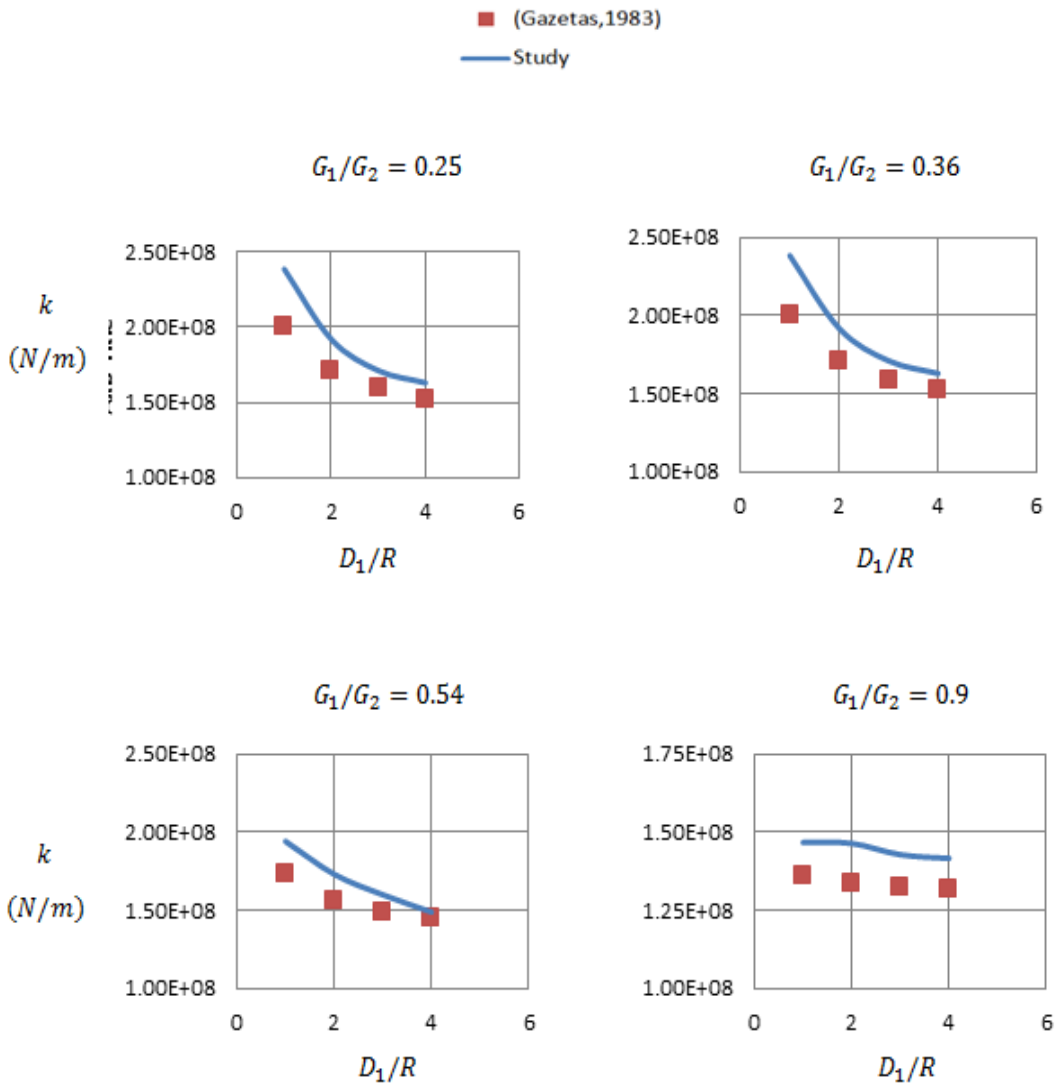
(Gazetas,1983)
Study
$G_1/G_2 = 0.25$
$G_1/G_2 = 0.36$
$G_1/G_2 = 0.54$
$G_1/G_2 = 0.9$
k
(N/m)
2.50E+08
2.00E+08
1.50E+08
1.00E+08
1.75E+08
1.25E+08
0
2
4
6
D_1/R

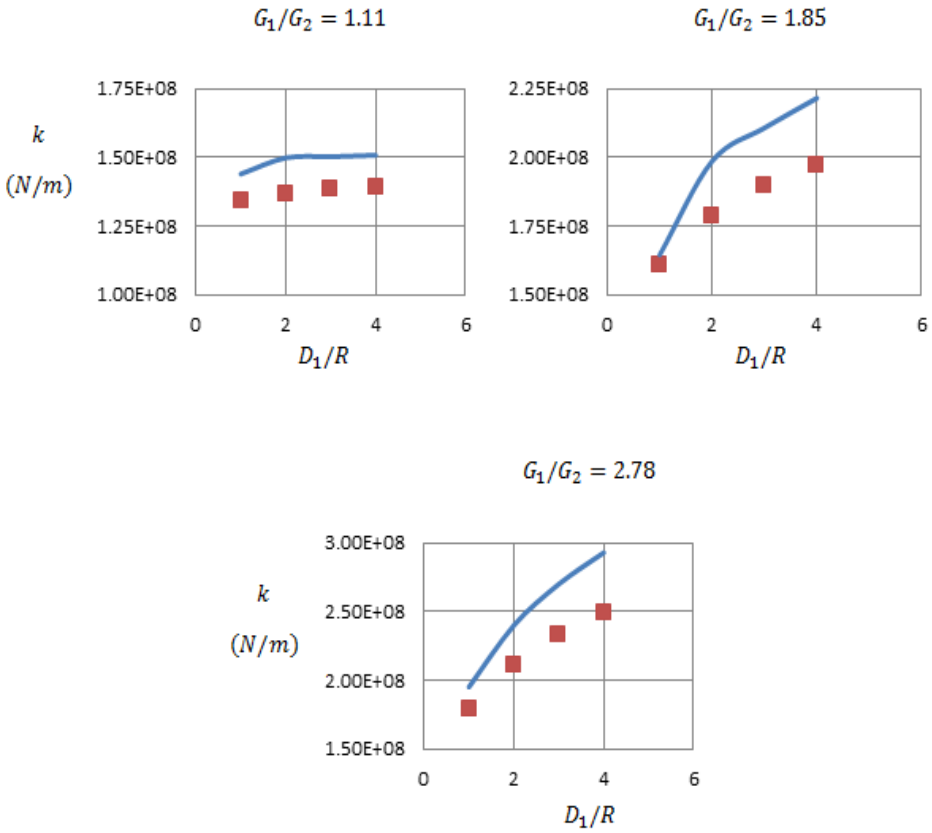

Figure 5.2: Comparison of spring constant k calculated in this study and that calculated by (Gazetas, 1983)

5.2.2. Effect on Natural Frequency

The existence of a second layer affects the static stiffness of the foundation which will result in an effect that extends to the natural frequency of the system, since the natural frequency depends on the static stiffness as given by Equation 2.5: $f_n = \sqrt{k/m}$. Where k is the static spring constant and m is the mass of the footing. An increase in static stiffness will increase the natural frequency (i.e., delay the occurrence of natural oscillation) and a decrease will do the opposite. The variation of natural dimensionless frequency,a_0 with the ratio D_1/R is given in Figure 5.3. Dimensionless frequency id calculated as $a_0 = \omega R/v_{s2}$. Where ω is the frequency in $radians/seconds$, R is the radius of the footing and v_{s2} is the shear wave velocity of the bottom layer. From Figure 5.3, it can be noted that the existence of a stronger layer beneath a weaker one (i.e., $G_1/G_2 < 1$) will result in a smaller dimensionless natural frequency and it gets smaller as the depth to the stronger layer increases. In contrary, the existence of a weaker layer beneath a stronger one (i.e., $G_1/G_2 > 1$) will result in a high dimensionless natural frequency as D_1/R is small but this natural frequency increases as the depth to the weaker layer increases. Also in cases at which $G_1/G_2 < 1$ the smaller the values of G_1/G_2 the smaller the dimensionless natural frequency at the same D_1/R. The opposite is noticed when $G_1/G_2 > 1$. The larger G_1/G_2 the larger the natural frequency is, at the same D_1/R.

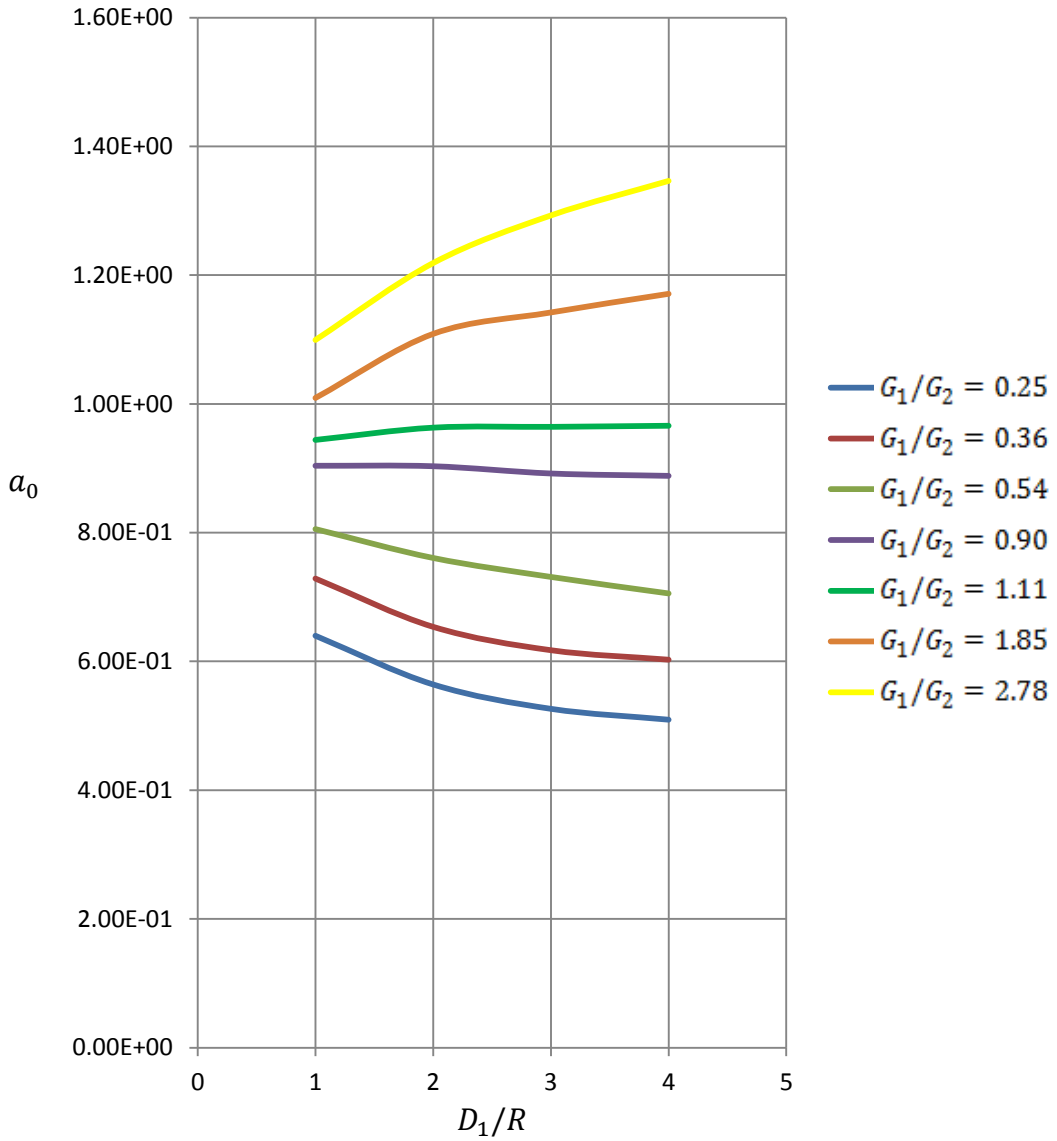

Figure 5.3: Variation of dimensionless natural frequency with D_1/R at different G_{eq}

5.1.3. Effect on Geometric Damping

The geometric damping ζ calculated using the Lysmer analog according to the equation in Table 2.1 as

$$\zeta = \frac{0.425}{\sqrt{B_z}} \tag{5.7}$$

Where B_z is mass ratio and independent of the soil properties. This means that at any value for the shear modulus of the elastic half space, the damping ratio is constant. This was found to be true when simulating the homogeneous elastic half space as was show in section 4.4. However, in simulating 2 layers, the response of the system starts to become dependent on the value of the ratio of the shear modulus of top layer to that of the bottom one G_1/G_2 and the depth to the second layer D_1. This property is very important, as the geometrical damping controls the damped natural frequency and the amplification of the vibration at any frequency. Even more, when $G_1/G_2 > 1$, and at $D_1/R > 2$ (where R is the radius) the amplification curve (i.e., the Plot of frequency against dynamic displacement) becomes different than that of a single degree of freedom system. In a typical amplification curve for a single degree of freedom system, the dynamic displacement amplitude is greater than one at the beginning then rises to a peak at the natural frequency and finally drops to lower than one. There is no fluctuation in the curve. The dynamic displacement is always greater than the static one before the natural frequency, but wmhen $D_1/R > 2$, it was found that the amplification starts at values lower than the static displacement before rising to the peak at natural frequency. This was detected when analysis was done at $D_1/R = 3$, so at values of $D_1/R \in (2, 3)$, the response is unknown. An example of such

cases where the response starts to become irregular is given at $G_1/G_2 = 1.36$ and $D_1/R = 4$ and is presented in Figure 5.4 while the typical response is given in Figure 5.5 for $D_1/R = 2$ and $G_1/G_2 = 0.9$.

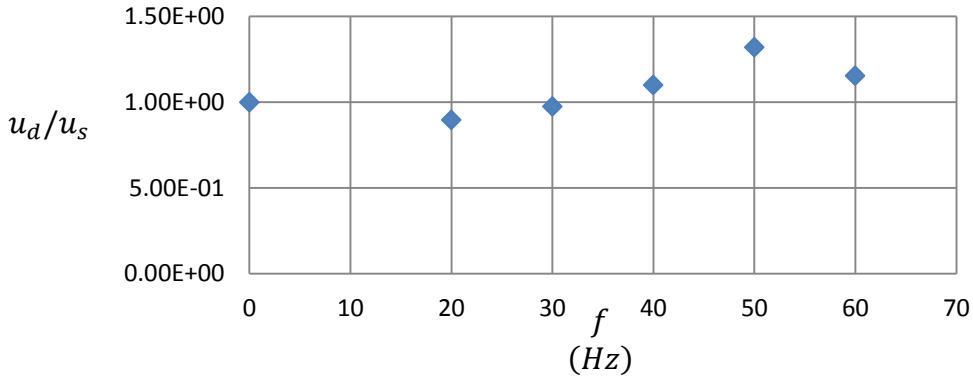

Figure 5.4: Example of irregular behavior detected at D_1/R =4 and G_1/G_2 =1.36

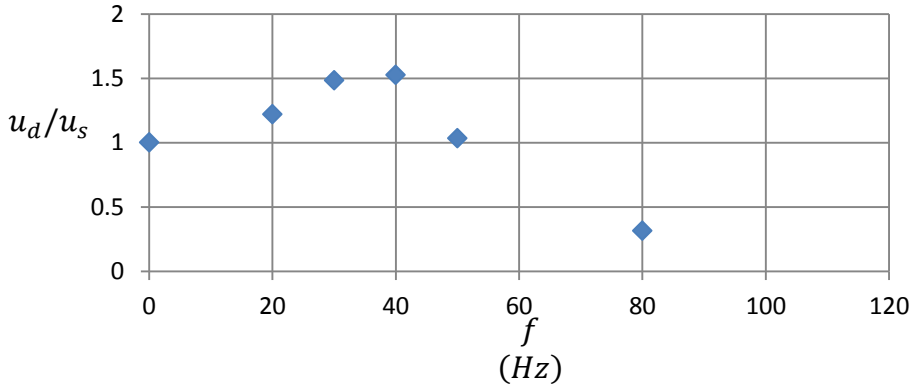

Figure 5.5: Typical response of single degree of freedom system for D_1/R =2 and G_1/G_2=0.9.

From Figure 5.4, the data collected by the finite element shows that the amplification is less than 1 at the lower frequencies and then the amplification starts to get higher as the frequency gets closer to the natural damped frequency until finally, the amplification gets lower again when the frequency is greater than the natural damped frequency. Figure 5.5 shows the typical single degree of freedom response where amplification is always greater than one before the natural frequency

As mentioned earlier, the geometric damping in the case of 2 layers starts to become dependent on the ratios of the shear modulus of top layer on bottom G_1/G_2, then the ratio of shear wave velocities, v_{s1}/v_{s2} will also affect the damping and the depth to the bottom layer relative to the radius D_1/R. Depending on the values of these ratios, the value of the damping could increase or decrease compared to what is calculated by the Lysmer analog, which is independent of the shear modulus and properties of the half space. Figure 5.6 shows how variations in shear wave velocity ratio of the top and bottom layer along with variations of depth of the top layer affects the geometric damping calculated by Lysmer's analog of the system. In Figure 5.6 damping is shown normalized over that calculated by Lysmer's analog according to Equation 5.7.

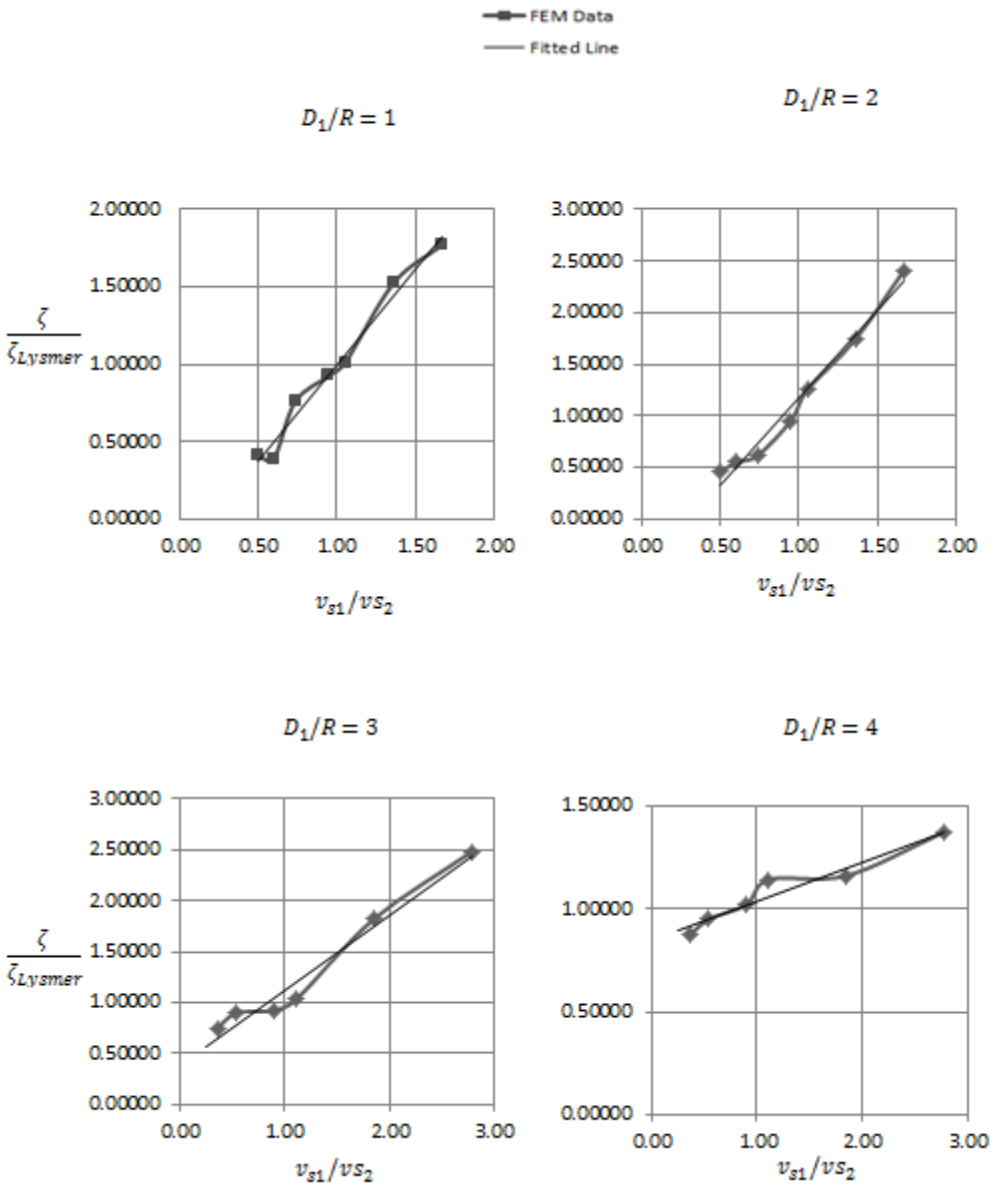

Figure 5.6: Geometric Damping variation with v_{s1}/v_{s2} at different D_1/R.

In Figure 5.6 the damping calculated by the Lysmer analog is reduced when $v_{s1}/v_{s2} < 1$. This means higher amplification of dynamic loads and a natural frequency that is close to the undamped natural frequency. On the contrary, if $v_{s1}/v_{s2} > 1$, the damping ratio will be almost doubled or even more than doubled depending on the ratio of D_1/R. As mentioned earlier the damping obtained using fitted data represent the response fairly well with some deficiencies in representing the actual obtained data. The effect of a second layer on the damping ratio starts to be reduced as the depth increases. This is seen as the slope of the straight line becomes less steep as the depth increases.

5.3. Results and discussion for embedded footing

5.3.1. Effect on static response

Embedment of a foundation within a soil medium will increase its stiffness as a result of friction between the soil and the foundation side wall. In this study the footing was circular and was analyzed when partially embedded to full embedment. The effect of embedment on the static stiffness is plotted in figure 5.7. The stiffness value is normalized over the stiffness when the footing is not embedded.

The increase in the vertical stiffness due to embedment has no significant variation within the same value of D_e/t as shown in Figure 5.7. D_e is the depth of embedment and t is the thickness of the footing. In addition, from Figure 5.7, as expected when the depth of embedment increases, the vertical stiffness will increase significantly. This increase is due to the increase of the contact area between the footing and the soil.

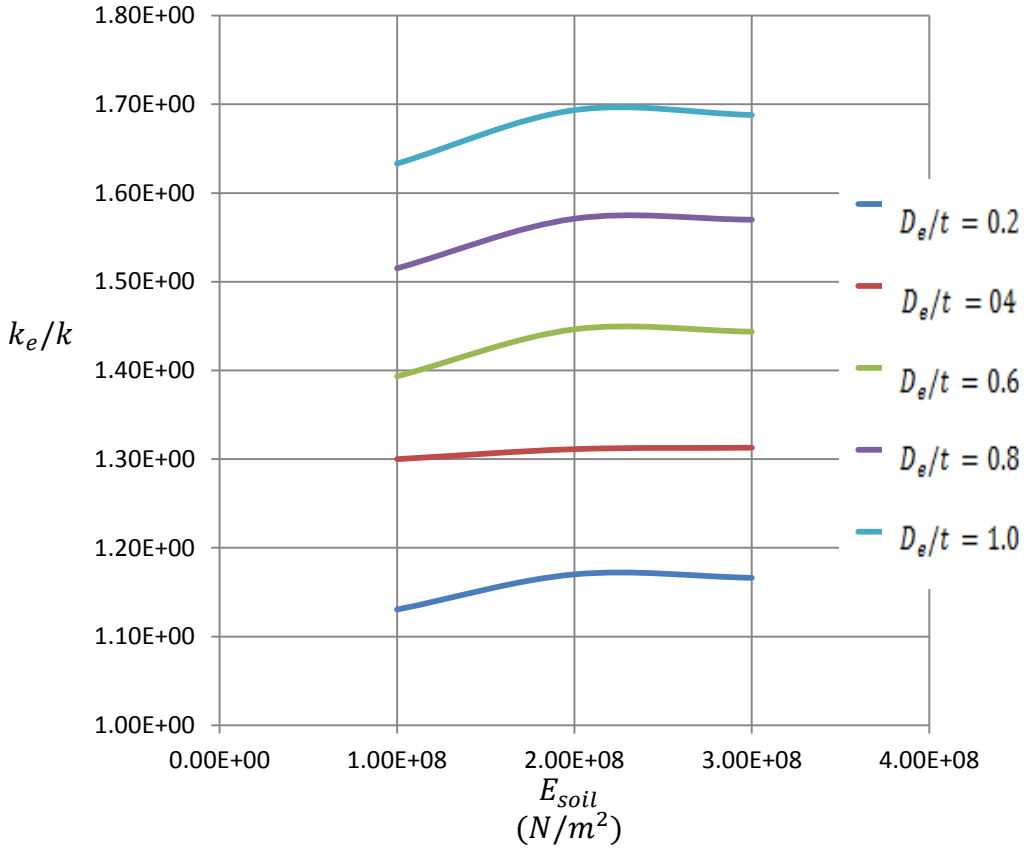

Figure 5.7: Variation of k_e/k with soil modulus of elasticity at different D_e/t

5.3.2. Effect on natural frequency

The increase in vertical static stiffness will increase the natural frequency of the system. This will result in a delayed damped natural frequency. The natural frequency of the system can be calculated using equation 2.5 as

$$f_n = \sqrt{\frac{k}{m}} \tag{5.8}$$

Where f_n is the natural frequency, k is the spring constant and m is the mass of the footing. By using the corrected vertical stiffness (see Figure 5.7) in the equation as

the spring constant, the natural frequency can be obtained and it will be higher than that obtained for surface footing.

5.3.3. Effect on Geometrical Damping

An increase in geometrical damping is expected. This increase is due to the increase of the surface of the footing. In a non-embedded foundation the wave can only travel downward from the base of the footing, while embedded the sides of the footing provides additional directions, which the wave can travel through. So it would be logical that the more the foundation is embedded in the ground the more the damping ratio will increase. The increase in damping ratio normalized over the non-embedded foundation's damping ratio (i.e., calculated in Lysmer's solution) is plotted against D_e/t in Figure 5.8. It is important to note that the increase in damping is strictly dependent on the depth of embedment and is independent of the shear wave velocity of the soil.

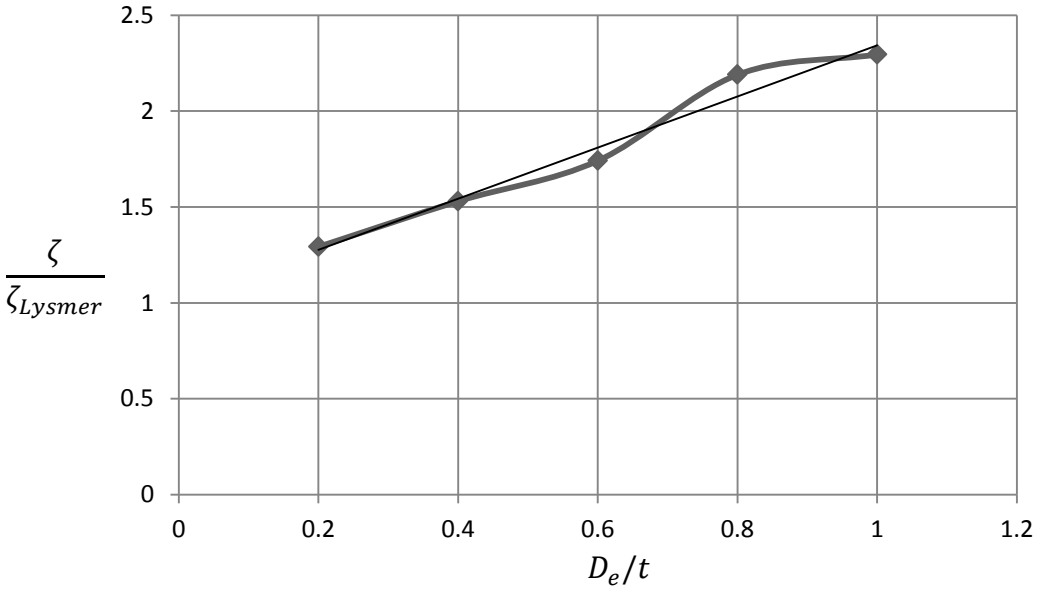

Figure 5.8: Normalized damping values corrected for embedment

An immediate increase of the damping ratio is seen with an embedment level of 20%. This trend continues approximately linear as seen from Figure 5.8.

5.3.4. Comparison of results of embedded footing with work of (Novak & Beredugo, 1972)

Novak and Beredugo provided a solution for the problem of embedded footing. Their solution gives the following equations for the static stiffness and damping ratio

$$k = GR[C_1 + \frac{G_s}{G}\frac{D_e}{R}S_1] \tag{5.9}$$

$$\zeta = \frac{1}{2\sqrt{b}}\frac{C_2 + S_2\frac{D_e}{R}\sqrt{\frac{G_s\rho_s}{G\,\rho}}}{\sqrt{C_1\frac{G_s}{G}\frac{D_e}{R}S_1}} \tag{5.10}$$

Where C_1, C_2, S_1 and S_2 are constants that depend on Poisson's ratio. G is the shear modulus and ρ is the mass density of soil. The subscript s is used to denote the side soil properties. In this study both side soil and bottom soil have the same properties. D_e is the embedment depth,. R is the radius of the foundation, and b is a mass ratio that equals $m/\rho R^3$. (see Figure 5.9)

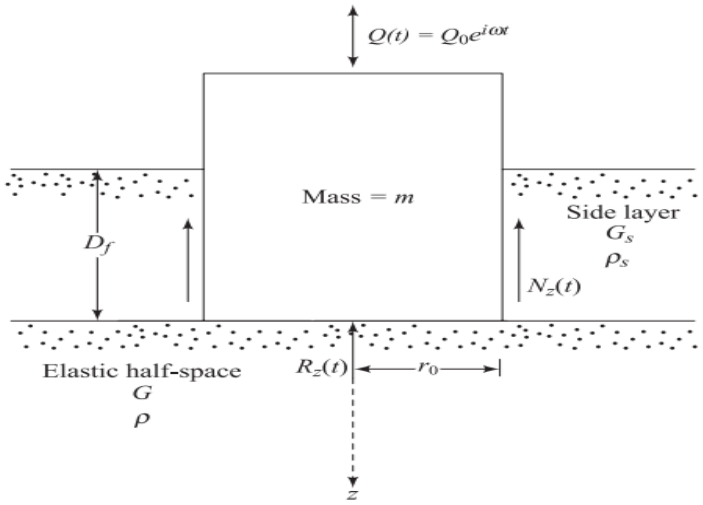

Figure 5.9: Details for solution of Novak and Beredugo after (Das & Ramana, 2010)

Note that in Figure 5.9, D_f is D_e and r_0 is R. According to this solution the values of the constants are $C_1 = 6.58$, $C_2 = 6.08$, $S_1 = 2.7$ amd $S_2 = 6.7$. This is for a Poisson's ratio of 0.4. Comparison of the Novak and Beredugo solution for static stiffness is given in Figure 5.10, while comparison of damping ratio values is given in Figure 5.11. From Figure 5.10, the static stiffness calculated by this study almost matches exactly the solution of Novak and Beredugo. From Figure 5.11, the damping ratio is showing the same linear trend but with a greater damping ratio predicted by the solution of Novak and Beredugo. This solution provided by is essentially frequency dependent. The values of the constants are function of the frequency of the applied load. Assumptions are made so that the constants become frequency independent (Das & Ramana, 2010). This study showed that damping is frequency independent. The damping ratio calculated is the same across all frequencies of loading for an embedded footing. This could explain the difference of the damping ratio calculated and the one resulting from this study. The Novak and Beredugo solution can be used to calculate damping when the footing is on the surface (i.e.,

$D_e = 0$). The problem then is that the damping calculated will be the same regardless of the ratio G_1/G_2 (or G_s/G in Novak and Beredugo). The damping calculated by this study depends greatly on the ratio of G_1/G_2 as was previously discussed in Section 5.1.3. The use of the Novak and Beredugo solution to calculate damping when the footing is on the surface is not valid when there are two layers beneath the footing.

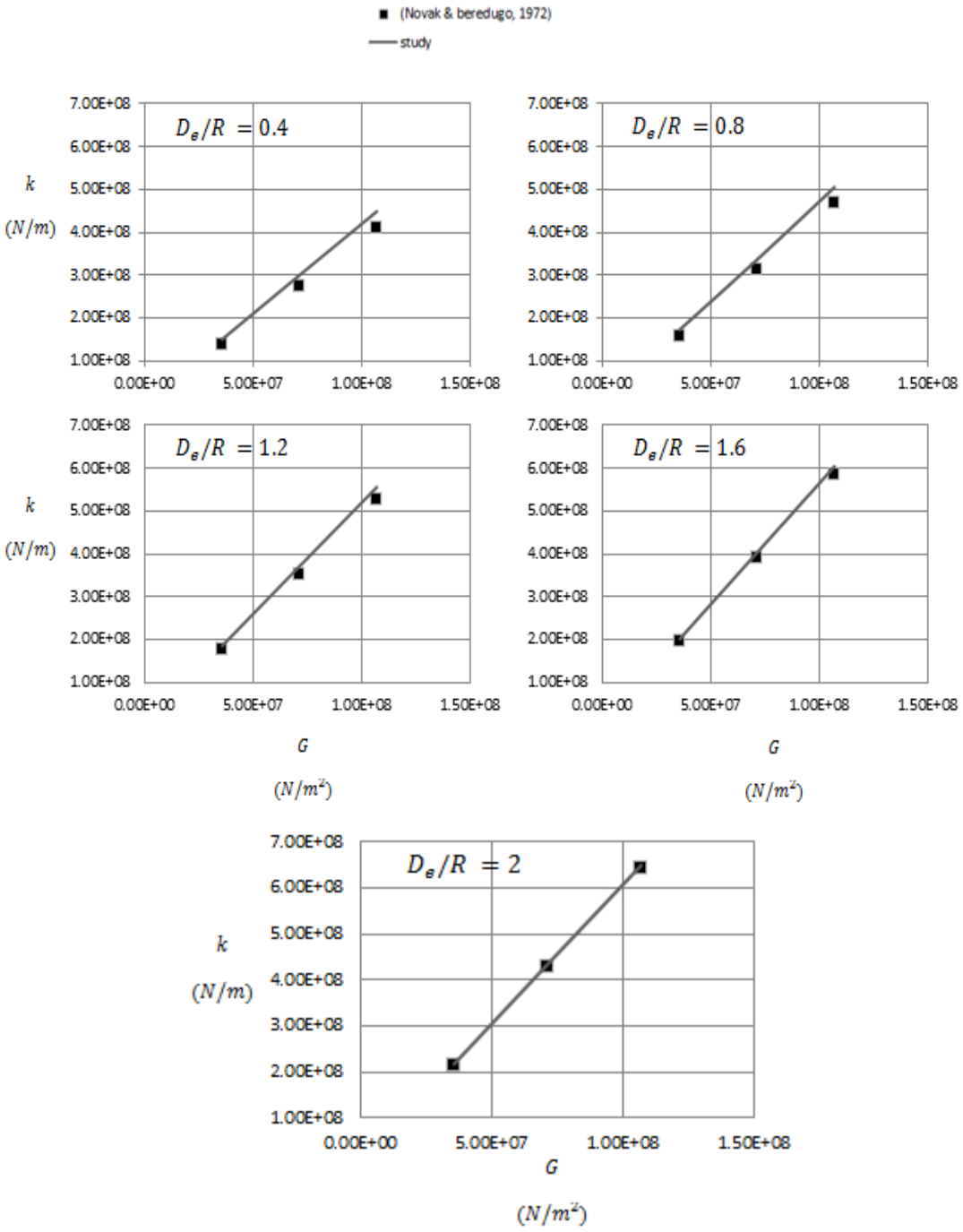

Figure 5.10: Comparison of static stiffness with solution of Novak & Beredugo

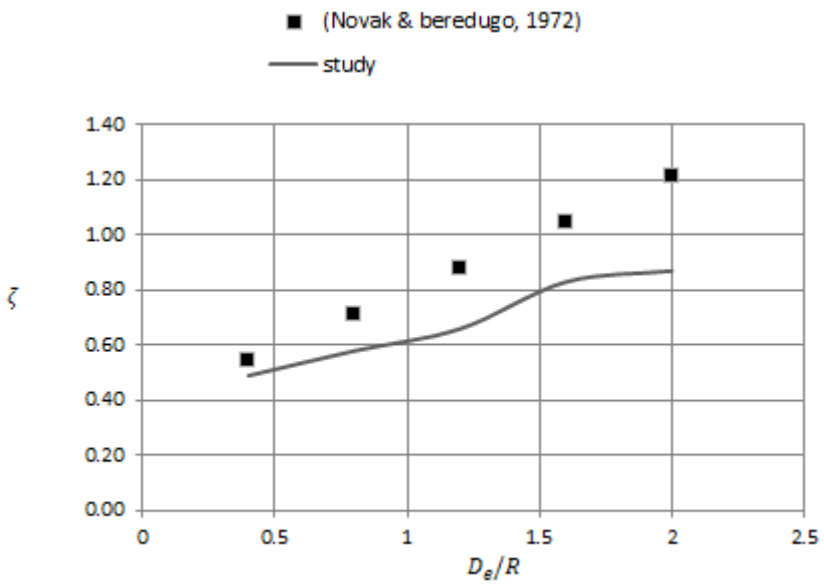

Figure 5.11: Comparison of damping ratio with Novak & Beredugo

6. Conclusion

A numerical procedure was used to solve two problems, one of a footing supported by two layers and the other one, a footing embedded in a homogenous elastic half space. Both footing were subject to a vertical dynamic force. Based on results of the numerical analysis, charts and recommendations are produced that will assist in the design of machine foundation that are subject to vertical dynamic load.

Current existing methods available use equations that determine the response of footings subject to dynamic loads assuming soil as a homogenous elastic half space.

For footings on two layers of soil, Figure 5.1 gives values of an equivalent shear modulus G_{eq}. This equivalent shear modulus can be used to represent the soil and it depends on the shear modulus of the top layer G_1, the shear modulus of the bottom layer G_2, and the depth of the top layer D_1 relative to the radius of the footing.

The figure shows that when shear modulus of both top and bottom layer are equal (i.e. $G_1 = G_2$) the equivalent shear modulus G_{eq}/G_1 is equal to 1. This is true for any value of the ratio of depth of the top layer to the radius of the footing D_1/R.

The effect of a second layer on the static response of the system is significant as the depth of the top layer is small. The lower the ratio of the depth of the top layer to the radius of the footing, D_1/R, the higher the effect in equivalent shear modulus. (Increase or decrease in shear modulus depends on G_1/G_2). The effect starts to diminish as D_1/R increases. When the depth of the top layer is 4 times the radius of the footing the values of G_{eq}/G_1 were found to be in the range of 0.82 to 1.3

The second layer adds to the strength of the top layer (i.e. increase in equivalent shear modulus) when it is stronger than the bottom layer. Decrease in the equivalent shear modulus is observed if the bottom layer is significantly weaker than the top one. For example at $D_1/R = 1$ and $G_1/G_2 = 2.78$, i.e., low top layer depth and significantly stronger top layer relative to lower one, the value of G_{eq}/G_1 was found to be close 0.55.

Figure 5.3 shows the natural frequency of the system as a dimensionless frequency a_0 where

$$a_0 = \frac{\omega R}{v_{s2}} \tag{6.1}$$

Where ω is the frequency in radians per seconds, R is the radius of the footing in m and v_{s2} is the shear wave velocity of the bottom layer. When the shear modulus of the top layer and the bottom layer shear are equal (G_1/G_2 =1) values of the natural frequency are the same for any value of D_1/R. When the top layer is stronger than the bottom one (i.e. $G_1/G_2 > 1$), the natural frequency increases with the increase of the ratio D_1/R. This increase is significantly higher for $D_1/R = 4$ than for $D_1/R = 2$. When the bottom layer is stronger the natural frequency decreases as D_1/R increases. It is higher at D_1/R and gets smaller as D_1/R decreases.

Geometrical damping is independent of the properties of the elastic half space in cases of homogenous elastic half space. It was found that this is not true for footing on two layers of soil with different shear moduli. Figure 5.6 shows the effect of ratio of shear wave velocities on the geometric damping. When the shear wave velocity of the top layer is slower than the bottom one (i.e., $G_1/G_2 < 1$ consequently $v_{s1}/v_{s2} <$

1) the geometric damping would be less than that calculated by Lysmer's method for a homogenous half space. The value of the geometric damping then increases linearly as the ratio of v_{s1}/v_{s2} increases. This is true for all values of D_1/R. The effect of the second layer starts to diminish as the depth of the top layer increases and the top layer depth starts to become large enough to simulate an infinite homogenous half space. At $D_1/R = 4$ values of the damping resulted from the study varied from 0.9 ζ_{Lysmer} to 1.4 ζ_{Lysmer} where ζ_{Lysmer} is the damping calculated for homogenous half space calculated by Lysmer's Method.

Effect of embedment of the footing was also studied for different embedment depths. The footing was embedded in a homogenous soil. The effect on the static and dynamic response was also determined..

The static stiffness of the system increases as the embedment depth increases. This is expected as side wall contact of the footing with the elastic half space would provide additional resistance compared to a surface footing. Figure 5.7 shows the static spring constant of embedded footing normalized over that of a surface footing. Within the same embedment depth, the value of the spring constant didn't increase significantly with a significant increase in the soil shear modulus. As shear modulus increase of 3 times resulted in far less than double the increase in embedded static stiffness.

As the depth of embedment increases the static stiffness gets a more significant increase at the same value of the shear modulus.

The effect of embedment on the geometrical damping is seen as a linear increase with the depth of embedment but it was found that it is independent of

variations of the shear modulus. Figure 5.8 shows the increase of the geometrical damping compared to that of the case of a surface footing.

Comparison of this data with available literature was also provided in this study. Comparison of the static stiffness of a surface footing on 2 layered soil was compared with an equation provided by Gazetas, 1983. Agreement was found in the pattern of the curve of the static stiffness but this study resulted in a stiffness that is higher than that calculated by Gazetas. This is due to the fact that Gazetas' equation doesn't take into account the stiffness of the footing while in this study the footing stiffness was part of the simulation. The comparison is shown in Figure 5.2.

The static stiffness of the embedded footing was compared with the work of Novak & Beredugo, (1972). The results of this study is in close agreement with that of the solution provided by Novak & Beredugo. This is shown in Figure 5.10.

Figure 5.11 shows comparison of the obtained damping of this study with that provided by Novak & Beredugo. The obtained damping was found to be less than that calculated by Novak & Beredugo. Furthermore, the damping calculated by Novak & Beredugo was frequency dependent which was the assumption they made on their solution. This study found that the geometrical damping of an embedded footing is frequency independent and a single value of damping can represent the dynamic response of the system very accurately at different frequencies and different embedment depths.

Appendix A.1

Sample Calculation for results interpretation procedure

A procedure of how the results are acquired and obtained is discussed in Section 5.1. The following is a detailed example of how the data obtained through finite element analysis was interpreted .to obtain G_{eq}, k and ζ. Refer to Figure 5.6 for the material properties used in this example.

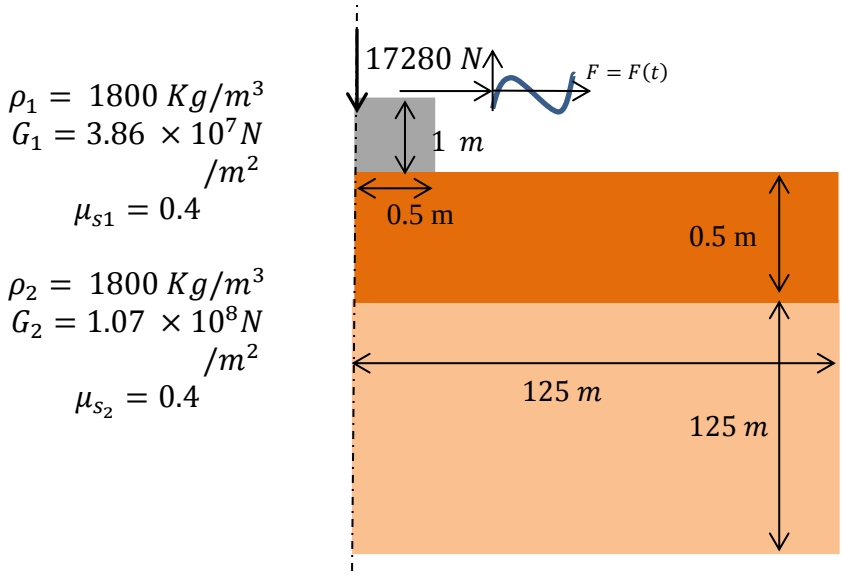

Figure A.1: Geometry and material properties for sample calculation

From Figure A.1, for $v_{s1} = \sqrt{G_2/\rho_1} = 146\ m/s$ and $v_{s2} = \sqrt{G_2/\rho_2} = 244\ m/s$, then $v_{s1}/v_{s2} = 0.36$ and $D_1/R = 1$ the results of FEM are obtained at different frequencies and presented in Table A.1.

Table A.1: Results of FEM for sample calculation

Frequency (Hz)	0	20	55	60
u^*	7.25×10^{-5}	8.45×10^{-5}	2.4×10^{-4}	1.42×10^{-4}
u_d/u_s	1	1.03	3.10E+00	3.31E+00

Note that in Table A.1 u^* at $0\ Hz$ is u_s and at any other frequency u^* is u_d. These values of displacements are obtained at the center of the footing at the soil-footing interface as discussed in section 5.1.

Now, the static spring stiffness is calculated as $k = F/u_s$ and $k = 2.38 \times 10^8\ N/m$. The equivalent shear modulus $G_{eq} = (1-\mu)k/(4R) = 7.14 \times 10^7 N/m^2$. The natural frequency f_n is calculated as $\sqrt{k/m}$ and $f_n = 56.59\ Hz$. The geometric damping is obtained using curve fitting of the dynamic data and Equation 2.20. This was done through Mathematica using the following command lines

```
Data = {{0,1},{20,1.05},{55,3.1},{560,3.31}};
Model = 1/Sqrt[(1-(f/56.59)^2)^2+4*D^2*(f/56.59)^2];
FindFit[data, {model,{D>0}}, D, f]
```

D in the previous command lines is the geometric damping. f is the frequency in Hz. The resulted damping is 0.16 which is close to what is calculated previously and presented in Figure 5.5 but different due to the fact that 3 data points were used in this sample calculation but the actual data used was 8 data points.

Bibliography

1. Bathe, K.-J. (2006). *Finite Element Procedures*. Klaus-Jurgen Bathe.
2. Das, B., & Ramana, G. V. (2010). *Principles of Soil Dynamics*. Cengage Learning.
3. Davis, R. O., & Selvadurai, A. P. S. (1996). *Elasticity and Geomechanics*. Cambridge University Press.
4. Gazetas, George. "Analysis of machine foundation vibrations: state of the art."*International Journal of Soil Dynamics and Earthquake Engineering* 2.1 (1983): 2-42..
5. Hadjian, A. H., & Luco, J. E. (1977). On the importance of layering on impedance functions. In *Proc. 6th WCEE* (pp. 1675-1681).
6. Hardin, B. O., & Black, W. L. (1968). Vibration Modulus of Normally Consolidated Clay. *Journal of the Soil Mechanics and Foundations Division*, *94*, 353–370.
7. Hardin, B. O., & Richart, J. F. E. (1963). Elastic wave velocities in granular soils. *ASCE Proceedings Journal of the Soil Mechanics and Foundations Division*, *89*, 33–65.
8. Lambe, H. (1904). On the Propagation of Tremors Over the Surface of an Elastic Solid. *Philosophical Transactions of the Royal Society of London. Series A, Containing Papers of a Mathematical or Physical Character*, *203*(1904), 1–42.
9. Logan, Daryl. "First Course In Finite Element Analysis." *Brooks/Cole* (2002).

10. Lysmer, J., & Richart, F. E. (1966). Dynamic response of footings to vertical loading. *Journal of the Soil Mechanics and Foundations Division*, *92*(1), 65-91.
11. Novak, M., & Beredugo, Y. O. (1972). Vertical vibration of embedded footings .*Journal of the Soil Mechanics and Foundations Division*, *98*(12), 1291-1310.
12. Quinlan, P. M. (1953). The elastic theory of soil dynamics. *ASTM Special Technical Publication*, (156), 3-34.
13. Reissner, E. (1936). Stationäre, axialsymmetrische, durch eine schüttelnde Masse erregte Schwingungen eines homogenen elastischen Halbraumes.*Archive of Applied Mechanics*, *7*(6), 381-396.
14. Richart, F. E., & Whitman, R. V. (1967). Comparison of footing vibration tests with theory. *Journal of Soil Mechanics & Foundations Div*,93,143-168.
15. Rollins, K. M., Evans, M. D., Diehl, N. B., & III, W. D. D. (1998). Shear modulus and damping relationships for gravels. *Journal of Geotechnical and Geoenvironmental Engineering*, *124*(5), 396-405.
16. Sung, T. Y. (1953). *Vibrations in semi-infinite solids due to periodic surface loading* (Doctoral dissertation, Harvard University).
17. Varga, R. S. (2009). *Matrix iterative analysis* (Vol. 27). Springer Science & Business Media..
18. Verruijt, A. (2010). *An introduction to soil dynamics* (Vol. 24). Springer Science & Business Media.
19. Zhang, J., & Tang, Y. (2007). Radiation damping of shallow foundations on nonlinear soil medium.